Chem Soc Rev

# Trianionic pincer and pincer-type metal complexes and catalysts.



| | |
|---|---|
| Journal: | *Chemical Society Reviews* |
| Manuscript ID: | CS-CRV-03-2014-000111.R2 |
| Article Type: | Review Article |
| Date Submitted by the Author: | 26-May-2014 |
| Complete List of Authors: | O'Reilly, Matthew; University of Florida, Chemistry<br>Veige, Adam; University of Florida, Chemistry |
| | |

# Trianionic pincer and pincer-type metal complexes and catalysts.

*Matthew E. O'Reilly and Adam S. Veige**

University of Florida, Center for Catalysis, P.O. Box 117200, Gainesville, Florida, 32611.

veige@chem.ufl.edu

**Table of Contents**

**Abstract:** Trianionic pincer and pincer-type ligands are the focus of this review. Metal ions from across the periodic table, from main group elements, transition metals, and the rare earths, are combined with trianionic pincer ligands to produce some of the most interesting complexes to appear in the literature over the past decade. This review provides a comprehensive examination of the synthesis, characterization, properties, and catalytic applications of trianionic pincer metal complexes. Some of the interesting applications employing trianionic pincer and pincer-type complexes include: 1) catalyzed aerobic oxidation, 2) alkene isomerization, 3) alkene and alkyne polymerization, 4) nitrene and carbene group transfer, 5) fundamental transformations such as oxygen-atom transfer, 6) nitrogen-atom transfer, 7) $O_2$ activation, 7) C−H bond activation, 8) disulfide reduction, and 9) ligand centered storage of redox equivalents (i.e. redox active ligands). Expansion of the architecture, type of donor atoms, chelate ring size, and steric and electronic properties of trianionic pincer ligands has occurred rapidly over the past ten years. This review is structured according to the type of pincer donor atoms that bind to the metal ion. The type of donor atoms within trianionic pincer and pincer-type ligands to be discussed include: $NCN^{3-}$, $OCO^{3-}$, $CCC^{3-}$, redox active $NNN^{3-}$, redox active $ONO^{3-}$, $ONO^{3-}$, and $SNS^{3-}$. Since this is the first review of trianionic pincer and pincer-type ligands, an emphasis is placed on providing the reader with in-depth discussion of synthetic methods, characterization data, and highlights of these complexes as catalysts.

## 1. Introduction

The Pincer Movement is a military maneuver that involves a simultaneous attack of an advancing army by two flanking units at the sides in an effort to surround the enemy unit. Hannibal's defeat of the Romans in 216 BC at the Battle of Cannae[1] is recognized as the first, and one of the most successful deployments of the movement. Another historic application includes confederate army General Lee's implementation of the Pincer Movement against a significantly larger Union opponent (Gen. Joseph Hooker) in the Battle of Chancellorsville[2] during the American Civil War. One of the most famous executions of the Pincer Movement occurred during the Battle of Stalingrad (August 23, 1942 – February 2, 1943)[3-4] under the code name Operation Uranus (launched November 19, 1942). During a fierce and casualty-heavy fight for the control of Stalingrad, the Soviet Army executed a pincer movement against the German 6th Army, Romanian 3rd and 4th Armies, and the German 4th Panzer Army (Figure 1). Within a few weeks nearly 300,000 soldiers were surrounded, signaling a significant turning point in the Eastern European war front of WWII.[3-4]

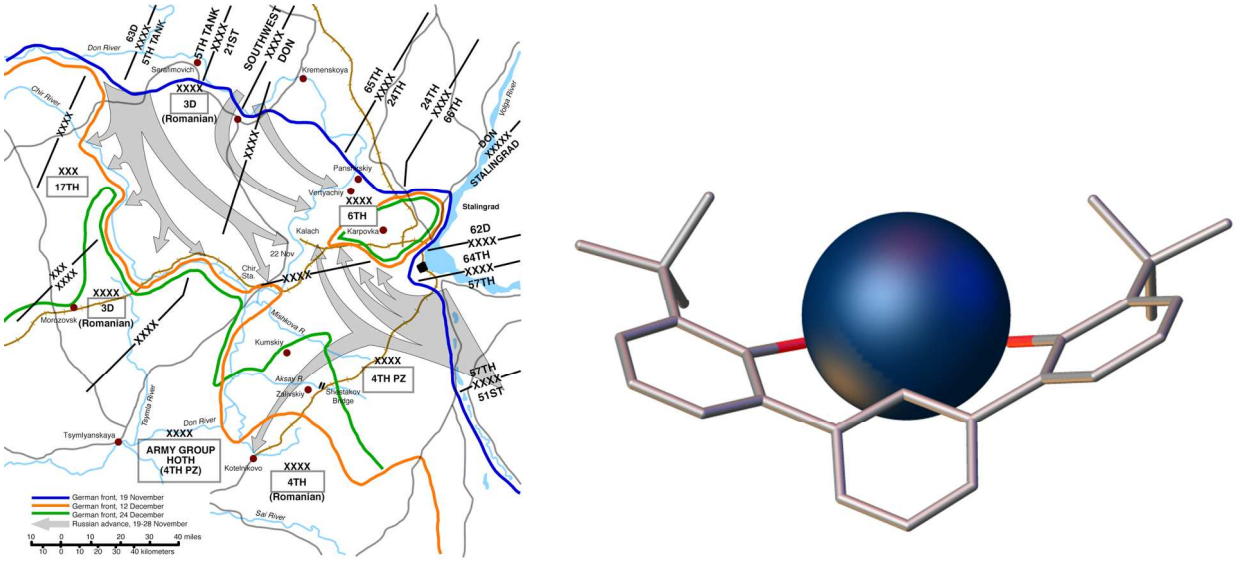


**Figure 1.** Left: The Soviet Army's execution of the Pincer Movement against German forces during the Battle of Stalingrad (November 19th, 1942): Operation Uranus.[5] Right: Pincer ligand chelating a metal ion.

The concept of surrounding an enemy unit is synonymous to chelating ligands in transition metal chemistry. A pincer ligand binds to a metal ion through a central M-C bond and two flanking donor groups (Figure 1). In the same way the military maneuver surrounds an enemy unit with no escape route, a pincer ligand surrounds a metal ion and effectively eliminates all reasonable kinetic opportunities for metal ion escape. Since their introduction in the 1970's, pincer and pincer-type ligands have been a versatile ligand class for transition and main group metal ions providing, fertile ground for discovering new applications in catalysis.[6-31] The pincer ligand, as designed by Moulton and Shaw,[32-37] contains an anionic carbon between two pendant neutral donors (originally phosphines). Somewhat loosely defined due to the myriad of plausible derivatives, *pincer-type* ligands, for the purposes of this review, replace the central carbon atom donor of pincer ligands with an anionic heteroatom.[38-41] Unifying this class of ligand however, is the important concept that they all constrain three donor atoms to the metal ion meridional plane. Straightforward modifications to the general pincer architecture permits exquisite control over the electronic and geometric properties of metal complexes. Historically, pincer and pincer-type ligands have been extensively applied with metal ions in low oxidation states, whereas applications employing metal ions in high oxidation states are only now emerging with the introduction of multi-anionic variants. In particular, *trianionic* pincer and pincer-type ligands are well-suited to explore the chemistry of high-valent metal ions ($M^{n+}$; $n \geq 3$). Incorporating the near-maximum anionic charge into the tridentate ligand structure provides the prerequisite electronic stabilization for high-valent metals. In addition, pincer ligands only occupy three coordination sites, resulting in coordinatively unsaturated metal complexes that are poised to enter into catalytic cycles. The term trianionic pincer does not appear in the literature until 2007,[42] however, a few examples of these ligands were reported prior to that date, including an $NNN^{3-}$ by Schrock in 1996,[43-44] and an $OCO^{3-}$ in 2006 by Kawaguchi.[45] Veige reported the first $NCN^{3-}$ version in 2007,[42] and since then number of derivatives has expanded significantly. Another important development is the use of trianionic pincer redox-active ligands, with the first $NNN^{3-}$ example appearing in 2004 by Gambarotta and Budzelaar.[46] An ONO redox active ligand was known for many decades,[47-50] but it was Heyduk and coworkers in 2008[51] that elucidated their potential, and expanded this area to include

catalysts.[52-53] It is now thoroughly established that storing redox equivalents within ligand-centered oxidation state changes is a potent approach to conducting multi-electron chemistry.[54-57] Some of the most interesting and exemplary cases of redox-active ligands happen to be trianionic pincers. Proof of trianionic pincer ligands' current and future potential comes in the form of numerous and diverse chemical applications in a relatively short period of time (<10 years), and now include catalyzed aerobic oxidation,[58] alkene isomerization,[59] alkene[60] and alkyne[61-62] polymerization, nitrene[52, 63] and carbene[53] group transfer, and fundamental transformations such as oxygen-atom transfer,[64] nitrogen-atom transfer,[65] $O_2$ activation,[66] C−H bond activation,[67] and disulfide reduction.[68] This review covers the current progress and strategic design of implementing trianionic pincer ligands in transition metal catalysis.

## 2. $NCN^{3-}$ trianionic pincer ligands

In the Veige laboratories, the initial focus centered on trianionic $NCN^{3-}$ pincer ligands, which were attractive due to their easy synthesis, their amenability to both steric and electronic modifications, and allowed a direct comparison to *monoanionic* NCN pincer ligands.[69] Despite numerous variations, relatively few examples of NCN trianionic pincer ligated complexes were synthesized, due in part to difficulty with metalating. In contrast to monanionic pincer ligands, ligating three anionic donors presents unique challenges.

### *2.1. $NCN^{3-}$ group 4 complexes*

This section provides a survey of metalation strategies for $NCN^{3-}$ trianionic pincer ligands. One successful approach to metalation is a triple salt metathesis reaction that involves treating a trilithio salt of the $NCN^{3-}$ pincer ligand with a metal halide. Some early examples of $NCN^{3-}$ trianionic pincer metalation via triple salt metathesis involve proligands **1** and **4** with $HfCl_4$.[42] Proligands **1** and **4** contain similar $NCN^{3-}$ pincer designs. The only difference is the slightly larger aryl group, 2,6-($^i$Pr)$_2$C$_6$H$_3$, of **4** relative to **1**, (2,6-(CH$_3$)$_2$C$_6$H$_3$). Refluxing either proligand **1** or **4** with methyl lithium yields [NCN]Li$_3$ salts **2** (Scheme 1) and **5** (Scheme 2) as suitable ligand precursors for metalation. Treating **2** with $HfCl_4$ in

benzene at room temperature yields complex **3** containing two pincer ligands bound to the hafnium metal center in a 54% yield. Coordinating two pincer ligands to a single hafnium metal center (over-metalation) presents one of the significant challenges in metalation strategies.[42] To avoid over-metalation, the slightly bulkier aryl group on the pendant arms of ligand **4** relative to **1** provides sufficient steric bulk to repel the approach of a second pincer ligand. Thus, treating **5** with $HfCl_4(THF)_2$ at -35 °C yields the $NCN^{3-}$ trianionic hafnium pincerate complex **6** in 16% yield. Treating in situ generated **6** with methyl lithium substitutes the chlorides for methides to provide complex **7** in 35% yield (Scheme 2).

**Scheme 1.** Synthesis of pincerate complex **3** via triple salt metathesis.

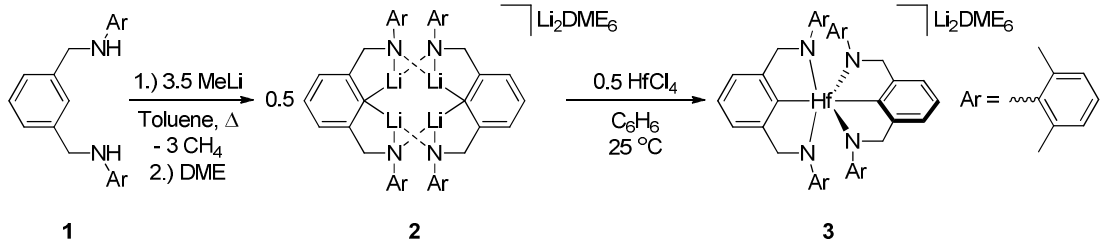


**Scheme 2.** Synthesis of pincerate complexes **6** and **7**.

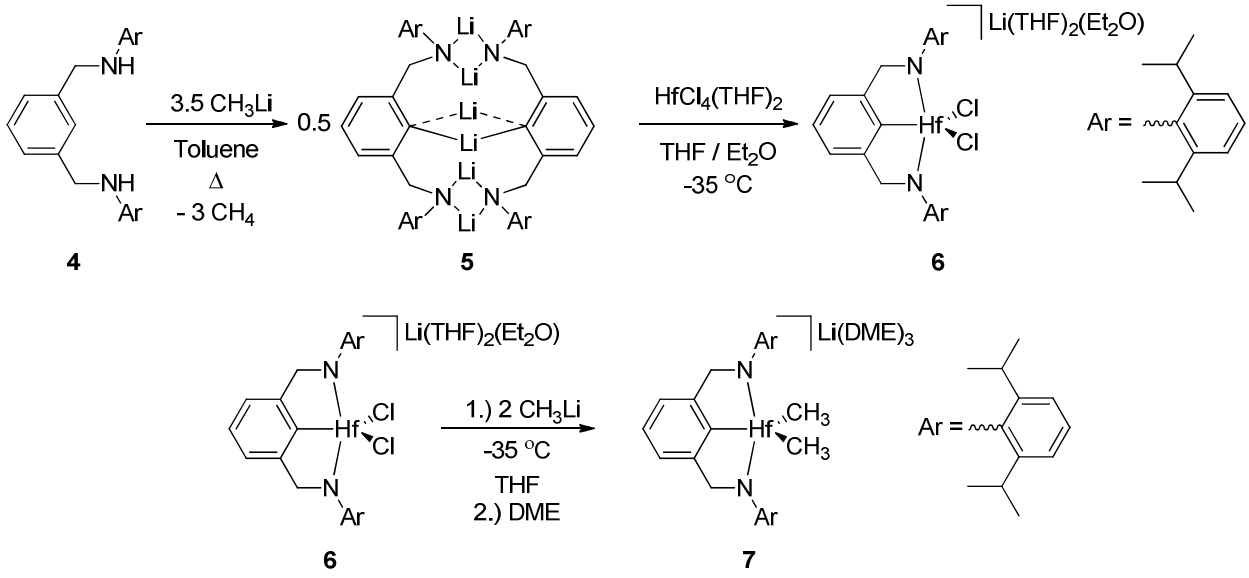

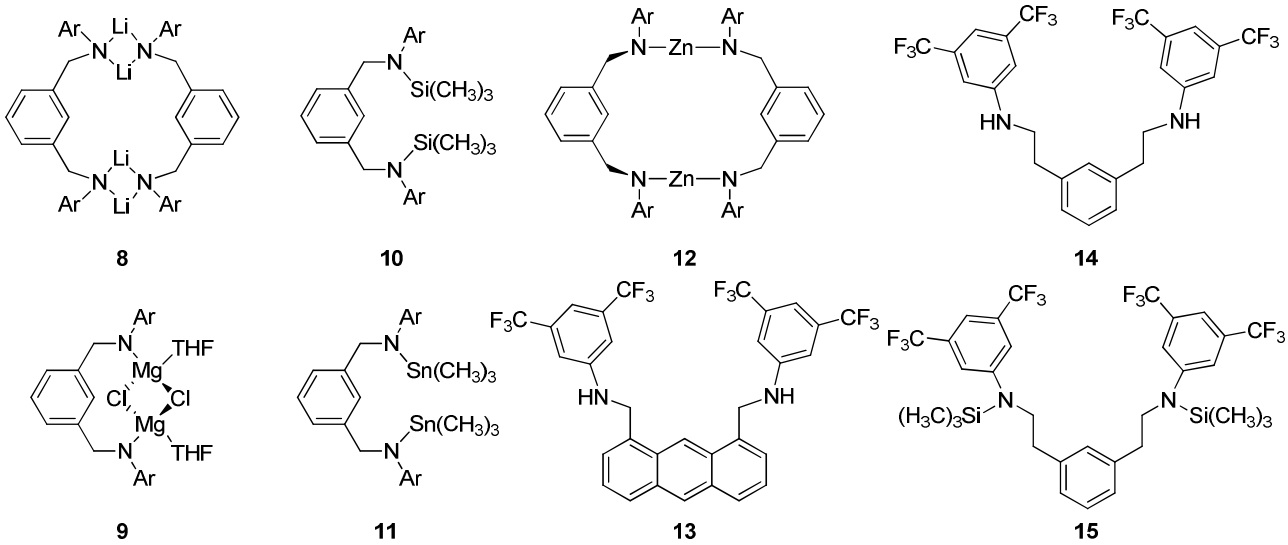


**Figure 2.** $NCN^{3-}$ trianionic proligands **8-15**, {**8-12**, Ar = 2,6-($^{i}$Pr)$_2$C$_6$H$_3$}.

Despite the successful metalation of the $NCN^{3-}$ trianionic pincer ligand with hafnium via triple salt metathesis, this synthetic methodology gave poor yields. Figure 2[70] presents several synthetic modifications to proligand **4**. Ligand precursors **8**, **9**, and **12** are diamido salts of proligand **4** with lithium, magnesium, and zinc counter cations, respectively.[70] The various salts offer an opportunity to investigate the role of the cation during salt metathesis. The test reaction involves treating $ZrCl_2(N(CH_3)_2)_2(THF)_2$[71] with the salt proligand to yield a trianionic pincer complex via double salt metathesis and pincer C-H$_{pincer}$ deprotonation by the internal amide (Scheme 3). However, treating **8** with $ZrCl_2(N(CH_3)_2)_2(THF)_2$[71] yields the zirconium complex [2,6-$^{i}$PrNCN]Zr(N(CH$_3$)$_2$)$_2$ (**16**). The solid state structure of **16** reveals the pincer is in the dianionic form and chelates through the amido N-atoms, but the pincer C-H$_{pincer}$ proton remains intact and aminolysis in an attempt to synthesize **17** does not occur even after prolonged heating at 90 °C. Though proligands **9** and **12** are good candidates for metalation via a double salt metathesis, they do not address the more substantial challenge of activating the pincer C-H$_{pincer}$ bond.

**Scheme 3.** Synthesis of complex **16** featuring a pincer in the dianionic form.

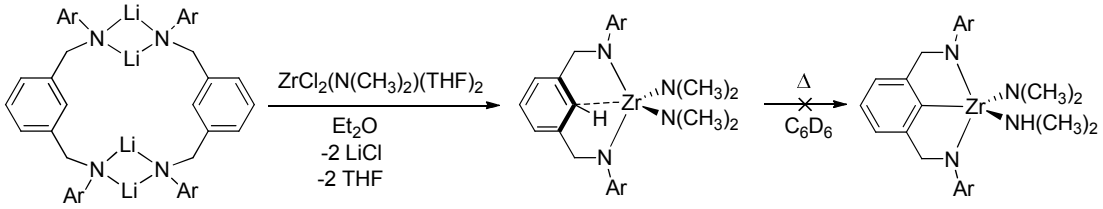


**8** **16** **17**

Better suited for metalation approaches that do not involve salt metathesis, proligands **10**, **11**, and **15** replace the NH bond with either $-Si(CH_3)_3$ and $-Sn(CH_3)_3$ to serve as potential leaving groups.[70] When treated with a metal halide ($M'Cl_4$; M = Ti, Zr, Hf), these proligands should abstract halides releasing $(CH_3)_3MCl$ (M = Sn and Si) to form chelating diamido metal complexes. However, no reaction occurred after heating proligands **10**, **11**, or **15** with either $TiCl_4$, $ZrCl_4$, or $HfCl_4$ in toluene (Scheme 4).

**Scheme 4.** Reactions between **10**, **11**, and **15** with $TiCl_4$, $ZrCl_4$, and $HfCl_4$.

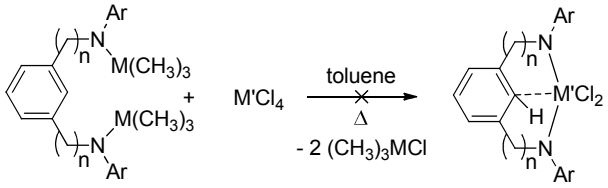


**10**: n = 1, M = Si, Ar = 2,6-($^i$Pr)$_2$C$_6$H$_3$
**11**: n = 1, M = Sn, Ar = 2,6-($^i$Pr)$_2$C$_6$H$_3$
**15**: n = 2, M = Si, Ar = 3,5-$(CF_3)_2C_6H_3$
M' = Ti, Zr, Hf

One explanation for the difficult metalation of proligands **1** and **4** may arise from the acute N-M-N bite angle of the pincer complex. For example, the NCN hafnium complexes **3**, **6**, and **7** contain an N-Hf-N bite angle of ~140°. To alleviate the constrained N-M-N bite angle, proligands **13** and **14** incorporate an extra carbon linker between the central aryl ring and the amido donor, thus encouraging the amido donors to span a *trans* angle of 180°. However, treating complex **13** with $Hf(N(CH_3)_2)_4$ yields the bimetallic complex **18** (Scheme 5).[70] Similar results were obtained when treating proligand **14** with $Zr(N(CH_3)_2)_4$. The resulting complexes **18** and **19** contain two metal ions bridged through the amido donors of two separate ligands and may be useful as precursors for cooperative bond activations in catalytic transformations.

**Scheme 5.** Synthesis of dinuclear complexes **18** and **19** with the flexible proligands **13** and **14**, respectively.

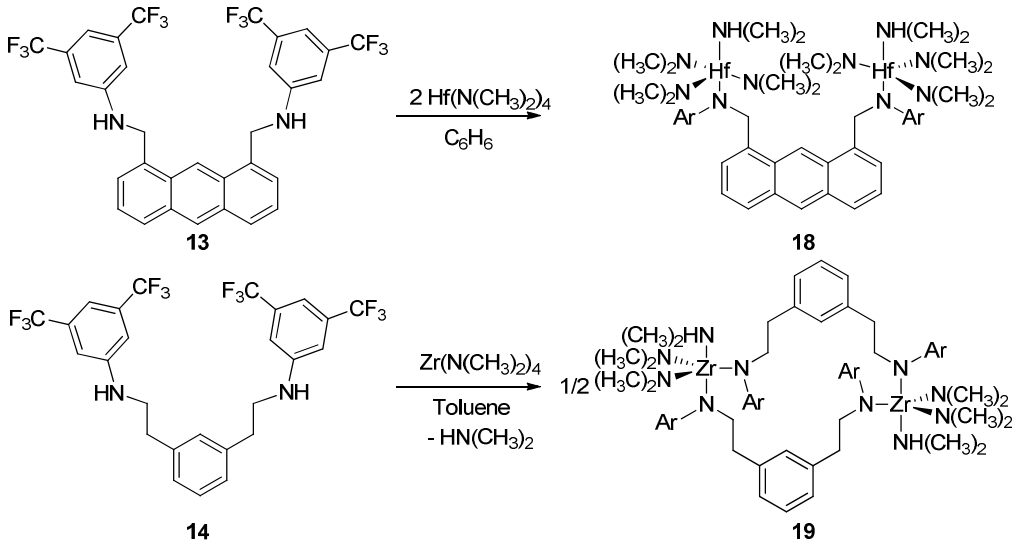


*2.2. $NCN^{3-}$ chromium complexes*

The reaction between proligand **8** and $CrCl_2CH_3(THF)_3$[72] in THF proceeds at -80 °C via double salt metathesis and methane elimination to yield the NCN trianionic pincer chromium(III) complex **20** (Scheme 6).[59] The Cr(III) metal center of **20** resides in a strongly electron-donating environment afforded by the σ- and π-donation of the $NCN^{3-}$ trianionic pincer ligand, inducing a strong proclivity towards higher oxidation states. Consequently, complex **20** readily deoxygenates styrene-oxide to form the $[NCN]Cr^{V}O$ complex **21** and styrene (Scheme 7).[59] However, complex **21** is exceptionally stable, and does not undergo oxygen-atom transfer (OAT) to $PPh_3$ (Scheme 7). This reactivity is consistent with the very strong electronic donation afforded by the $NCN^{3-}$ ligand that stabilizes Cr(V) over Cr(III).

**Scheme 6.** Synthesis of $[NCN]Cr^{III}(THF)_3$ (**20**), (Ar = 2,6-($^{i}$Pr)$_2$C$_6$H$_3$).

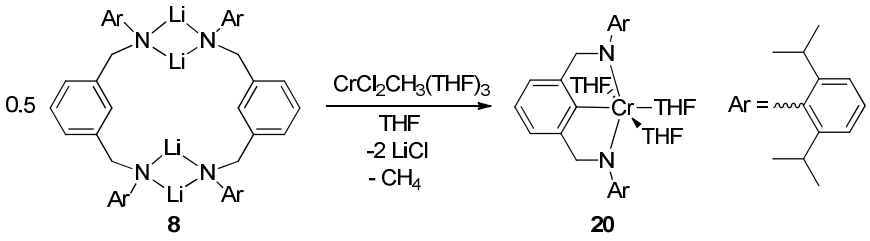

**Scheme 7.** Deoxygenation of styrene-oxide by **20** to yield **21**.

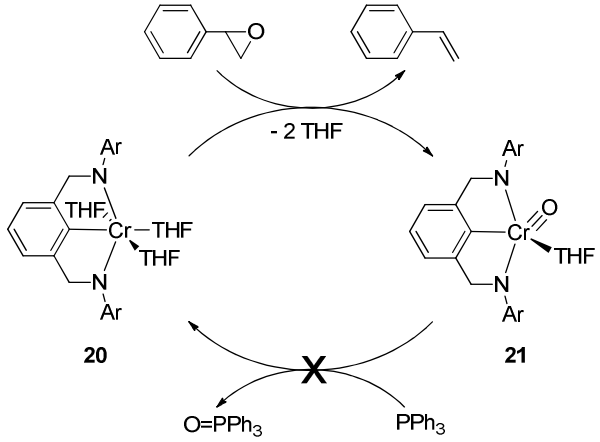


*2.1.1. Catalytic alkene isomerization*

Changing the solvent from THF to $Et_2O$ for the reaction between **8** and $CrCl_2CH_3(THF)_3$[72] drastically alters the outcome of the reaction. While only **20** forms in THF, conducting the reaction in diethyl ether results in disproportionation yielding Cr(III) (**20**), Cr(IV) (**22**), and Cr(II) (**23**) species (Scheme 8). The Cr(IV) species **22** is a rare Cr(IV) mono-alkyl complex.[73] While Cr(III) alkyl complexes are ubiquitous, chromium(IV) alkyls are destabilized by the higher oxidation state, and readily decompose via bond homolysis, valence disproportionation, and reductive elimination.[74] However, complex **22** is stable at room temperature in solution and in the solid state, which is again attributable to the strong σ- and π-donation from the $NCN^{3-}$ pincer ligand.

**Scheme 8.** The disproportionation synthesis of **20**, **22**, and **23** from proligand **8**, (Ar = 2,6-($^i$Pr)$_2$C$_6$H$_3$).

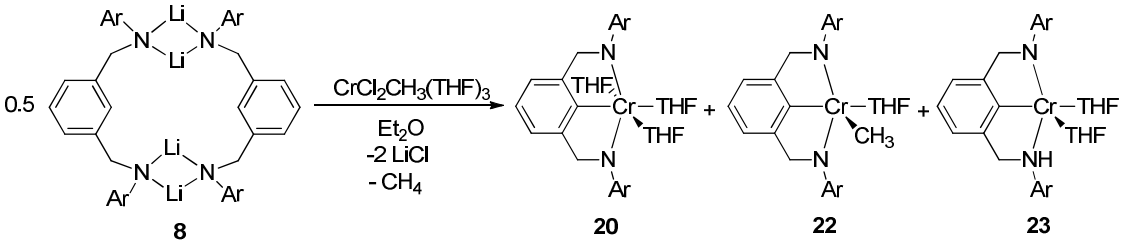

Heating complex **22** at 80 °C in the presence of 1-hexene or 1-octene over the course of 48 h catalyzes the isomerization these terminal olefins to predominantly 2-hexene and 2-octene with 95% yield.[59] Tracking the reaction progress versus time for the isomerization of 1-hexene and 1-octene revealed a 4 h induction period at 80 °C for complex **22** prior to isomerization. Heating complex **22** at 80 °C for 24 h prior to the addition of 1-hexene, eliminates the induction period. Complex **23** was identified as the active catalyst. Treating **8** with $CrCl_2$ in THF at -80 °C (Scheme 9) provides complex **23** directly, and indeed, it isomerizes 1-hexene and 1-octene at 85 °C without an induction period.[59]

**Scheme 9.** Synthesis of the active isomerization catalyst **23**, (Ar = 2,6-($^i$Pr)$_2$C$_6$H$_3$).

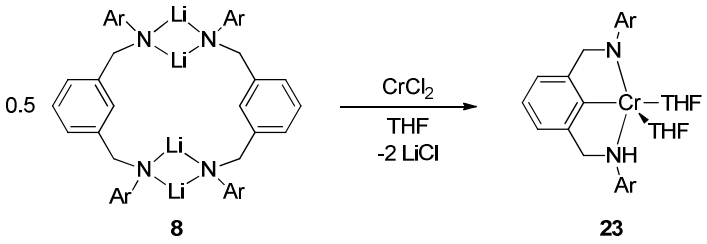


**8** **23**

Evidence supports a radical mechanism in the transformation of **22** to **23** at elevated temperatures in benzene-$d_6$ (Scheme 10). The byproducts arising from this transformation are $CH_4$ and biphenyl-$d_{10}$, which were confirmed by GC analysis. Conducting the reaction in the presence of a radical scavenger, TEMPO (2,2,6,6-tetramethylpiperidin-1-yl), traps the $CH_3$• radical and forms TEMPO-$CH_3$.

**Scheme 10.** Bond homolysis of complex **22** to yield **23**.

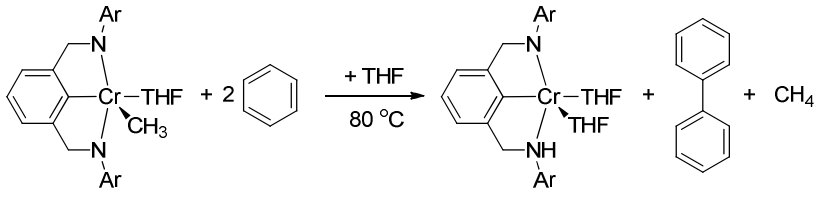


**22** **23**

*2.2.2. Catalytic ethylene polymerization*

Homogeneous ethylene polymerization catalysts are important models for the heterogeneous Phillips catalyst,[75-76] but are predominantly chromium(III) complexes. Despite the rarity of chromium(IV) catalysts for ethylene polymerization,[77-82] they are predicted to be highly active.[79] Complex **22** is a highly active precatalyst in the presence of triisobutylaluminum (TIBA) as co-catalyst.[60] The catalytic activity is dependent on the ratio of the co-catalyst TIBA and **22**. At an optimal amount of co-catalyst, complex **22** is classified as a highly-active catalyst with an activity of 7,020 kg/molCr/h.

*2.3. $NCN^{3-}$ uranium complexes*

Gambarotta et al. used the dianionic ligand[83] precursor $Li_2(NC^HN)(THF)_4$ (**124**) to form U(III) (**25**) and U(IV) (**26**) complexes (Scheme 11).[84] For both U(III) (**25**) and U(IV) (**26**), the central ring C-$H_{pincer}$ bond remains intact and the ligands are dienamides. Heating the U(III) (**25**) complex in THF for 6 h at 80 °C cleaves the C-$H_{pincer}$ to provide the U(IV) complex **27** bearing a trianionic pincer ligand. An alternative synthesis of **27** involves treating the U(IV) complex **26** with one equiv potassium naphthalenide in THF at 25 °C. In the reduction pathway the uranium remains in the 4+ oxidation state. Additional reductions of **26** employing various reductants, equivalents, and conditions lead to other complexes bearing trianionic pincer ligands, but are not illustrated here. Instead, Scheme 11 highlights the important and interesting step that converts the dianionic pincer ligand into its trianionic form.[84]

**Scheme 11.** Synthesis of uranium complexes highlighting the reductive C-H bond activation pathway to from a trianionic pincer.

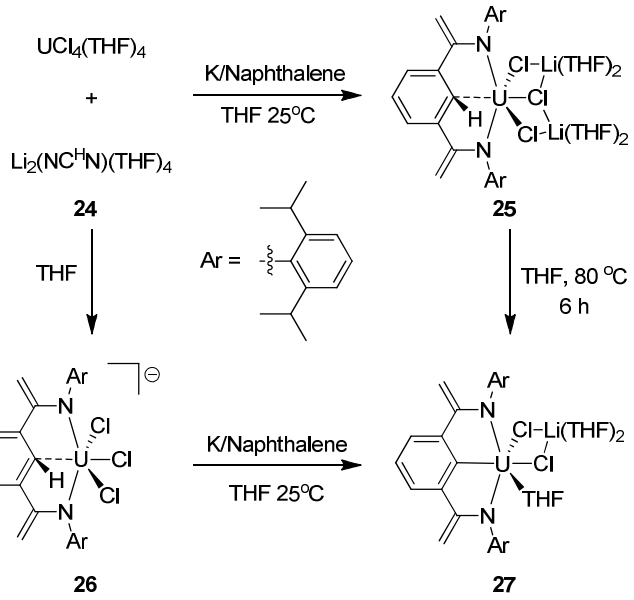


Overall, $NCN^{3-}$ ligands remain underexplored but offer ample opportunities for further investigation with the promise of rich chemistry. However, metalation will certainly be the limiting factor to their future expansion.

## 3. $OCO^{3-}$ trianionic pincer ligands

### *3.1. $OCO^{3-}$ titanium complexes*

Alkane elimination is a viable route to activate the central pincer C-H bond to yield trianionic pincer complexes. Treating [$^t$BuCH$_3$OCO]H$_3$ (**28**) with tetrabenzyl titanium yields the chelating diphenolate titanium dibenzyl complex **29** (Scheme 12).[85] Upon heating, complex **29** liberates toluene forming the monobenzyl OCO titanium complex that readily dimerizes to form **30**.

**Scheme 12.** Synthesis of dinuclear {[$^t$BuCH$_3$OCO]Ti(CH$_2$Ph)}$_2$ (**30**) via the reaction of [$^t$BuCH$_3$OCO]H$_3$ (**28**) with Ti(CH$_2$Ph)$_4$.

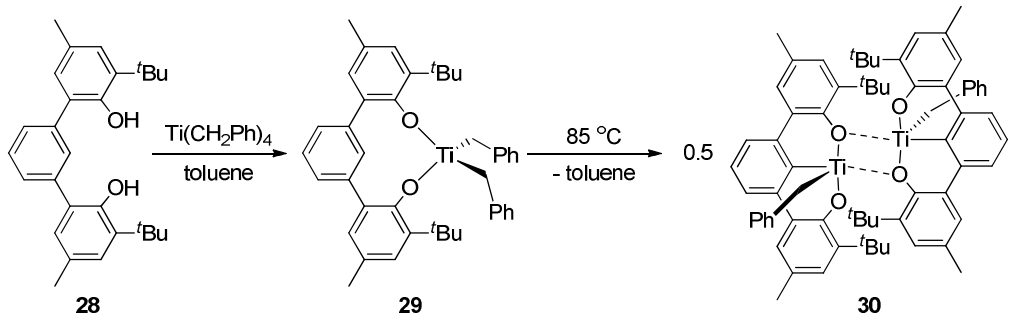


Two possible mechanisms for the activation of the pincer C-H bond are proposed in Scheme 13.[86] Pathway A follows a direct σ-bond metathesis of the pincer C-H bond by the benzyl ligand. Pathway B indirectly activates the pincer C-H bond by forming a titanium benzylidene via α-hydrogen abstraction prior to 1,2-CH activation. To examine these pathways, a series of deuterium labeling studies, replacing either the pincer C-*H* or the benzyl -C*H*$_2$- protons with deuterium, result in scrambling of deuterium atoms in both the free toluene and benzyl ligands. For instance, direct activation of the pincer C-D bond via Pathway A yields toluene-$d_1$, whereas in Pathway B deuterium atoms are transferred to form Ti—CH(D)C$_6$H$_5$. Pathways A and B are viable as competing mechanisms for the activation of the central CH bond backbone, since both deuterated products are observed.

**Scheme 13.** Competing mechanistic pathways for C-H$_{pincer}$ bond activation. Pathway A: direct σ-bond metathesis. Pathway B: α-hydrogen abstraction followed 1,2-CH bond activation.

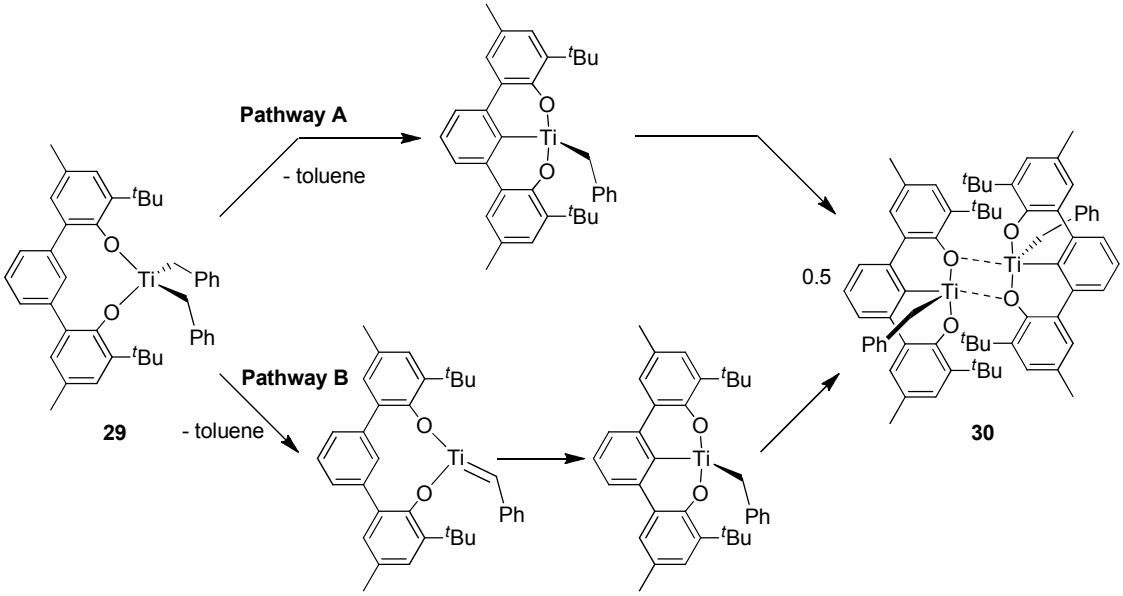

### *3.2. $OCO^{3-}$ zirconium complexes*

Similar to the metalation of **29** with titanium, treating [$^t$BuOCO]$H_3$ (**31**) with tetrabenzylzirconium yields the chelating diphenolate zirconium dibenzyl complex **32** (Scheme 14).[87] Subsequent heating in benzene readily activates the pincer C-H bond of **32**. In the absence of donor ligands, the trianionic pincer zirconium complex dimerizes to form **33**. Dimerization presents a significant problem for applications in catalysis. For example, complex **33** is unreactive towards CO, $H_2$, or ethylene. Dimerization is avoidable by adding donor ligands $P(CH_3)_3$ or THF to provide the corresponding trianionic $OCO^{3-}$ pincer complexes **34** and **35**, respectively.

**Scheme 14.** Synthesis of [$^t$BuOCHO]Zr($CH_2Ph)_2$ (**32**) and subsequent reactivity by heating or addition of $P(CH_3)_3$ or THF to yield {[$^t$BuOCO]Zr($CH_2Ph$)}$_2$ (**33**), [$^t$BuOCO]Zr($P(CH_3)_3)_2$($CH_2Ph$) (**34**), and [$^t$BuOCO]Zr$(THF)_2$($CH_2Ph$) (**35**).

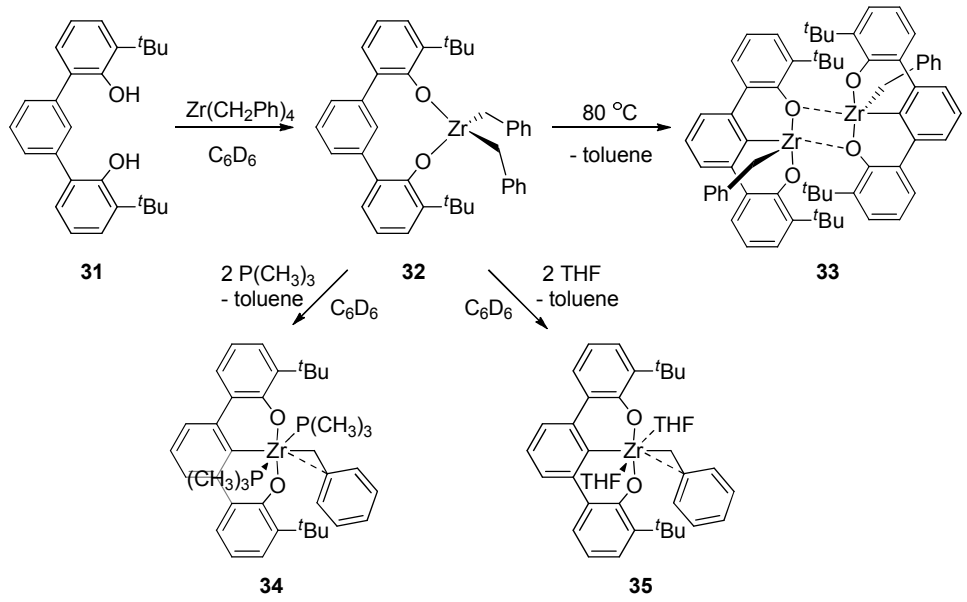


Treating the diphenolate precursor **32** with two equivalents of pyridine does not activate the central pincer C-H bond as in the case of $P(CH_3)_3$ and THF. Instead, the pyridine's *o*-C*H* protons are activated to release free toluene and complex **36** (Scheme 15).[87] Adding a third equivalent of pyridine activates the diphenolate backbone to yield the trianionic pincer ligand complex **37**. The more sterically encumbered 2-methylpyridine first binds to form complex **38**, and adding a second equivalent activates

the *o*-CH of one 2-methylpyridine and the methyl C-H bond of the second 2-methylpyridine to form complex **39**.

**Scheme 15.** Addition of pyridine and 2-methylpyridine to yield complexes **36**, **37**, **38**, and **39**.

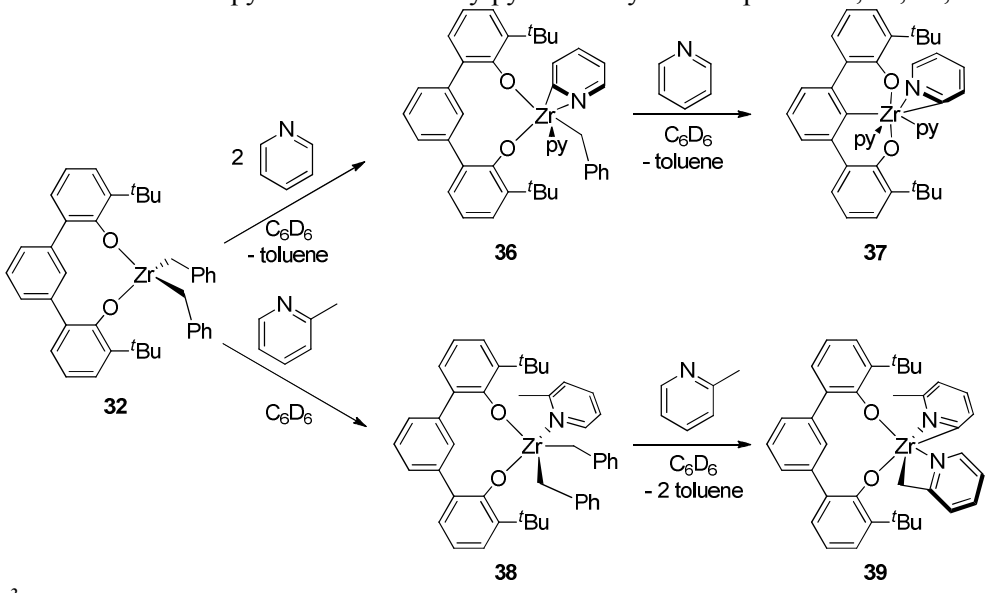


### *3.3. $OCO^{3-}$ tantalum complexes*

In contrast to $NCN^{3-}$ trianionic pincer ligands, the $OCO^{3-}$ trianionic pincer allows for easier metalation conditions with better yield. This observation may in part be attributable to the more acidic protons on the phenol versus the aniline. Bercaw et al.[88] demonstrated two practical approaches to metalating the trianionic pincer ligand [$^t$Bu$_2$OCO]H$_3$ (**40**) with $TaCl_2(CH_3)_3$ (Scheme 16). The first approach involves treating **40** with benzyl potassium to generate a dipotassium salt in situ. The salt reacts with $TaCl_2(CH_3)_3$[89-91] in a double salt metathesis to yield a diphenolate intermediate. The intermediate eliminates methane via σ-bond metathesis to yield the dimethyl complex **41**. The second method involves heating [$^t$Bu$_2$OCO]H$_3$ (**40**) with $TaCl_2(CH_3)_3$ to yield the dichlorotantalum complex **43** via three methane elimination steps. The latter reaction proceeds by attaching the two pendant alkoxides yielding complex **26** as an isolable intermediate prior to the final methane elimination to attach the pincer aryl group.

**Scheme 16.** Synthesis of **41** via double salt metathesis and methane elimination, and **43** via triple methane elimination.

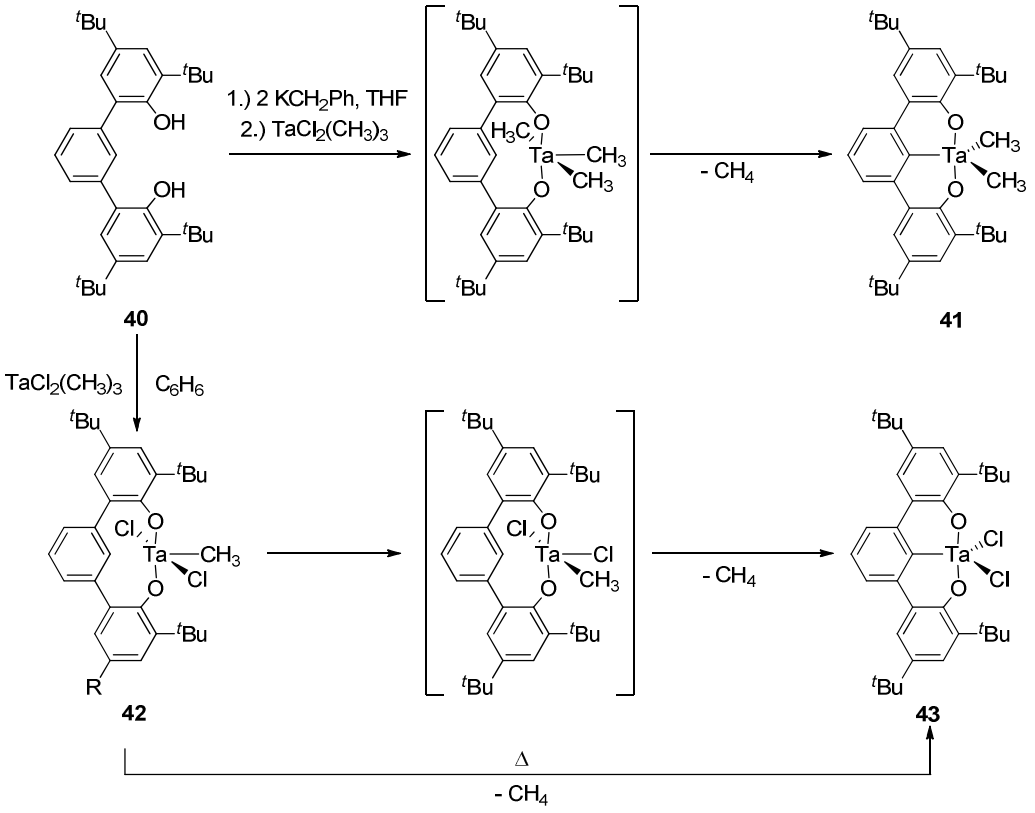


While the depicted mechanism for the formation of complex **43** appears straightforward, mechanistic studies probing C-H bond activation through deuterium labeling studies yielded some interesting results.[88] Upon treating the partially deuterated [$^t$Bu$_2$OCO] ligand **40-*d*$_2$** and **40-*d*$_3$** with $TaCl_2(CH_3)_3$, the corresponding complex **42** contained deuterium atoms in the central aryl ring of the pincer (Scheme 16). The H/D exchange in both cases is above 75% (**40-*d*$_1$** = 84% and **40-*d*$_2$** = 75%), suggesting the C-H$_{pincer}$ is almost completely exchanged with alcohol protons. To account for the nearly quantitative H/D exchange, Bercaw et al. propose the mechanism in Scheme 17. Activation of the pincer C-H bond occurs prior to the second alcoholysis step rather than complex **42** in Scheme 16. An analogous and isolable example of the proposed intermediate that contains a protonated pendant arm and an intact pincer C-M bond is the [2,6-$^i$PrNCN(H)]Cr(THF)$_2$ complex **23**, presented in Schemes **8**, **9**, and **10**.

**Scheme 17.** Deuterium atom exchange upon metalation of deuterated ligands **40-*d*$_2$** and **40-*d*$_3$** with $TaCl_2(CH_3)_3$ (top) and mechanism of H-atom exchange between phenol -O*H* and pincer C*H* protons during metalation (bottom).

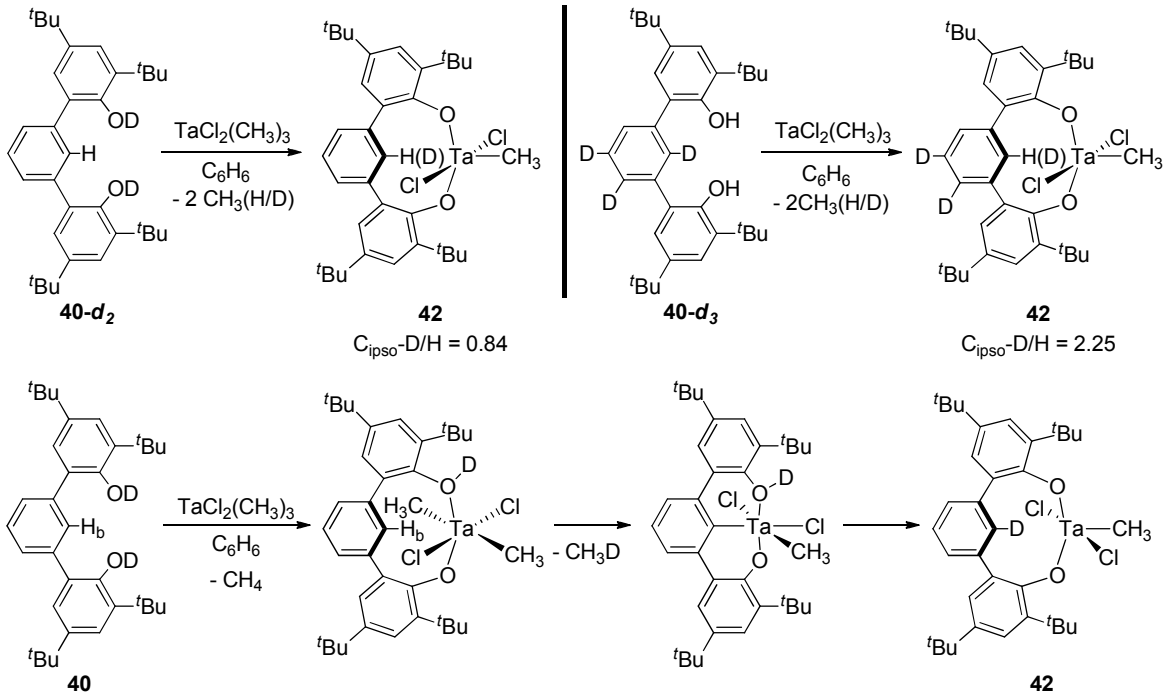


The reactivity of complex **41** was explored with unsaturated substrates that might undergo insertion into the Ta—$CH_3$ bond. Instead, benzophenone and benzonitrile insert into the pincer $C_{pincer}$-Ta bond of **41** to yield complexes **44** and **45**, respectively (Scheme 18). In contrast, the sterically bulky *tert*-butyl-isonitrile inserts into the Ta—$CH_3$ bond yielding complex **46**.[92] Similar insertion reactivity of the pincer metal-carbon bond is observed for an OCO molybdenum(IV) complex (see section 3.5) and OCO tungsten alkylidynes (see section 3.6).

**Scheme 18.** Insertion of $Ph_2CO$, PhCN, and $^t$BuNC into Ta-C bonds of **41** to yield **44**, **45**, and **46**.

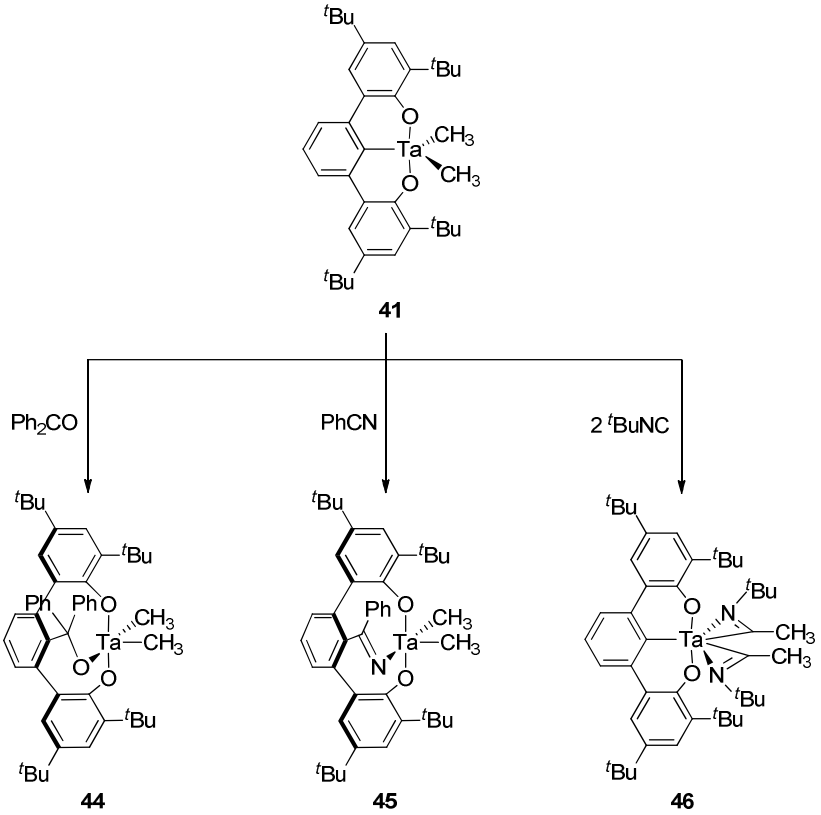


A particularly useful approach to metalating trianionic pincer ligands is to first attach the pendant arms followed by C-H activation of the central aryl ring of the pincer by σ-bond metathesis, as in the case of NCN and OCO versions. Kawaguchi et al. successfully extended this strategy to the benzylic C-H bonds of **47** in the synthesis of the $OCO^{3-}$ tantalum complex $[OCHO]Ta(CH_3)_2$ (**48**), Scheme 19.[45] The goal was to generate a bisphenoxide carbene pincer. Addition of $[Ph_3C][B(C_6F_5)_4]$ to **48** results in hydride abstraction to produce the cationic carbene complex $\{[OC:O]Ta(CH_3)_2\}\{B(C_6F_5)_4\}$ (**49**). Complex **49** is unreactive towards olefins and it treating with $PPh_3$ results in phosphine addition to the carbene atom. The authors note that structural data implicate the *o*-quinone methide resonance of **49** as an important contributor, akin to *N*-heterocyclic carbenes.

**Scheme 19.** Synthesis of the trianionic pincer tantalum complex **48** and its subsequent conversion to the bisphenoxide-carbene complex **49**.

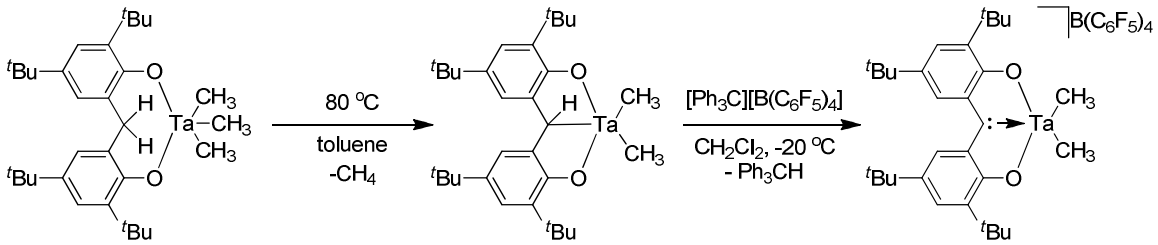


### *3.4. $OCO^{3-}$ chromium complexes*

Oxygenase catalysis,[93-95] a subset of oxidation catalysis that delivers and inserts oxygen-atoms into substrates, commonly features early first row transition metals with salen, porphyrin, and corrole based ligands. These tetradentate ligands serve as biomimetic models of cytochrome P450,[96-97] and in the case of manganese salen complexes, they are used extensively as catalysts for the epoxidation of olefins.[98-100] Continued research in oxygenase catalysis focuses predominantly on using milder and more environmentally benign oxidants such as $O_2$ and $H_2O_2$, but current systems suffer several drawbacks that lower the potential catalytic activity. One hindrance is the formation of inert $\mu$-oxo dimers that effectively lower the concentration of active catalytic species in solution (Scheme 20). The second problem is turnover suppression by coordination of the oxidized substrate (product inhibition) to the metal ion coordination sphere. Thus ligand designs that eliminate product inhibition as a deactivation pathway are highly desirable.

**Scheme 20.** General mechanism for substrate oxidation that includes reversible formation of a M-O-M intermediate and product inhibition.

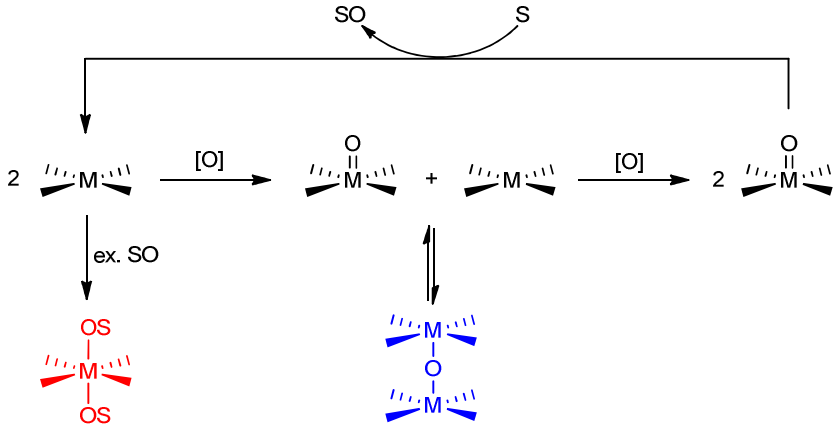

Changing from a fixed tetradentate ligand scaffold to trianionic pincer ligands provides an additional coordination site for substrates/reactants to access (Scheme 21). Additionally, the newly formed coordination site experiences a strong *trans* influence from the pincer metal-carbon bond, thereby weakening ligation.

**Scheme 21.** Creating an additional open coordination site by replacing tetradentate porphyrin, corrole, and salen based ligands with tridentate trianionic pincer ligands.

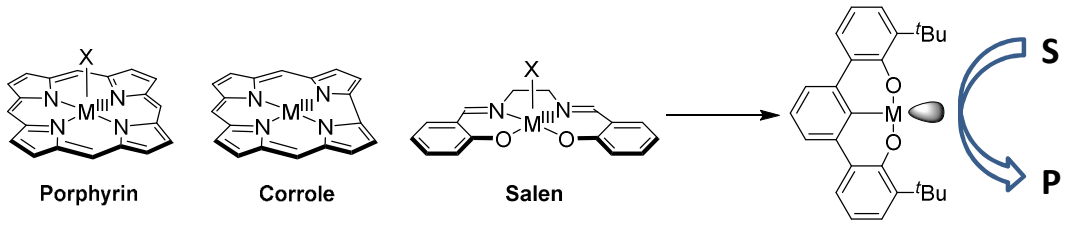


Treating the dipotassium salt of the OCO ligand, [$^t$BuOCHO]$K_2$•$(THF)_{1.5}$ (**50**) with $CrCl_2CH_3(THF)_3$[72] yields [$^t$BuOCO]$Cr^{III}(THF)_3$ (**51**) via double salt metathesis and methane elimination (Scheme 22).[58] The molecular structure of **51** contains an octahedral chromium metal center featuring a $C_2$-symmetric trianionic OCO pincer ligand and three coordinated THF molecules.

**Scheme 22.** Synthesis of [$^t$BuOCO]$Cr^{III}(THF)_3$ (**51**).

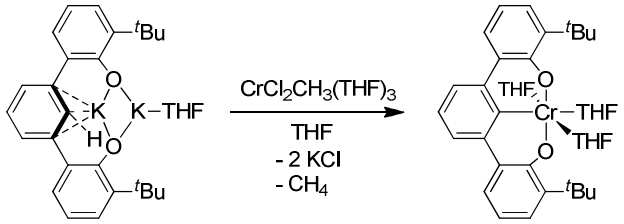


*3.4.1. Autocatalytic $O_2$ reduction*

Complex **51** readily reduces $O_2$ to yield the $d^1$ Cr(V) complex [$^t$BuOCO]$Cr^V$(≡O)(THF) (**52**). The mechanism of the $O_2$ reduction step by **51**, was investigated through a series of kinetic experiments. The data indicate the $O_2$ reduction is accelerated by the formation of product **52**, in an autocatalytic mechanism.[66] The identity of the autocatalytic intermediate was investigated by combining equimolar

solutions of **51** and **52** in toluene.[66] EPR analysis of the sample at 4.5 K concluded the formation of the S=2 $Cr^{IV}$-O-$Cr^{IV}$ dimer **53** (Scheme 23). In addition, a single crystal X-ray structural analysis confirmed the assignment.

Supporting the $\mu$-oxo dimer as the autocatalytic intermediate, complex **53** instantly reacts with $O_2$ in dichloromethane ($CH_2Cl_2$) to yield the $Cr^{V}O$ product **52**. Scheme 23 depicts the overall mechanism of $O_2$ activation by **51** including the formation of complex **53** via the autocatalytic Pathway B.

**Scheme 23.** Dioxygen activation by **51** including the product-catalyzed Pathway B.[66] Reprinted with permission from J. Am. Chem. Soc. **2011**, *133*, 13661-13673. Copyright (2011) American Chemical Society."

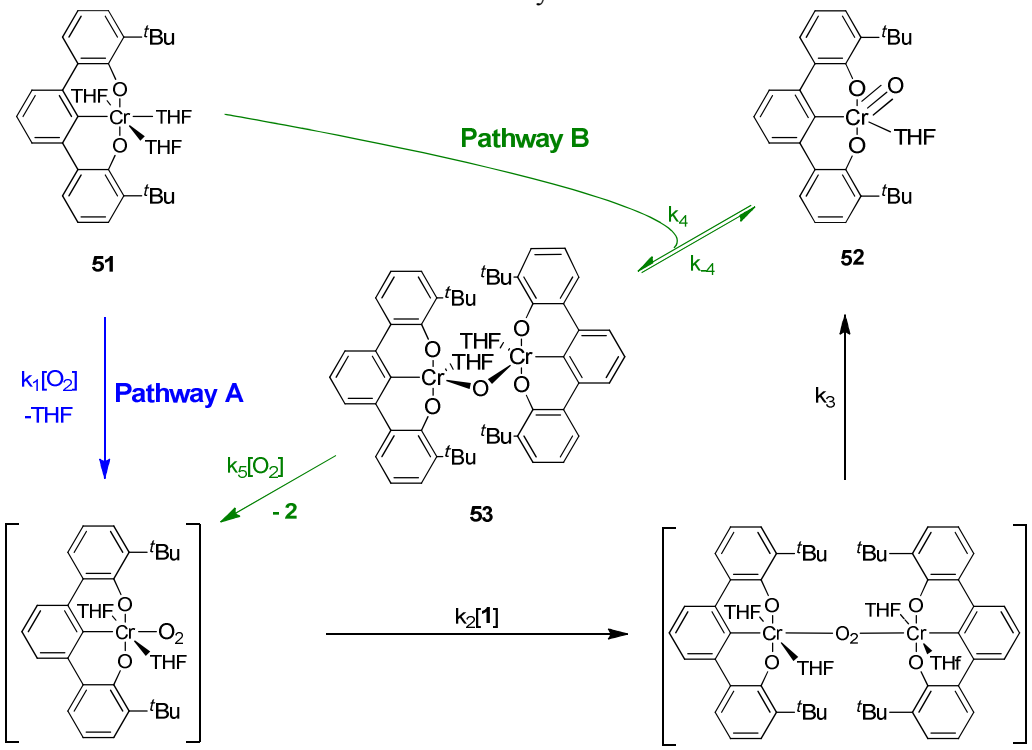


*3.4.2. Catalyzed aerobic oxidation*

Complex **51** also catalyzes the aerobic oxidation of $PPh_3$ at room temperature with a TON = 200. The advantage of the trianionic [$^t$BuOCO]$^{3-}$ pincer ligand during aerobic oxidation catalysis is clearly evident. In contrast to other aerobic oxidation catalysts, the rate of $O_2$ activation by **51** in THF *accelerates* at higher concentration of oxidized product $OPPh_3$. The reactive $Cr^{III}$ intermediate that forms in the

presence of excess $OPPh_3$ was isolated. Scheme 24 depicts the synthesis of the 5-coordinate Cr(III) complex **54** featuring the $[^tBuOCO]^{3-}$ ligand and *only* two $OPPh_3$.[58] The Cr(III) ion adopts a square pyramidal geometry leaving the coordination site *trans* to the Cr-$C_{pincer}$ bond vacant. The open coordination site of **54** provides dioxygen unhindered access to the metal center, which is in stark contrast to similar chromium catalysts employing tetradentate ligands. Open access leads to increased reactivity towards $O_2$, thus increasing the initial concentration of $OPPh_3$ in the system accelerates the $O_2$ activation.

**Scheme 24.** Synthesis of complex **54**. Reprinted with permission from J. Am. Chem. Soc. **2011**, *133*, 13661-13673. Copyright (2011) American Chemical Society."

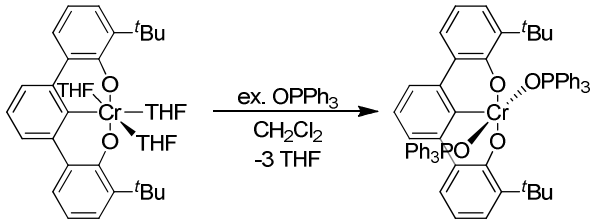


**51** **54**

An intriguing result is the OAT rate is not affected by the choice of solvent (THF, $CH_2Cl_2$ with 50 μL THF, and $CH_3CN$) or the presence of additional $OPPh_3$. These results contrast the well-documented OAT rate enhancement by donor ligands.[72, 98, 101-102] Adding the strong two electron donor $H_2C{=}PPh_3$ to **52** in toluene replaces the THF ligand to form the phosphorane adduct **55** (Scheme 25). However, complex **55** does not transfer its oxo ligand to $PPh_3$. The strongly donating ylide ligand stabilizes the Cr(V) over the Cr(III) oxidation state.

**Scheme 25.** Synthesis of **55**.

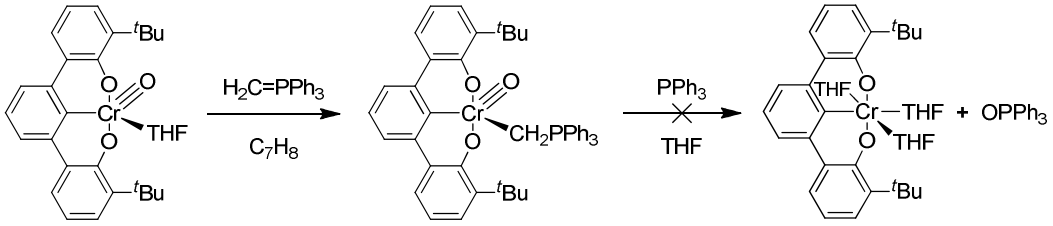


**52** **55** **51**

Donor ligands do serve a purpose during OAT as evidenced by a second study investigating direct OAT from the $Cr^{IV}_2(\mu\text{-O})$ dimer **53**. Complex **53** forms from the comproportionation of **51** and **52** in the absence of a coordinating solvent during OAT in $CH_2Cl_2$, but itself is not a competent OAT reagent and the reaction requires over 20,000 s to complete. In contrast, in THF complex **52** requires only ~100 s. Hence, the role of the donor ligand (i.e. THF) is to prevent $\mu$-O dimer formation. The reaction exhibits no rate dependence on the concentration of $PPh_3$, indicating that OAT occurs after the rate limiting dissociation of the dimer **53** (Scheme 26).[64] This confirms that oxidation rate suppression in many systems is likely due to either irreversible, or a significant equilibrium toward $\mu$-oxo dimer formation. Access to complex **53** provided the first opportunity to directly examine this potential pathway.

**Scheme 26.** Mechanism of OAT from **53** to $PPh_3$ to yield **56**.

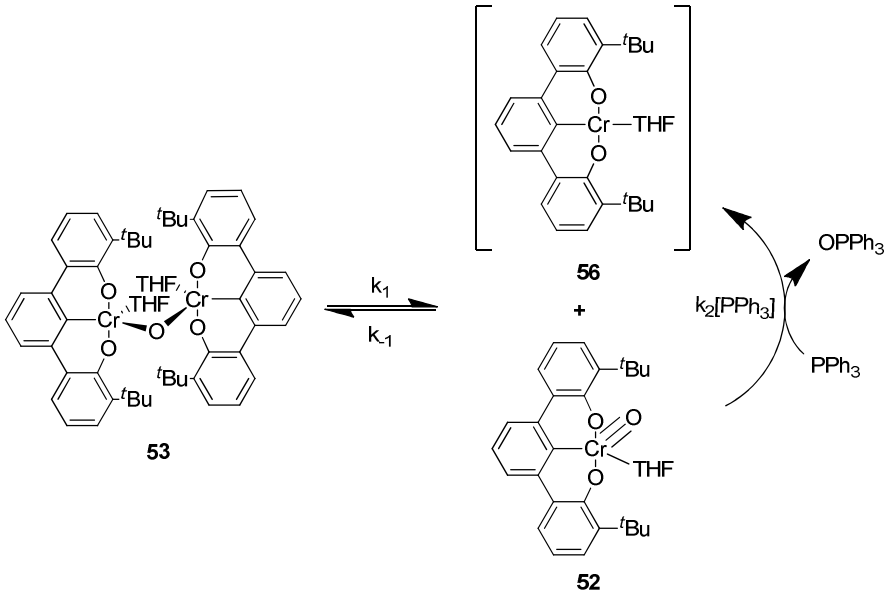


*3.5. $OCO^{3-}$ molybdenum complexes*

Treating [$^t$BuOCO]$H_3$ (**31**) with $Mo(N(CH_3)_2)_4$ readily activates both the O-H and the pincer C-H bonds at -35 °C to yield [$^t$BuOCO]$Mo(N(CH_3)_2)(NH(CH_3)_2)_2$ (**57**). Subsequent treatment of **57** with $NaN_3$ in dimethylformamide (DMF) produces the anionic molybdenum(VI) nitride dimer **58** (Scheme 27).[65] The anionic $Mo^{VI}\equiv N$ reacts with mild electrophiles ($(CH_3)_3SiCl$ and $CH_3I$) yielding neutral imido complexes [$^t$BuOCO]$Mo{=}NR(N(CH_3)_2)$ (**59-R**, R = $-Si(CH_3)_3$, $-CH_3$) (Scheme 28).[65]

**Scheme 27.** Synthesis of [$^t$BuOCO]Mo(N(CH$_3$)$_2$)(NH(CH$_3$)$_2$)$_2$ (**57**) and {Na(DMF)}$_2$ {[$^t$BuOCO]Mo≡N(N(CH$_3$)$_2$)}$_2$ (**58**).

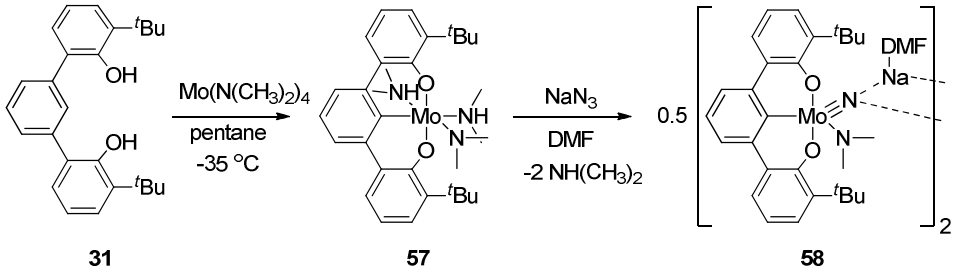


**Scheme 28.** Nitrido alkylation with mild electrophiles ($CH_3I$, $(CH_3)_3SiCl$) to yield **59-R** and N-atom transfer to acid chlorides to produce nitriles.

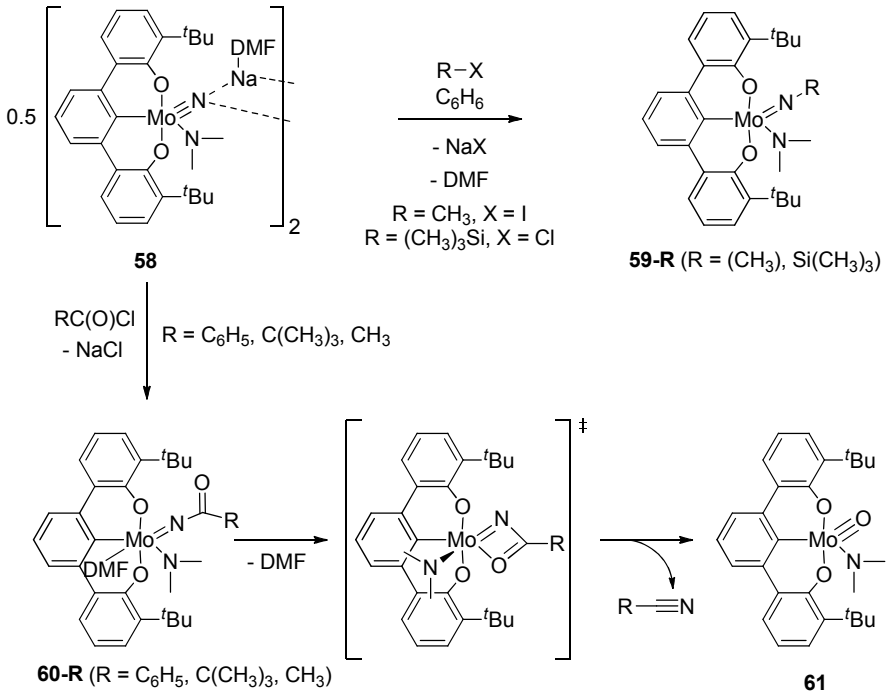


An application of **58** is the complete N-atom transfer to acid chlorides to produce nitriles. Complex **58** reacts with acid chlorides to form the acyl-imido species Mo(NC(O)R) (**60-R**; R = $C_6H_5$, $C(CH_3)_3$, and $CH_3$). Subsequent heating at 60 °C completes the N-atom transfer to form free nitrile and the molybdenum(VI)-oxo complex **61**. The mechanism of nitrogen atom transfer was investigated through a series of kinetic experiments. Adding free DMF to the reaction solution of **60-C(CH$_3$)$_3$** suppresses the rate of N-atom transfer, indicating a reversible loss of DMF upon formation of an

azametallacyclobutene intermediate (Scheme 28). Consistent with the formation of an azametallacyclobutene intermediate, the larger acyl group substituents within **60-R** impede the cyclization, leading to increased reaction times (R = $CH_3$ (1.5 h); $C_6H_5$ (3 h); $C(CH_3)_3$ (7 h)).[65]

**Scheme 29.** Synthesis of the diphenolate molybdenum alkylidene complex [$^t$BuOCHO]Mo(=NAr)(=CHC$(CH_3)_2$Ph) (**63**) and conversion to the trianionic pincer alkylidene {[$^t$BuOCO]Mo(=NAr)(=CHC$(CH_3)_2$Ph)}{$CH_3PPh_3$} (**64**) (Ar = 2,6-($^i$Pr)$_2C_6H_3$).

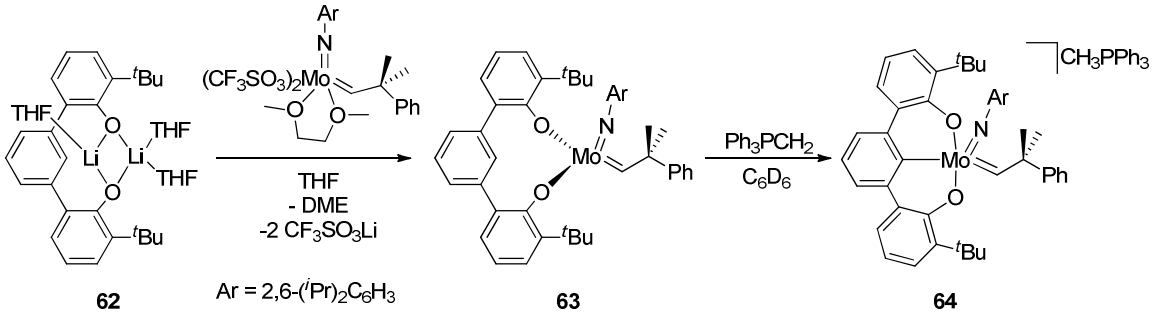


An area of active research is the preparation of group 6 alkylidynes supported by trianionic pincer ligands. The constrained meridional coordination of a trianionic pincer ligand provides an opportunity to maximize the cycloaddition rate of alkynes to metal-alkylidynes.[103] The synthetic challenge to building an alkylidyne complex lies in attaching the trianionic pincer ligand while keeping the M≡C functionality intact. Treating Schrock's alkylidene complex $(CF_3SO_3)_2$Mo(=NAr)(=CHC$(CH_3)_2$PH)[104] with the dilithio salt [$^t$BuOCHO]$Li_2$ (**62**) provides the diphenolate complex **63** (Scheme 29).[105] Adding the ylide base $H_2C$=$PPh_3$[106] deprotonates the pincer C-H proton to yield the anionic molybdenum alkylidene {[$^t$BuOCO]Mo(=NAr)(=CHC$(CH_3)_2$Ph)}{$CH_3PPh_3$} (**64**).

**Scheme 30.** Insertion of terminal alkynes into the Mo-$C_{pincer}$ bond.

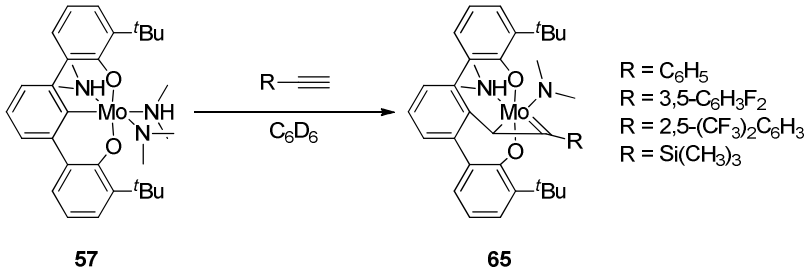


**57** **65**

Another approach to obtain a molybdenum alkylidyne complex is to employ Cummins' low oxidation state route by reacting Mo(IV) complexes with terminal alkynes.[107-108] Treating complex **57** with PhC≡CH results in a completely different outcome; as intended, the molybdenum ion undergoes two-electron oxidation but the alkyne inserts into the Mo-$C_{pincer}$ bond to yield the molybdenacyclopropylidene complex **65** (Scheme 30).[105] Changing the electronic or steric properties of the terminal alkyne did not alter the outcome of the reaction in the cases of {3,5-($C_6H_2F_2$)}-C≡CH, {3,5-($CF_3$)$_2$$C_6H_2$}C≡CH, or ($CH_3$)$_3$SiC≡CH.

### *3.6. $OCO^{3-}$ tungsten complexes*

Other approaches to yield a group 6 trianionic pincer alkylidyne were met with complications. Treating [$^t$BuOCHO]$K_2$ (**50**) with W(≡C$^t$Bu)$Cl_3$(DME)[109] yields the diphenolate tungsten alkylidyne [$^t$BuOC*H*O]W(≡C$^t$Bu)Cl (**66**), which was characterized by NMR spectroscopy (Scheme 31).[103] However, [$^t$BuOC*H*O]W(≡C$^t$Bu)Cl could not be separated from impurities that form during the salt metathesis.

**Scheme 31.** Synthesis of the diphenolate alkylidyne complex [$^t$BuOC*H*O]W(≡C$^t$Bu)Cl (**66**).

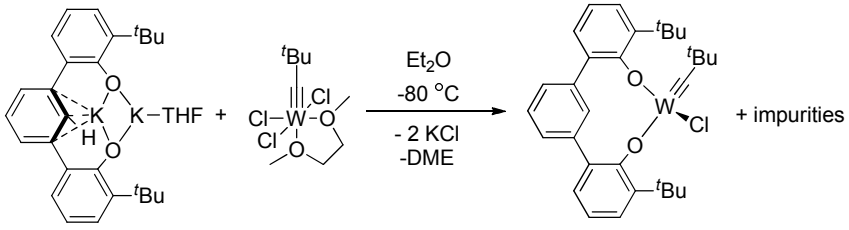


**50** **66**

Metalation of [$^t$BuOCO]H$_3$ (**31**) with a tungsten alkylidyne via alkane elimination requires extensive heating. Heating a sealed tube of **31** and W(≡C$^t$Bu)(CH$_2$$^t$Bu)$_3$[109-110] in benzene at 110 °C takes 5 days to produce the dinuclear complex **67** (Scheme 32).[103] The bridging $^t$BuOCHO ligand adopts two conformations that are separable via fractionally crystallization and characterized by single crystal X-ray crystallography.

**Scheme 32.** Synthesis of the dinuclear complex **67** via alkane elimination from reaction of [$^t$BuOCO]H$_3$ (**31**) with W(≡C$^t$Bu)(CH$_2$$^t$Bu)$_3$.

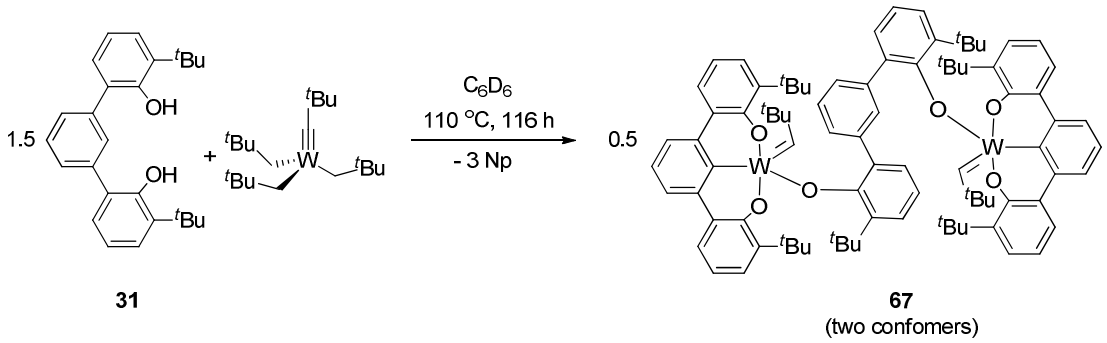


**31** **67** (two confomers)

Another approach to the synthesis of a trianionic pincer supported tungsten alkylidyne involves treating [$^t$BuOCO]H$_3$ (**31**) with W(≡C$^t$Bu)(OAr)$_2$(CH$_2$$^t$Bu) {where Ar = 2,6-($^i$Pr)$_2$C$_6$H$_3$}.[111] The reaction, in comparison to W(≡C$^t$Bu)(CH$_2$$^t$Bu)$_3$, proceeds rapidly and is complete within 2 h at 80 °C to yield the tungsten alkylidene [$^t$BuOCO]W(=CH$^t$Bu)(OAr) **68** (Scheme 33). A more facile route to **68** involves treating **31** with W(≡C$^t$Bu)(O$^t$Bu)$_3$ followed by addition of HOAr. The reaction between **31** and W(≡C$^t$Bu)(O$^t$Bu)$_3$ occurs immediately at ambient temperature to liberate free *tert*-butanol.[103]

**Scheme 33.** Synthesis of the trianionic pincer alkylidene complex [$^t$BuOCO]W(=CH$^t$Bu)(OAr) **68** by treating [$^t$BuOCO]H$_3$ (**31**) with W(≡C$^t$Bu)(CH$_2$$^t$Bu)(OAr)$_2$ or W(≡C$^t$Bu)(O$^t$Bu)$_3$/ArOH (Ar = 2,6-($^i$Pr)$_2$C$_6$H$_3$).

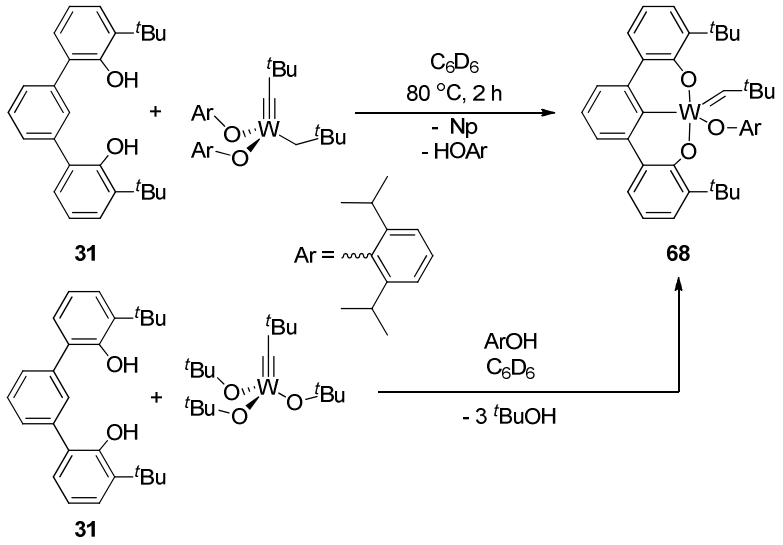


The synthesis of the alkylidene complexes **63**, **64**, and **68** provided a roadmap to the preparation of a trianionic pincer alkylidyne. Treating **31** with W(≡C$^t$Bu)(O$^t$Bu)$_3$[112] attaches the phenoxide donors of the OCO pincer ligand by removing two equivalents of *tert*-butanol to form the diphenolate complex [$^t$BuOCHO]W(≡C$^t$Bu)(THF) **69.** Again, adding the ylide base $CH_2$=$PPh_3$ to **69** deprotonates the pincer C-H proton to yield the anionic tungsten alkylidyne pincer complex {[$^t$BuOCO]W(≡C$^t$Bu)(O$^t$Bu)}{$CH_3PPh_3$} **70**. The remaining *tert*-butoxide on **70** is removed by addition of methyl triflate and replaced with $Et_2O$ to yield the neutral tungsten alkylidyne complex [$^t$BuOCO]W(≡C$^t$Bu)($Et_2O$) (**71**) (Scheme 34).[62] Despite isolating crystals of **71**, residual [$CH_3PPh_3$][OTf] persists as a impurity in the sample. To remove the impurity, adding several drops of THF to an $Et_2O$ solution of complex **71** precipitates the remaining [$CH_3PPh_3$][OTf] yielding the tungsten alkylidyne complex [$^t$BuOCO]W(≡C$^t$Bu)(THF)$_2$ (**72**).

**Scheme 34.** Synthesis of [$^t$BuOCO]W(≡C$^t$Bu)(THF)$_2$ (**72**).

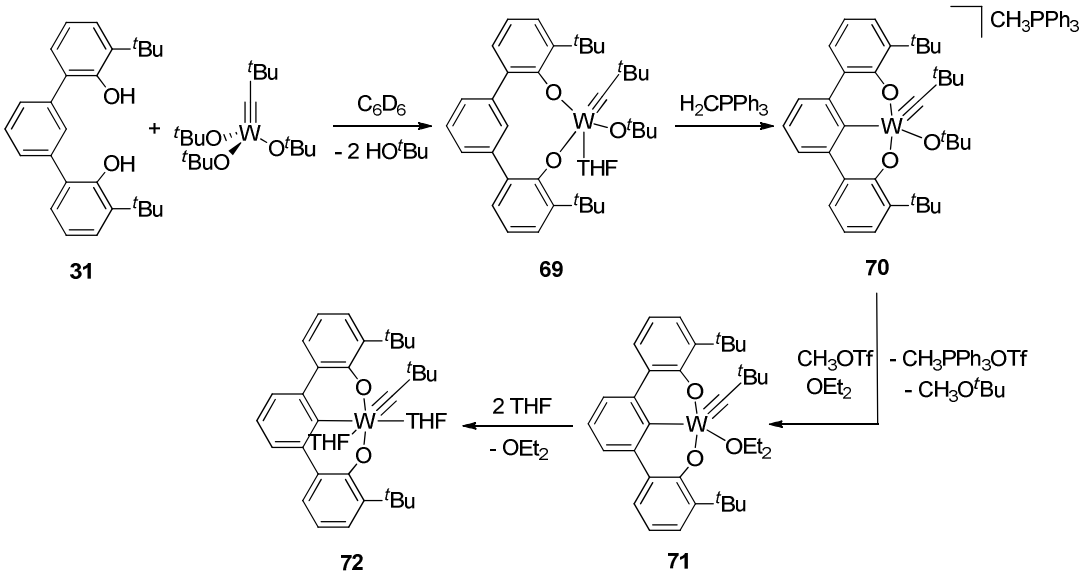


*3.6.1. Catalytic alkyne polymerization*

Foreshadowed by the insertion of alkynes into the M-$C_{pincer}$ bond of **57**, complex **72** does not react with internal alkynes (3-hexyne and 1-phenylpropyne) to yield alkyne metathesis products. However, complex **72** readily reacts with terminal alkynes to yield poly(alkynes) (Scheme 35). The resulting polymers have impressively high molecular weight (relative to polystyrene standard) and contain a ~96% head-to-tail structure.[62]

**Scheme 35.** Alkyne polymerization by **72**.

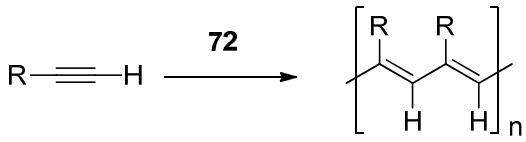


Initially, the proposed mechanism of polymerization involved alkyne insertion into a metallacyclobutadiene and chain growth via subsequent alkyne insertions to expand the ring. This ring expansion mechanism is widely regarded as the operating polymerization of 2-butyne by several alkylidyne metathesis catalysts.[113-115] To investigate the possible role of metallacycle intermediates, treating complex **72** with only two equivalents of phenylacetylene at -35 °C forms two new tungsten

containing products in a 2:1 ratio and was clear indication that an alternative mechanism was operating. The two complexes comprise isomers featuring a new *tetraanionic* pincer ligand (Scheme 36).[61] The major products **73** and **74** are the result of a formal insertion of the W≡CR bond into the pincer W-$C_{pincer}$ aryl bond. The formation of **74** indicates that a tungstenacyclobutadiene is a likely intermediate in this transformation. The mechanism of this transformation is the subject of an ongoing study.

**Scheme 36.** Alkylidyne α-carbon insertion into the pincer W-C bond.

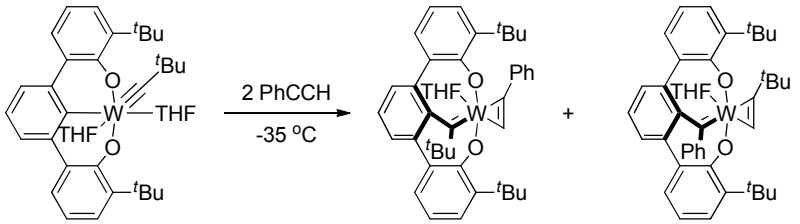


**72** **73** **74**

Though complexes **73** and **74** initially form in a 2:1 ratio, the tetraanionic ligands are not locked in their conformation. Upon prolonged heating at 85 °C in benzene, both complexes **73** and **74** gradually convert to an equilibrated mixture of **73** and **74** in a 1:5 ratio, respectively. Kinetic studies reveal that **73** is a significantly more active catalyst than **74**. Using this information, the catalytic polymerization of phenylacetylene and 1-decyne by **73** were optimized and yielded impressively high TONs of 17,233 (phenylacetylene) and 9620 (1-decyne), and activities of 5.64 x$10^6$ $g_{pol}$/mol/h (phenylacetylene) and 7.98 x$10^6$ $g_{pol}$/mol/h (1-decyne). The exceptionally high activity of catalyst **73** for alkyne polymerization is understood given the mechanism of polymerization. The proposed mechanism involves sequential insertion of alkyne monomer into a growing metallacycle. Evidence for this proposal comes in the form of a trapping experiment of the first insertion product. Treating complex **73** with the internal alkyne, 1-phenylpropyne, results in a single insertion into the tungstenacyclopropene ring to yield isomers **75** and **76** (Scheme 37).[61] This mechanism is well-known for cyclotrimerization of alkynes,[116-120] where after a third alkyne insertion, reductive elimination occurs to release benzenes. In complex **73**, the rate of insertion is much greater than the rate of reductive elimination, thus leading to polymerization. The high

rate of insertion is a consequence of constraining four anionic donor ligands to the meridional plane. This constraint provides a very open metal coordination sphere, thus favoring insertion over reductive elimination. See Scheme 37 for a truncated structure of **75** in which the metallacyclopentadiene unit is removed.

**Scheme 37.** Insight in the mechanism of alkyne polymerization: synthesis of metallacyclopentadienes **75** and **76** (top); and truncated structure of **75** (bottom).[61]

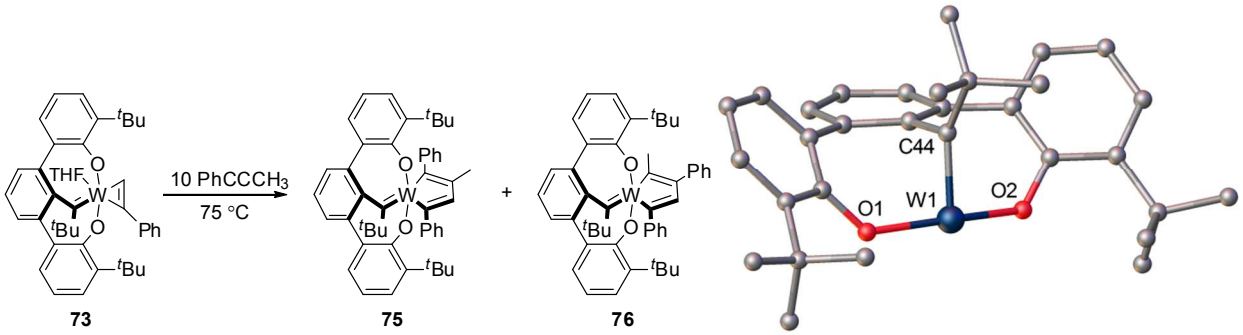


**73** **75** **76**

The most diverse and unique trianionic pincer ligand chemistry occurs with the use of $OCO^{3-}$ ligands. The added dimension of reactivity at the M-$C_{pincer}$ bond provides new avenues of research; access to the tetraanionic pincer ligand is a good example. Prior to employing an $OCO^{3-}$ trianionic pincer ligand though, it is important to consider that unsaturated substrates will likely react with the M-$C_{pincer}$ bond, and therefore an $OXO^{3-}$ pincer-type ligand would be the better choice if that is an undesirable outcome.

## 4. $CCC^{3-}$ trianionic pincer ligands

### *4.1. $CCC^{3-}$ tantalum complexes*

A new interesting class of trianionic pincer ligands developed by Parkin et al. is the $CCC^{3-}$ donor motif using 2,6-*p*-tolylphenyl as the ligand platform and starts with the relatively easy to access iodo derivative **77**.[121] Treating the lithium derivative **78** with $TaCl_2(CH_3)_3$[89-91] yields complex **79** with the ligand in the monoanionic form. Subsequent addition of two equivalents of $PMe_3$ to complex **79** yields the $[CCC]^{3-}$ trianionic pincer tantalum complex $[CCC]TaCl(CH_3)(P(CH_3)_3)_2$ (**80**), via two methane eliminations (Scheme 38). Alternatively, using $Ta(P(CH_3)_3)_2Cl_2(CH_3)_3$[122] as the metal precursor provides

access to complex **76** directly. The geometry of the 7-coordinate tantalum ion is a distorted pentagonal bipyramid with the two pendant pincer arms occupying bent axial positions.

**Scheme 38.** Synthesis of [CCC]TaCl($CH_3$)($P(CH_3)_3$)$_2$ (**80**).

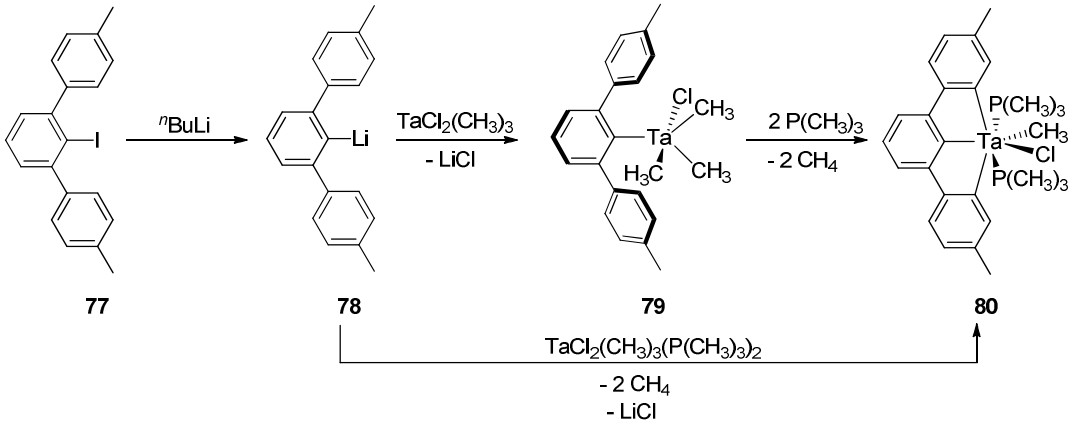


Over time, complex **80** converts into an equilibrated mixture of halide-methide exchanged products, [CCC]Ta($P(CH_3)_3$)$_2$($CH_3$)$_2$ (**81**) and [CCC]Ta($P(CH_3)_3$)$_2$$Cl_2$ (**82**) (Scheme 39). Complexes **81** and **82** are independently prepared by treating **80** with either $CH_3MgBr$ or $ZnCl_2$, respectively.

**Scheme 39.** Equilibrium mixture of **80** with **81** and **82**; and the direct synthesis of **81** and **82** upon addition of $CH_3MgBr$ or $ZnCl_2$, respectively.

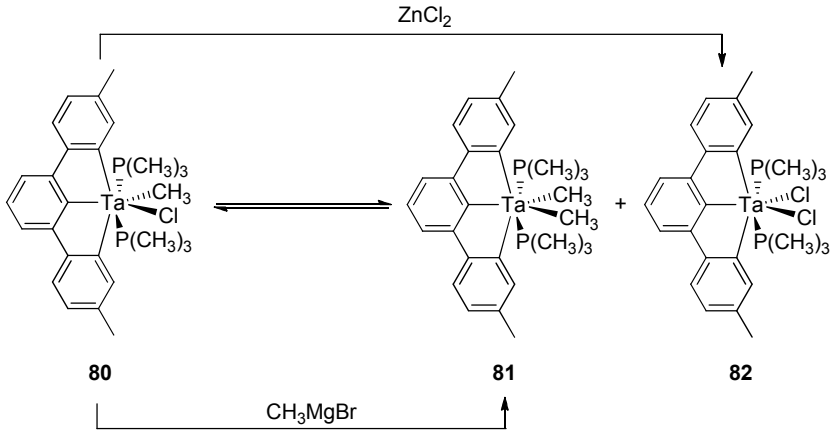


**Scheme 40.** Reduction of **82** with $KC_8$ to yield **83**.

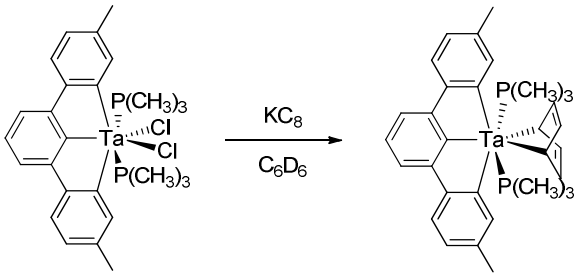


**82** **83**

Combining complex **82** with excess $KC_8$ reduces the tantalum(V) metal center by two electrons and eliminates two equivalents of KCl (Scheme 40). The reduced tantalum(III) species readily binds benzene to form complex **83**. According to a solid state structure of **83**, the coordinated benzene is reduced, and is better described as a dianionic 1,4-cyclohexadienediyl ligand ($C_6H_6^{2-}$) coordinated to a Ta(V) ion. The $C_6H_6^{2-}$ ring is puckered (fold angle = 17.1°) and the π-bonding is localized with alternating single and double bonds. The $CCC^{3-}$ ligand is an interesting contribution to the area of trianionic pincer ligands, and one clear advantage is the relatively easy access to proligand **77**, and by extension numerous other possible derivatives. One disadvantage though is that metalation to achieve a trianionic pincer requires activation of three aryl C-H bonds, which may be problematic in future metalation strategies. In $OCO^{3-}$ and $ONO^{3-}$ derivatives, the convenience of alcoholysis inherently provides multiple routes to metalation.

## 5. $NNN^{3-}$ trianionic pincer-type ligands

### *5.1. $NNN^{3-}$ tantalum complexes*

Schrock and coworkers were early pioneers in $NNN^{3-}$ trianionic pincer-type ligands, though their entry into a trianionic pincer-type ligand was somewhat unexpected. The first reported trianionic $NNN^{3-}$ pincer-type complex resulted from ligand degradation of the *tris*-amido-tripodal $[N_3N]^{3-}$ ligated tantalum complex **84** in the presence of a Grignard reagent (Scheme 41) to yield the trianionic $NNN^{3-}$ pincer-type complex **85**.[43-44]

**Scheme 41.** Degradation of a tripodal ligand to form the trianionic $NNN^{3-}$ pincer-type complex **85**.[43-44]

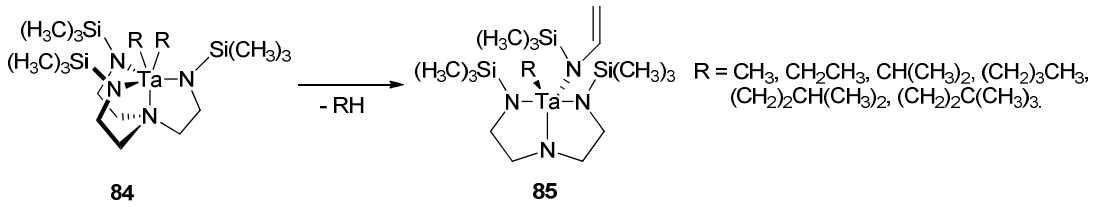


**84** **85**

Several $NNN^{3-}$ trianionic pincer-type ligands **86**, **87**, and **88** are easily synthesized directly, and metalated using $Ta(CH_3)_5$[123] to yield the respective complexes **89**, **90**, and **91** (Scheme 42).[124] Proligand **87** or **88** react swiftly with $Ta(CH_3)_5$ in $Et_2O$ at -35 °C to yield complexes **89** and **90**, respectively. Under similar conditions, treating proligand **88** with $Ta(CH_3)_5$ in $Et_2O$ at -35 °C initially eliminates two equivalents of methane to yield the isolable intermediate **91**. The NH proton on **91** appears as a broad singlet at 2.43 ppm in the $^1H$ NMR spectrum. Over time, complex **91** loses an additional equivalent of $CH_4$ to form complex **92**, which can be hastened by heating at 65 °C for 9 h.

**Scheme 42.** Synthesis of trianionic NNN pincer-type tantalum complexes **89**, **90**, and **92** from proligands **86**, **87**, and **88**, respectively.

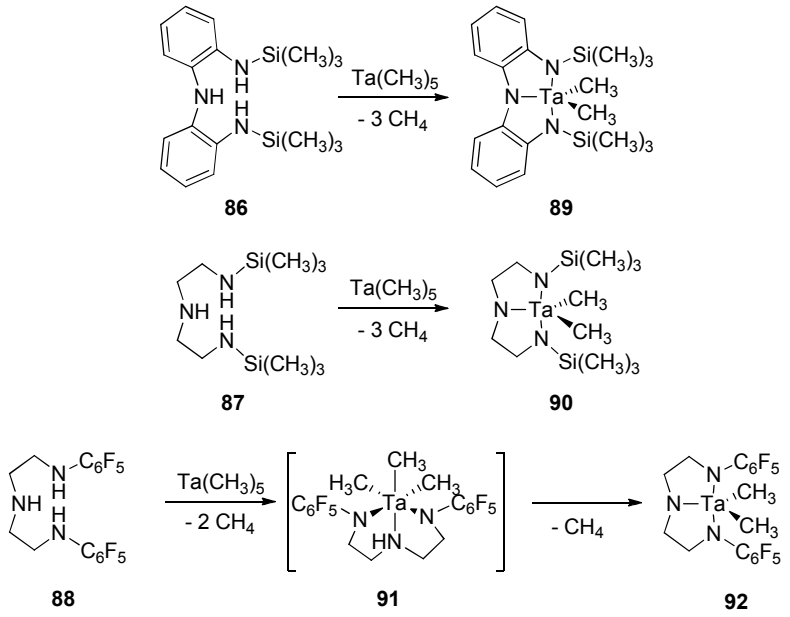


Treating complex **90** with the Lewis acid, $Al(CH_3)_3$, yields complex **93** (Scheme 43). In solution, complex **93** is $C_s$-symmetric yielding two different Ta-C*H*$_3$ resonances at 0.85 and 0.55 ppm in the $^1$H NMR spectrum. $B(C_6F_5)_3$ abstracts methide from **91** in toluene at -35 °C to form $CH_3B(C_6F_5)_3$ and leaves the central NH bond intact to give **94** (Scheme 44). Another route to complex **94** involves treating complex **92** with $\{Ph(CH_3)_2NH\}\{CH_3B(C_6F_5)_3\}$.[124]

**Scheme 43.** Reaction of $Al(CH_3)_3$ to **90** to form **93**.

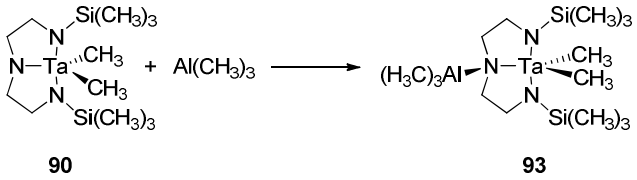


**Scheme 44.** Methide abstraction from **91** by $B(C_6F_5)_3$ to form **94**, and an alternative synthesis by protonation of **92**.

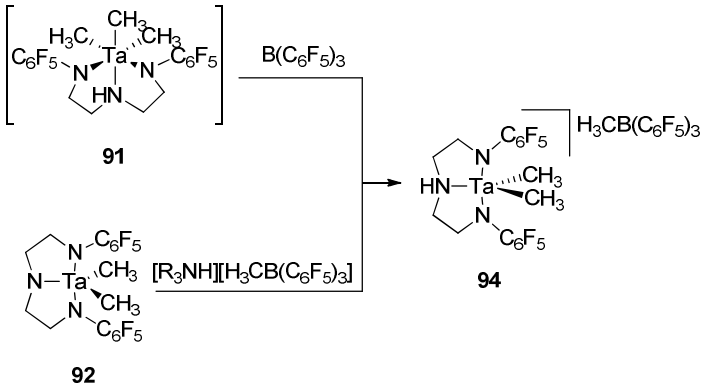


**Redox-active NNN$^{3-}$ ligands**

*5.2. NNN$^{3-}$ zirconium complexes*

Heyduk et al. employ trianionic pincer-type ligands that are redox-active. Presented in Scheme 45 is the NNN$^{3-}$ trianionic pincer-type ligand **A** and its one-electron oxidized dianionic radical form, **B** (semiquinone), and two-electron oxidized monoanionic form **C** (quinone).[125]

**Scheme 45.** Trianionic (**A**), dianionic/semiquinone (**B**), and monoanionic/quinone (**C**) of a redox active NNN pincer-type ligand.

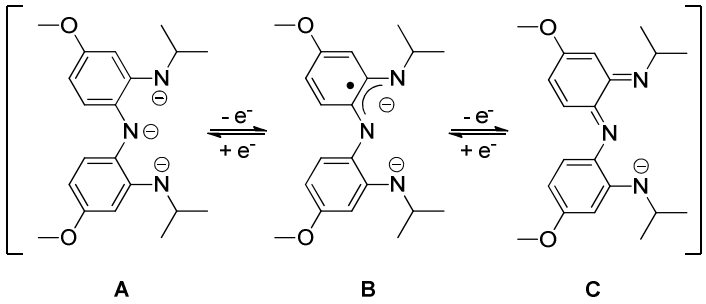


The trianionic pincer-type zirconium complex **96** was synthesized via triple salt metathesis with in situ generated [NNN]$Li_3$ (Scheme 46).[63] The resulting complex is $C_{2v}$-symmetric with two coordinated THF ligands that are easily replaced with pyridine or C≡N$^t$Bu. Complex **96** readily reacts with 0.5 equivalents of $PhICl_2$ yielding the semiquinonate containing oxidized complex **97** (Scheme 46). Complex **96** is paramagnetic with a ligand-based radical, giving rise to a singlet resonance at g =1.999 in the X-band EPR spectrum. In contrast to the previously discussed [NNN]$TaCl_2$ complex (see section 5.3),

adding a full equivalent of $PhICl_2$ to **96** oxidizes the pincer-type ligand to its quinonate form in **98** (Scheme 46). A possible explanation for the observed second oxidation is that **96** has an additional coordination site to mediate the electron transfer, whereas $[NNN]TaCl_2$ does not. Complex **96** reacts with organic azides to yield the bridging bisimido dimer complex **99**.[63] The dimer **99** is overall $C_{2v}$-symmetric, but the imido ligands are not equivalent. The pincer-type ligand is in the quinonate form as evidenced by the solid state structure. In solution, dimer **99** is quite stable and does not dissociate under thermal conditions. Moreover, complex **99** proved unreactive with olefins, alkynes, phosphines, sulfides, and isocyanides, even at elevated temperatures. Whereas formation of the coordinately saturated $[NNN]Ta(=NR)Cl_2$ (see section 5.3) prevents nitrene transfer to substrate, the analogous low coordinate [NNN]Zr(=NR)Cl is unreactive due to formation of the $\mu$-imido dimer.

**Scheme 46.** Synthesis of the NNN trianionic pincer-type zirconium complex **96** and reaction with $PhICl_2$ and $RN_3$.

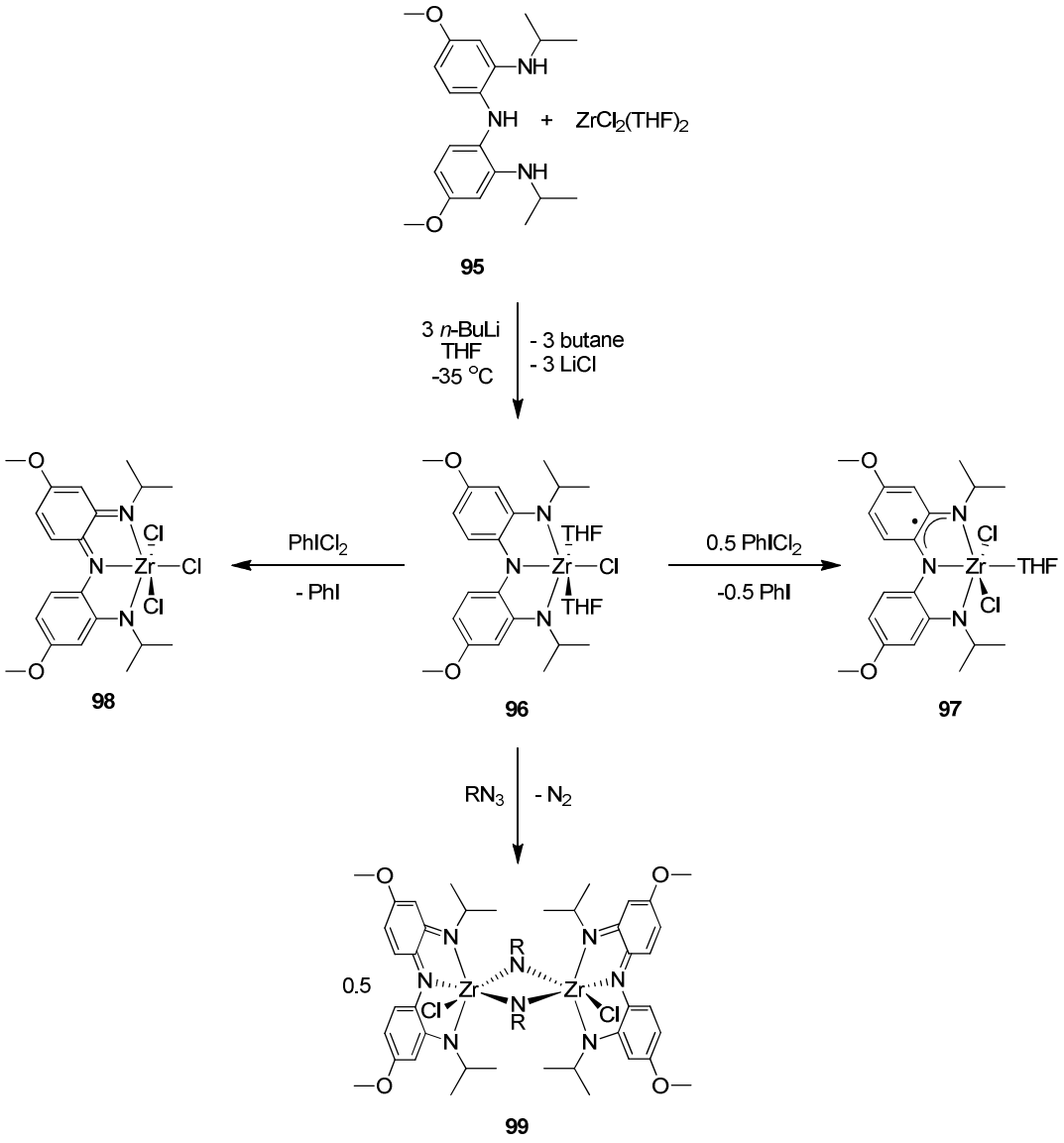


*5.2.1. Catalytic nitrene transfer*

Replacing the coordinated THF ligands of **96-THF** with C≡N$^t$Bu yields the *bis*-isonitrile complex **96-CN$^t$Bu**. Treating **96-CN$^t$Bu** with $RN_3$ does not yield dimer **99**, but rather forms the carbodiimide product, RN=C=N$^t$Bu (Scheme 47).[63] Complex **96-THF** catalyzes the complete conversion of 10 equivalents of both organic azide and isonitrile into carbodiimide, RN=C=N$^t$Bu. The catalyzed reaction proceeds at 55 °C via the proposed mechanism depicted in Scheme 47. The observed rate decreases with increasing concentration of C≡N$^t$Bu, supporting the reversible dissociation of one equivalent of C≡N$^t$Bu

prior to azide addition (intermediate **I**). Expulsion of $N_2$ from the coordinated azide in the rate-determining step yields the zirconium imido species **II**. The coordinated C≡N$^t$Bu allows migratory insertion to proceed instead of dimerization yielding **III** and **IV**.

**Scheme 47.** Mechanism for the catalytic nitrene transfer to CN$^t$Bu by **96-CN$^t$Bu**.

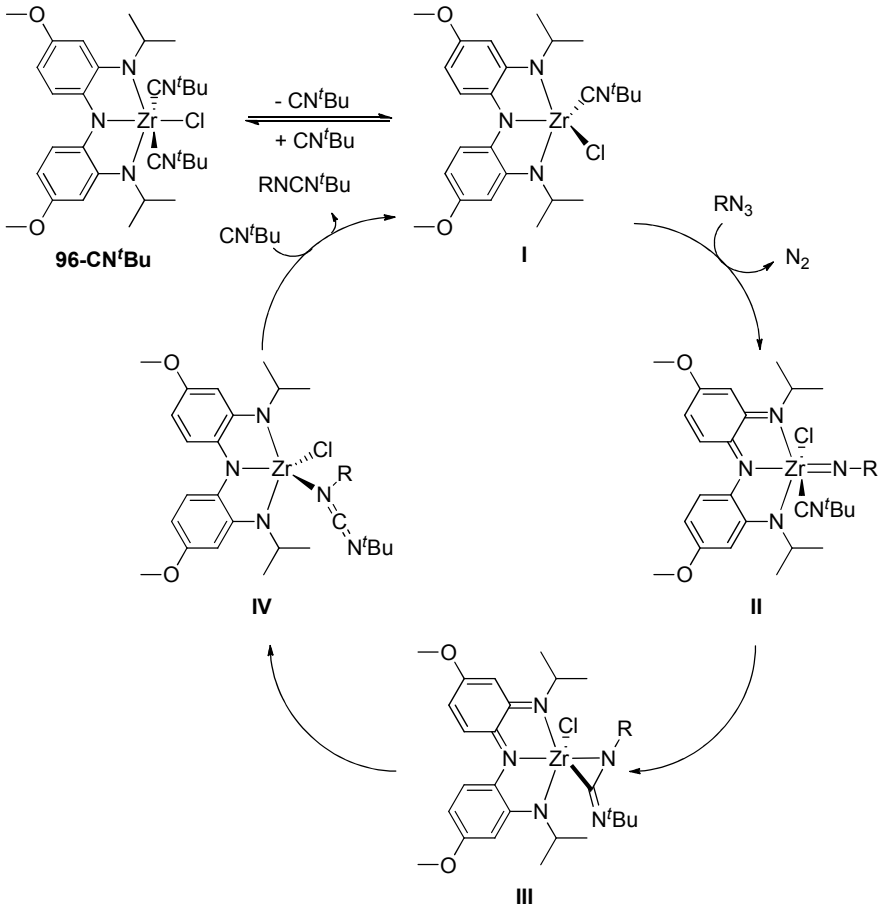

### *5.3. $NNN^{3-}$ tantalum complexes*

Treating proligand **95** with $TaCl_2(CH_3)_3$[89-91] at -35 °C results in three methane eliminations to yield the $NNN^{3-}$ trianionic pincer tantalum complex **100** (Scheme 48).[125] Complex **100** is $C_2$-symmetric in the solid state, with the central and pendant N-atoms residing 2.082(3) and 1.963(2) Å from the Ta metal center, respectively. Within the solid state structure of **100**, the Ta-N, C-C, and C-N bond lengths are consistent with Ta(V) and the ligand in the trianionic pincer-type form **A**.

**Scheme 48.** Metalation of protio-ligand **95** with $TaCl_2(CH_3)_3$ to yield **100**.

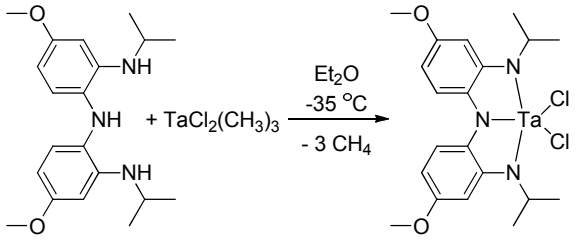


Treating complex **95** with C≡N$^t$Bu yields complex **100-CN$^t$Bu** (Scheme 49). Upon coordination of C≡N$^t$Bu, the C≡N stretch in the IR spectrum shifts to a higher frequency of 2203 $cm^{-1}$ than that of free CN$^t$Bu (2125 $cm^{-1}$). The shift to higher frequency supports assignment of a Ta(V) oxidation state, as opposed to a formally reduced Ta(III) species. Though Ta(V) is $d^0$, complex **100** is readily oxidized with 0.5 equivalents of $PhICl_2$ by removing an electron from the pincer ligand yielding the semiquinone dianionic ligand form, **B** (Scheme 49).[125] The resulting complex **101** is paramagnetic containing a single unpaired electron within the metal-ligand delocalized orbitals. The EPR spectrum contains an eight-peak multiplet centered at g = 1.897 arising from splitting of the I = 7/2 tantalum metal center. However, the peaks lying at the ends of the multiplet have a stronger intensity and are consistent with a ligand based radical. Thus, the electron is delocalized over the entire metal-ligand framework. Complex **101** does not react with additional $PhICl_2$, in contrast to the analogous $[ONO]^{3-}$ tantalum complex (Section 6.2).

**Scheme 49.** Reactions of **100** with $CN^tBu$, $PhICl_2$, $ArN_3$, and $Ph_2CNN$.[125]

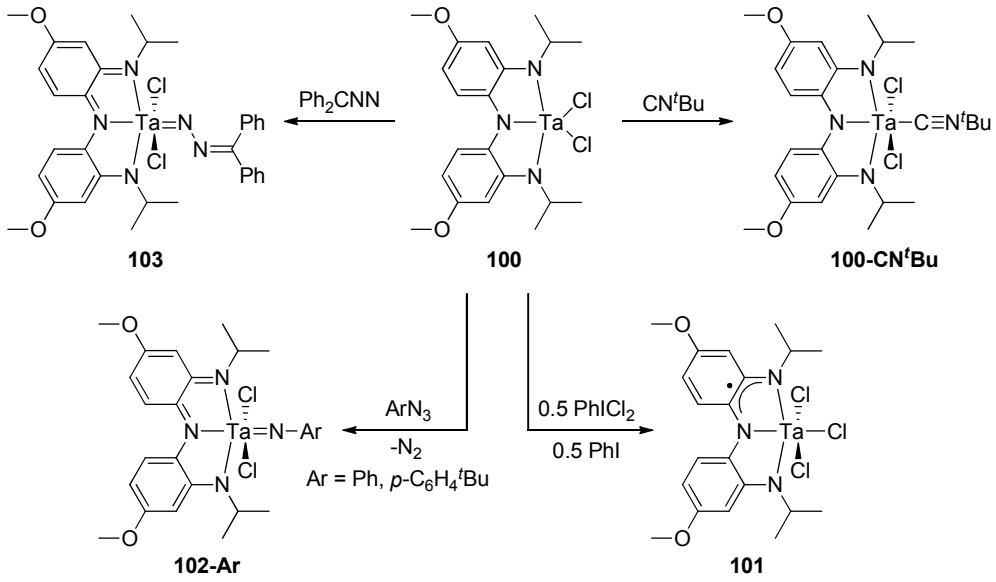


The expulsion of $N_2$ from an azide to form a metal-amido requires two electron oxidation of the metal center. The $NNN^{3-}$ trianionic pincer-type ligand, capable of a two electron oxidation by forming the quinone monoanionic pincer **C**, serves as a convenient electron reservoir to promote dinitrogen expulsion from an otherwise fully oxidized metal ion. Indeed, complex **100** reacts with tolyl- and phenylazide by emitting $N_2$ to yield the tantalum imido complex **102-Ar** (Ar = Ph, *p*-$C_6H_4$-$^t$Bu). Surprisingly, **100** does not react with alkylazides or the bulky 2,6-diisopropylphenylazide (Scheme 49).[125] The addition of pyridine to **100** prior to $ArN_3$ completely inhibits the reaction, further emphasizing the need for an accessible coordination site to complete the transformation. In an attempt to generate a tantalum carbene species, complex **100** was treated with $Ph_2C{=}N{=}N$. The trianionic $NNN^{3-}$ pincer-type ligand of **100** undergoes a similar two-electron oxidation when treated with (diazomethylene)dibenzene, but does not eject $N_2$. The isolated complex **103** contains the pincer ligand in the 2-electron oxidized quinone form (**C**), and the (diazomethylene)dibenzene is reduced to form a $Ta{=}N{-}N{=}CPh_2$ fragment (Scheme 49). Bond lengths and angles of the monoanionic NNN ligand within complex **103** are similar to those within complex **102-Ar**.

**Scheme 50.** Nitrene transfer reactions with **102-Ar**.

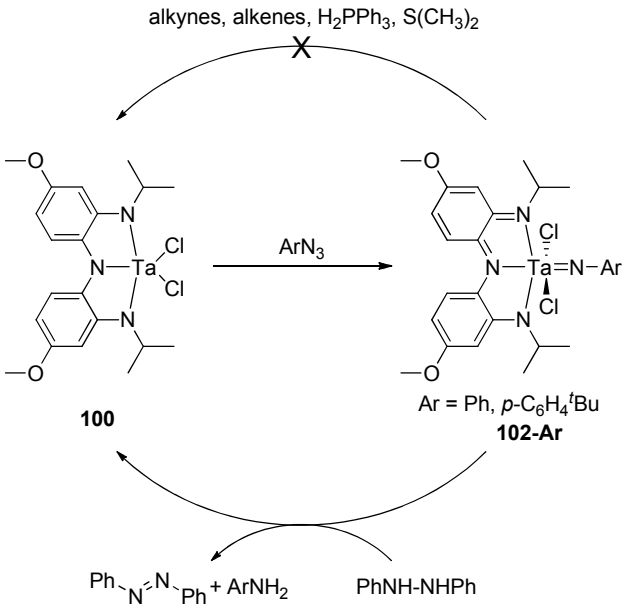


Complex **102-Ar** does not undergo nitrene transfer to olefins, alkynes, $S(CH_3)_2$, or $H_2PPh_3$. However, complex **102-Ar** will oxidize hydrazine to form azobenzene, arylamine, and complex **100** (Scheme 50).[126] These results suggest that complex **102-Ar** only undergoes proton-coupled electron transfer and not a two electron nitrene transfer. The coordinatively saturated metal ion in **102-Ar** prevents hydrazine from binding.

A series of redox active $NNN^{3-}$ pincer-type ligands were prepared with varying electron-donating and withdrawing groups to modify the redox potential of the $NNN^{3-}$ pincer-type ligand. Scheme 51 depicts the series of ligands **95a-f** and the respective tantalum complexes **100a-f**.[127] Coordinating C≡N$^t$Bu to **100a-f** yields complexes **100a-f-CN$^t$Bu**. Treating complexes **100a-f** with $[NBnEt_3]Cl$ coordinates a chloride ion to the Ta metal center, yielding complexes **104a-f** as stable complexes for electrochemical studies. The electrochemical reduction potentials are listed in Table 1 and are consistent with expected trends. The first and second oxidation/reduction waves are separated by ~0.4 V. The most significant change is the 0.270 V difference between the redox potentials of **104a** and **104b**. Complexes **100a-f-CN$^t$Bu** undergo a single electron oxidation upon addition of 0.5 equivalents of $PhICl_2$, or one equivalent

of *N*-chlorosuccinimide, to yield semiquinonate complexes **101a-f**. Despite the significant electrochemical potential changes observed, the corresponding EPR g-value of the semiquinone radical is only moderately affected, ranging between 29-33 G. The reaction of **100a-f-CN$^t$Bu** with azides forms the corresponding tantalum imido complexes, but they do not undergo nitrene transfer.

**Scheme 51.** Reactions of *para*-functionalized NNN pincer-type ligands ($OCH_3$, F, H, $CH_3$, $^t$Bu) with tantalum.

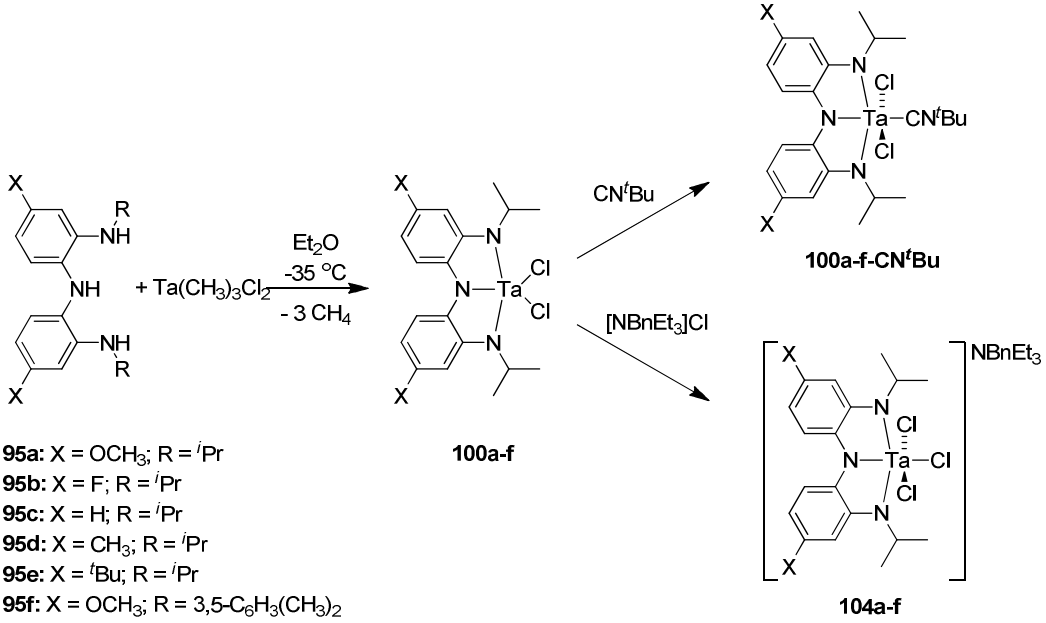


**95a:** X = $OCH_3$; R = $^i$Pr
**95b:** X = F; R = $^i$Pr
**95c:** X = H; R = $^i$Pr
**95d:** X = $CH_3$; R = $^i$Pr
**95e:** X = $^t$Bu; R = $^i$Pr
**95f:** X = $OCH_3$; R = 3,5-$C_6H_3(CH_3)_2$

**Table 1.** Electrochemical redox potentials of complexes **104a-f**. Eº2 (V vs $[Cp_2Fe]^{+/0}$).

| | $[NNN]TaCl_3^{0/-}$ | $[NNN]TaCl_3^{+/0}$ |
|---|---|---|
| **104a** | -0.17 | 0.23 |
| **104b** | 0.10 | 0.50 |
| **104c** | 0.02 | 0.47 |
| **104d** | -0.07 | 0.36 |
| **104e** | -0.02 | 0.42 |
| **104f** | -0.13 | 0.23 |

### *5.4. NNN$^{3-}$ iron complexes*

Bis(imino)-pyridine ligands[128] are another class of redox-active NNN pincer-type ligands for transition metal ions. In particular, *bis*(imino)-pyridine iron complexes are effective precatalysts for several important transformations.[129-132] Until recently, the trianionic form of the ligand within the

coordination sphere of a transition metal was unknown, though Gambarotta and Budzelaar synthesized and characterized a reduced trilithio salt of the ligand.[133] In 2013, Bart et al.[134] and Chirik et al.[135] independently expanded the *bis*(imino)-pyridine redox capabilities to include the trianionic form of the ligand. In Chirik's work, treating the neutral diradical iron(II) complex **105-R** (R = $CH_3$, Ph)[136] with 1.01 equiv of sodium naphthalenide in THF provided the corresponding anion, but characterization was complicated by the presence of two different coordination modes of the sodium ion. Performing the reaction in the presence of 15-crown-5, or 18-crown-6, sequestered the sodium ion within one environment and provided pure compounds (Scheme 52).[135] Spectroscopic and single crystal X-ray diffraction studies, in conjunction with computation, provide conclusive evidence that the reduction is ligand centered and the complexes **106-$R_{x,y}$** (x = 15, y = 5 (15-crown-5), x = 18, y = 6 (18-crown-6)) comprise iron(II) radical anions bearing a trianionic pincer ligand. The next redox event, upon addition of an additional electron, occurs at the metal center to give the low spin iron(I) radical dianion **107-$Ph_{18,6}$**, with the pincer unaffected and in the trianionic form. Bart[134] employed the phenyl *bis*(imino)-pyridine (i.e. R = Ph) in uranium coordination chemistry to achieve a trianionic pincer as well, see section 5.5 for further details.

**Scheme 52.** Sequential reduction of bis(imino) iron-dinitrogen complexes to synthesize the trianionic pincer-type Fe(II) radical anion **106-$R_{x,y}$** (R = $CH_3$, Ph; x = 15, y = 5 (15-crown-5), x = 18, y = 6 (18-crown-6)) and the Fe(I) radical dianion **107-$Ph_{18,6}$**.

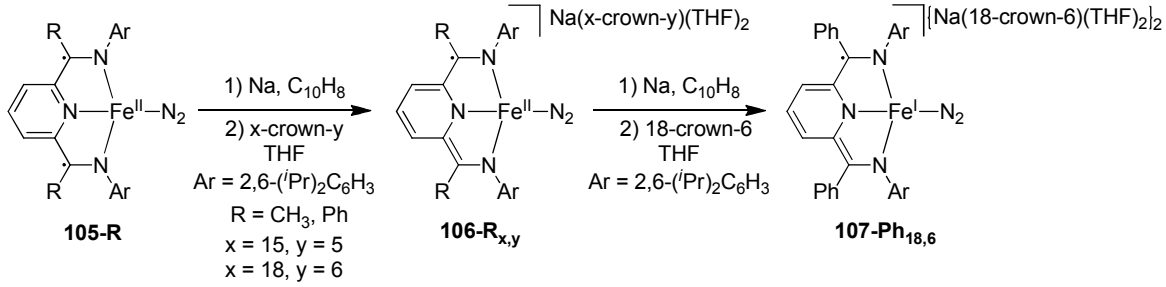


*5.5. $NNN^{3-}$ uranium, neodymium, and lanthanum complexes*

Only a few examples of lanthanide and actinide complexes bearing a trianionic pincer ligand are known. Gambarotta and Budzelaar reported neodyumium and lanthanum *bis*(imino)pyridine complexes

with the ligand in its trianionic form in 2004.[46] Reduction of the Ln(III) complexes **108-Ln** (Ln = La, Nd) with potassium naphthalenide forms the trianionic pincer-type complexes **109-Ln**, albeit in low yield (Scheme 53).[46] The reduction is ligand centered as the metal ions remain in the +3 oxidation state. In this case though, the proposal is that ligand centered reduction results in enough radical electron density at the methylidene C-atom, and is stable enough, to find a partner to dimerize. Other radical termination events are likely the cause of the low yields, and investigation into the reactivity of **109-Ln**, its full characterization, and mechanism of formation was not completed.

**Scheme 53.** Synthesis of **173-Ln** and proposed mechanism of dimerization.

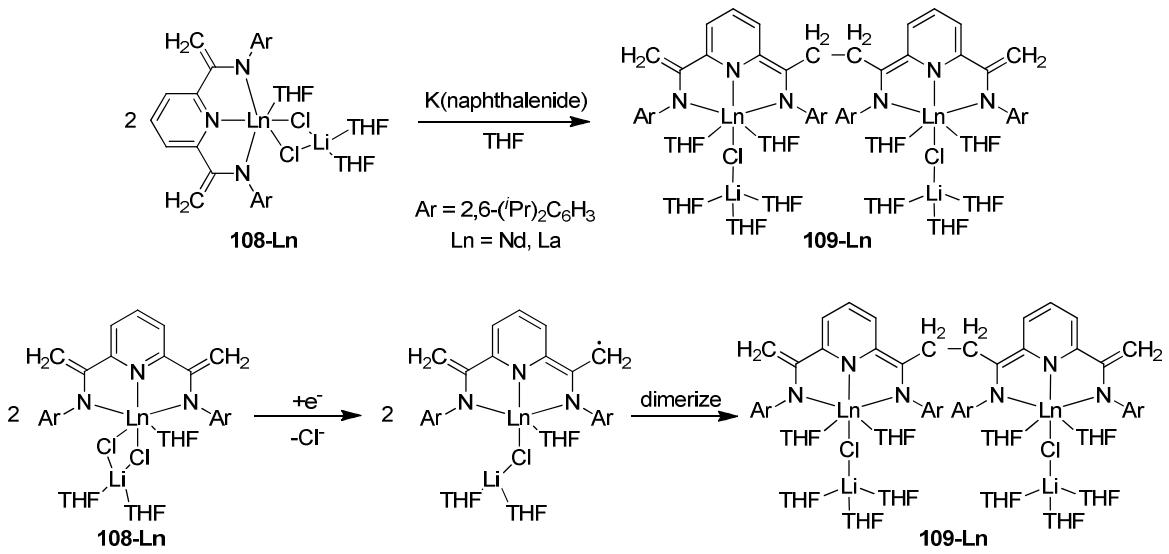


Continuing the trend of ligand centered reduction to generate a trianionic form of a pincer ligand, Bart et al. treated the U(III) precursor $Cp^*_2UI(THF)$[137] with the neutral *bis*(imino)-pyridine ligand $^{Mes}PDI^{Me}$ (**110**) under reducing conditions (2 equiv $KC_8$) in toluene to produce the U(IV) complex $Cp^*U(^{Mes}PDI^{Me})(THF)$ (**111**) (Scheme 54).[134] A single crystal X-ray analysis of **111** and a comparison of the ligand metric parameters with the reduced trilithio derivative of Gambarotta,[133] provide convincing evidence the ligand is in its trianionic form. One fascinating result is the uranium ion is oxidized from U(III) to U(IV) under reducing conditions. To convert the neutral *bis*(imino) ligand to the trianionic form requires three electron equivalents, clearly two originate from the external reagent (2 x $KC_8$) and one must come from U(III). Extracting the stored electron equivalents in a meaningful chemical reaction

occurs upon treating **111** with azobenzene. Reduction of azobenzene by **111** results in the formation of the *bis*(imido) U(V) species Cp*U(PDI)($NPh_2$)$_2$ (**112**) (Scheme 54).[134] The reduction requires four electrons, three from the ligand to return it to a neutral *bis*(imino)-pyridine, and one from U(IV), to give U(V). Interestingly, though the ligand in its trianionic form is poised to unleash three electrons Bart et al.[138] demonstrate that not all electron equivalents need to be deployed. Treating complex **111** with benzaldehyde produces the pinacolate complex **113**. Pinacolate formation is the result of C-C bond formation using electrons derived from the two-electron oxidation of the trianionic ligand. Upon two-electron oxidation of the trianionic pincer, X-ray structural data indicates the ligand adopts a charge separated radical anion resonance form. Changing the size of the Cp ligand alters the chemistry in two important ways. Reducing the Cp ligand size to 1-(7,7-dimethylbenzyl)cyclopentadienide ($Cp^p$) provides the analogous U(IV) complex **114** with the ligand in the trianionic form, but treating **114** with benzaldehyde results in decomposition. In contrast, treating **114** with two equivalents of benzophenone produces the pincolate complex **115.** The reaction again is the result of two electron oxidation of the trianionic ligand and C-C coupling. However, the lower electron donating capacity of the $Cp^p$ ligand alters the resonance form of the bis(imino) ligand. X-ray structural data indicate the ligand adopts a straightforward radical monoanion form. These results are good examples of the additional reactivity dimension afforded by redox-active ligands; and in light of the topic for this review, it deserves reemphasizing that the reducing equivalents are housed in a trianionic pincer. Controlling redox equivalents in trianionic pincer ligands is now well-established. The future challenge in this area will be to control the redox equivalents to complete purposeful chemistry. Another challenge is to build redox-active trianionic pincer complexes that are water stable. The highly charged nature of the ligand does not lend itself to water stability, therefore employing redox active ligands in water oxidation/reduction, at this time is not possible.

**Scheme 54.** Synthesis of the trianionic pincer-type complex Cp*U($^{Mes}$PDI$^{Me}$)(THF) (**111**) and demonstration of the subsequent release of stored electrons.

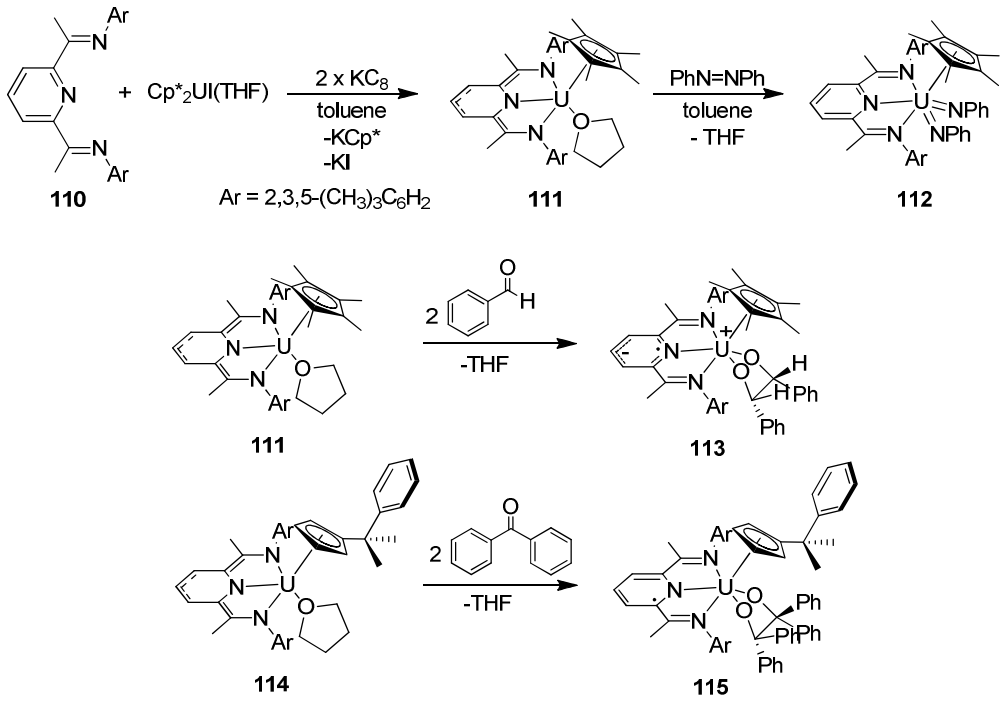


## 6. ONO$^{3-}$ trianionic pincer-type ligands

### *6.1. ONO$^{3-}$ group 4 complexes*

Trianionic pincer-type ONO$^{3-}$ ligands are similar to their NNN$^{3-}$ derivatives and can be either redox active, or dormant. Another example of ligand modification at the metal center to yield an ONO trianionic pincer-type complex involves first treating 6,6'-(quinoline-2,8-diyl)*bis*(2,4-*di*-*tert*-butylphenol) (**116**) with $TiBn_4$ to eliminate two equivalents of toluene and benzyl attack of the pyridine at the 4-positon to form the trianionic ONO pincer-type complex **117** (Scheme 55).[139] From the solid state structure of **117**, the large ring of the ONO pincer-type ligand is evidently flexible and allows the low-coordinate titanium metal ion to adopt a distorted tetrahedral geometry. The benzyl ligand coordinates $\eta^2$ to maximize electron donation to the unsaturated Ti(IV) ion. Metalation to obtain trianionic ONO pincer-type complexes with larger Zr and Hf metal ions results in similar insertion chemistry, but benzyl attack occurs at the pyridine 2-position and the N-donor is protonated. Thus, the ligand is a dianion and poised

for conversion to a trianionic pincer upon toluene elimination. From the solid state structure of **118-M** (M = Zr, Hf), the metal ion adopts a distorted trigonal bipyramidal geometry with the dibenzyl ligands coordinated in a $\eta^1$ fashion. Complexes **117** and **118-M**, are all active catalyst for ethylene/1-butene copolymerization with MAO/$[Ph_3C][B(C_6F_5)_4]$ as a cocatalyst.

**Scheme 55.** Synthesis of the trianionic ONO pincer-type titanium complex **117** and dianionic derivatives of Zr and Hf (**118-M**).

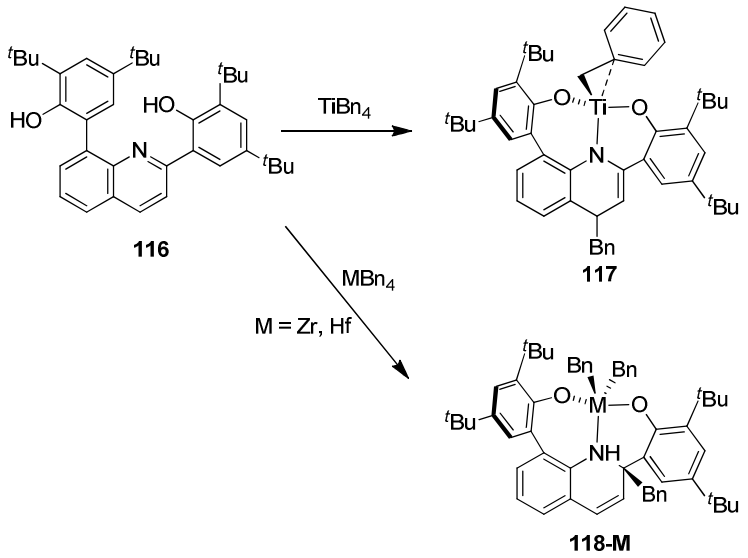


*6.2. ONO$^{3-}$ tantalum complexes*

Motivation for employing ONO ligands are the following: 1) activating the central C-H bond within NCN, OCO, and CCC pincer ligands create challenges for metalation, 2) the chemistry of trianionic pincer complexes with unsaturated substrates such as alkynes is susceptible to substrate insertion into the M-$C_{pincer}$ bond.[105] It should be noted that while undesirable for certain applications, formal insertion of an alkylidyne into the M-$C_{pincer}$ bond led to the discovery of complex **73**, a highly active alkyne polymerization catalyst.[61] Switching to an ONO pincer-type ligand circumvents insertion of unsaturated substrates. Additionally, trianionic pincer-type ligands that contain a central amido donor exhibit interesting structural and electronic properties arising from the central nitrogen lone pair, as in the

case of [NNN]Ta$(CH_3)_2$[124] and [ONO]Rh$(py)_3$.[140] Figure 3 depicts the [$CF_3$-ONO]$^{3-}$ ligand within a metal coordination sphere. The combination of electron-withdrawing fluorinated alkoxides and central amido donor create a push-pull electronic affect that typifies the highly active push-pull alkyne metathesis catalysts elaborated by Tamm et al.[141-144]

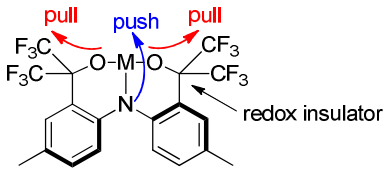


**Figure 3.** The unique push-pull design of the [$CF_3$-ONO]$^{3-}$ pincer-type ligand.

The [$CF_3$-ONO]$H_3$ trianionic pincer proligand **119** is accessible in high yields in only two steps. Additionally, the [$CF_3$-ONO] pincer-type ligand incorporates a push-pull effect of an electron-rich amido donor, electron-withdrawing fluorinated alkoxides, and a constrained amido lone pair that is exploitable in high-valent metal catalysis. As such, an investigation was conducted to develop synthetic approaches to access a variety of high-valent metal complexes. Tantalum is an ideal candidate to explore the coordination chemistry as demonstrated in earlier examples of OCO, and redox active ONO, and NNN, trianionic pincer complexes.

Treating proligand **119** with Ta$(N(CH_3)_2)_5$ provides a convenient route to access the amido-amine complex [$CF_3$-ONO]Ta$(N(CH_3)_2)_2(NH(CH_3)_2)$ (**120**) (Scheme 56).[145] One equivalent of $HN(CH_3)_2$, generated in the reaction, coordinates to form an octahedral metal center. Applying vacuum to **120** removes the coordinated amine to yield the 5-coordinate tantalum diamido complex [$CF_3$-ONO]Ta$(N(CH_3)_2)_2$ (**121**). However, further derivation of complex **121** with $(CH_3)_3SiCl$ to yield a [$CF_3$-ONO]$TaCl_2$ complex was unsuccessful.

**Scheme 56.** Metalation of $[CF_3\text{-ONO}]H_3$ (**119**) with tantalum.

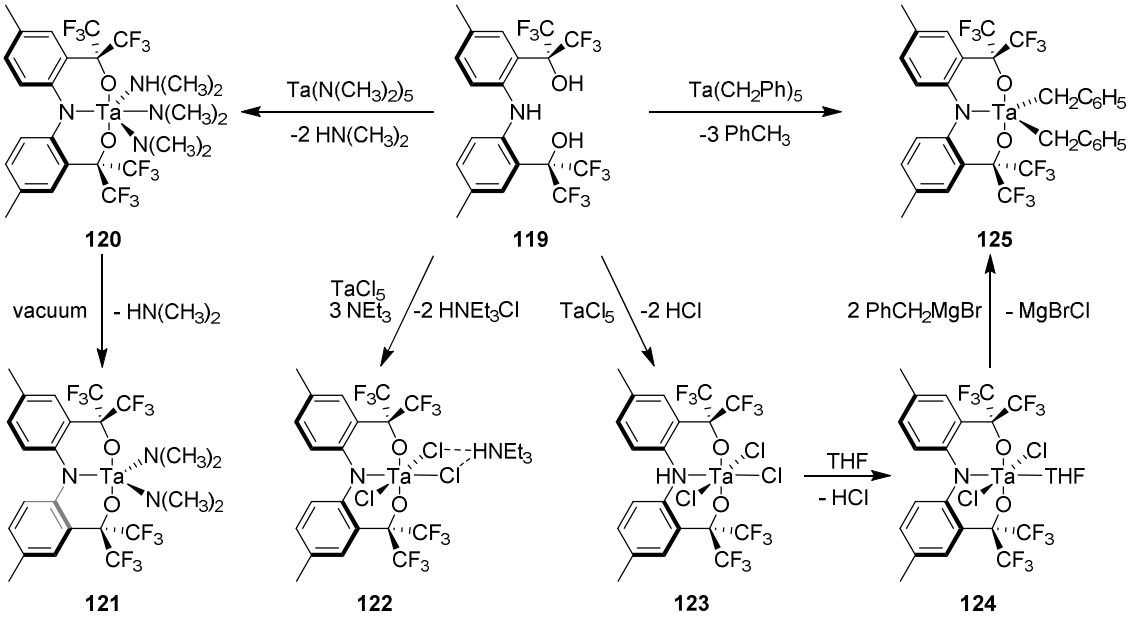


An attempt to access the $[CF_3\text{-ONO}]TaCl_2$ involved treating the proligand first with three equivalents of *n*-butyllithium prior to addition of $TaCl_5$, but this yielded a mixture of products. A more straightforward route involves treating $TaCl_5$ with proligand **119** directly. Subsequent addition of $HNEt_3$ removes any liberated HCl to provide the trianionic pincer tantalum complex $\{HNEt_3\}[CF_3\text{-ONO}]TaCl_3\}$ (**122**) bearing three chlorides (Scheme 56).[145] The initial reaction between $[CF_3\text{-ONO}]H_3$ and $TaCl_5$ proceeds even without the presence of a base. Refluxing a toluene solution of **119** and $TaCl_5$ drives off HCl(g) yielding $[CF_3\text{-ON}\mathit{H}\text{O}]TaCl_3$ (**123**) with the pincer N—H bond intact. The reaction is more easily accomplished by combining the reagents in $CH_2Cl_2$ and stirring under a static vacuum for several hours. Deprotonation of complex **123** is remarkably straightforward. Treating a $CH_2Cl_2$ solution of **123** with excess THF releases HCl, to yield the neutral dichloride complex $[CF_3\text{-ONO}]TaCl_2(THF)$ (**124**). Unfortunately, complex **124** gradually decomposes over several hours in solution, limiting its use in further derivatization. However, complex **124** can be prepared in situ with sufficient purity for further chemistry. Treating freshly prepared **124** with two equivalents of BnMgBr yields the dibenzyl tantalum complex **125** (Scheme 56).[145] Heating a solution of $TaBn_5$ with proligand **119** provides an alternative

route to **125**, which is thermally stable. Tantalum dialkyl complexes and $TaBn_5$ readily undergo H-atom abstraction at elevated temperatures, or with the addition of phosphine ligands to form alkylidene complexes. However, complex **125** does not display this chemistry.

As mentioned earlier, trianionic pincer and pincer-type ligands are not merely supporting frameworks; they are intimately involved in directing the outcome of chemical reactions at the metal center. Powerful examples are redox-active ONO and NNN pincer-type ligands that shuttle between semiquinonate, quinonate, and trianionic ligand forms. Transforming the ligand while coordinated has led to some of the most outstanding results from trianionic pincer complexes. For example, the highly active alkyne polymerization catalyst **73** forms from the reversible insertion of a tungsten alkylidyne into the OCO trianionic pincer ligand to yield a tetraanionic pincer ligand,[61] or in the case of alkene isomerization,[59] the trianionic NCN chromium(IV) methyl complex **22** decomposes into the active catalyst bearing a dianionic NCN ligand. While these examples lose the trianionic character of the ligand, it is possible to transform coordinated ligands into a trianionic pincer/pincer-type ligand. A notable example involves the picolinaldehyde ligand by Fandos and Otero et al.[146-148] Upon deprotonation of the dianionic ligand on **126** and two-electron reduction from the metal, the trianionic ONO pincer ligated complex **127** forms (Scheme 57). Supporting the assignment of a trianionic pincer ligand, the enolate C-H proton resonates at 7.69 ppm, significantly up-field from typical aldehyde resonances.

**Scheme 57.** Synthesis of the trianionic pincer-type tantalum complex **127** (top) and illustration of the inter-conversion of the monoanionic and trianionic forms of the ligand (bottom).

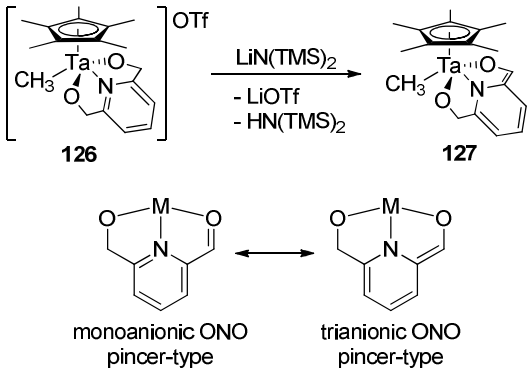

Adding phenylacetylene or trimethylsilylacetylene to **127** forms a C-C bond between the enolate carbon and the alkyne to form tantalum alkenyl complexes **128-R** (R = Ph, TMS) (Scheme 58).[147] The solid state structures of **128-R** contain the pyridine ligand *trans* to the $\eta^5$-Cp*, and the alkoxides occupy *trans* positions to each other. In a similar manner, C-C bond formation occurs upon treating complex **127** with dipyridylketone. Complex **129** contains similar structural features to **128-R**, except for replacing the alkenyl substituent with an alkoxide. Finally, related ONO-dicarboxylic acid pincer tantalum and iridium complexes were reported,[149-150] but within all derivatives the ligand remains in the dianionic form.

**Scheme 58.** C-C bond formation between the trianionic pincer ligand of **127** and alkynes.

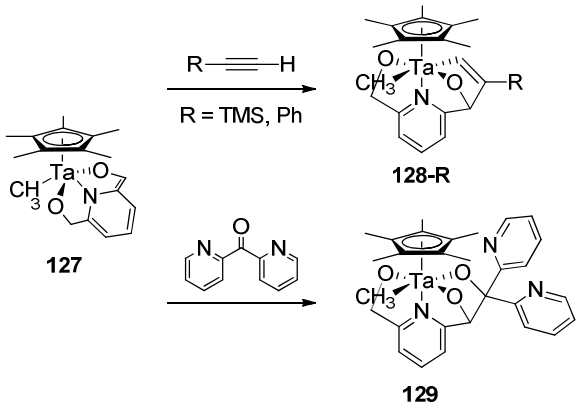


*6.3. $ONO^{3-}$ tungsten complexes*

The synthesis of a tungsten alkylidyne supported by a $[CF_3\text{-ONO}]^{3-}$ pincer-type ligand involves a similar synthetic strategy to that of [$^t$BuOCO]W(≡C$^t$Bu)(THF)$_2$ (**72**) (Section 3.6). Adding the $[CF_3\text{-ONO}]H_3$ (**119**) ligand precursor to W(≡CR)(O$^t$Bu)$_3$ {where R = $^n$Pr, $^t$Bu} results in double alcoholysis and proton transfer to the alkylidyne carbon (Scheme 59).[67, 151] The resulting complexes [$CF_3$-ONO]W=CH$^t$Bu(O$^t$Bu) (**130-$^t$Bu**)[151] and [$CF_3$-ONO]W=CHEt(O$^t$Bu) (**130-Et**)[67] are $C_1$-symmetric in solution giving rise to six separate aromatic proton signals in the $^1$H NMR spectra. The alkylidene proton is easily deprotonated by $CH_2$=$PPh_3$ to afford the anionic alkylidyne complexes {$CH_3PPh_3$}{[$CF_3$-ONO]W≡C$^t$Bu(O$^t$Bu)} (**131-$^t$Bu**) and {$CH_3PPh_3$}{[$CF_3$-ONO]W≡CEt(O$^t$Bu)} (**131-Et**).

**Scheme 59.** Synthesis of $[CF_3\text{-ONO}]^{3-}$ supported tungsten alkylidenes **130-R** and anionic alkylidyne **131-R** (R = Et, $^t$Bu).

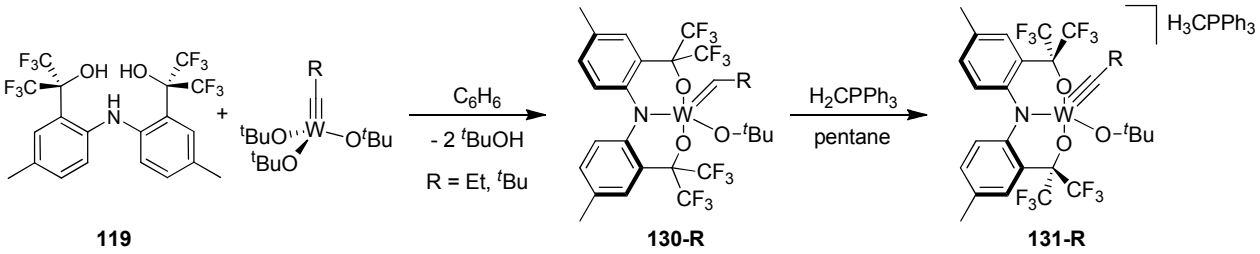


**119** **130-R** **131-R**

The DFT optimized structure of **131-Et** reveals an interesting electronic effect originating from the orientation of the nitrogen lone pair in the pincer backbone (Figure 4; right). The tungsten alkylidyne π-bond facing the nitrogen lone pair (HOMO-1) is delocalized into the nitrogen *p*-orbital. Similarly, the HOMO containing the nitrogen lone pair forms an anti-bonding interaction (HOMO). This interaction between the lone-pair and the alkylidyne π-bond is analogous to the electronic structure of organic enamines (Figure 4; left). Appending an amine to an alkene (hence, enamine)[152-153] increases the nucleophilicity of the α-carbon, by pushing electron density two atoms away from the nitrogen. By similar merit, **131-$^t$Bu** and **131-Et** experience enhanced nucleophilicity at the alkylidyne carbon and the bonding combination is given the term "inorganic enamine".[50,133]

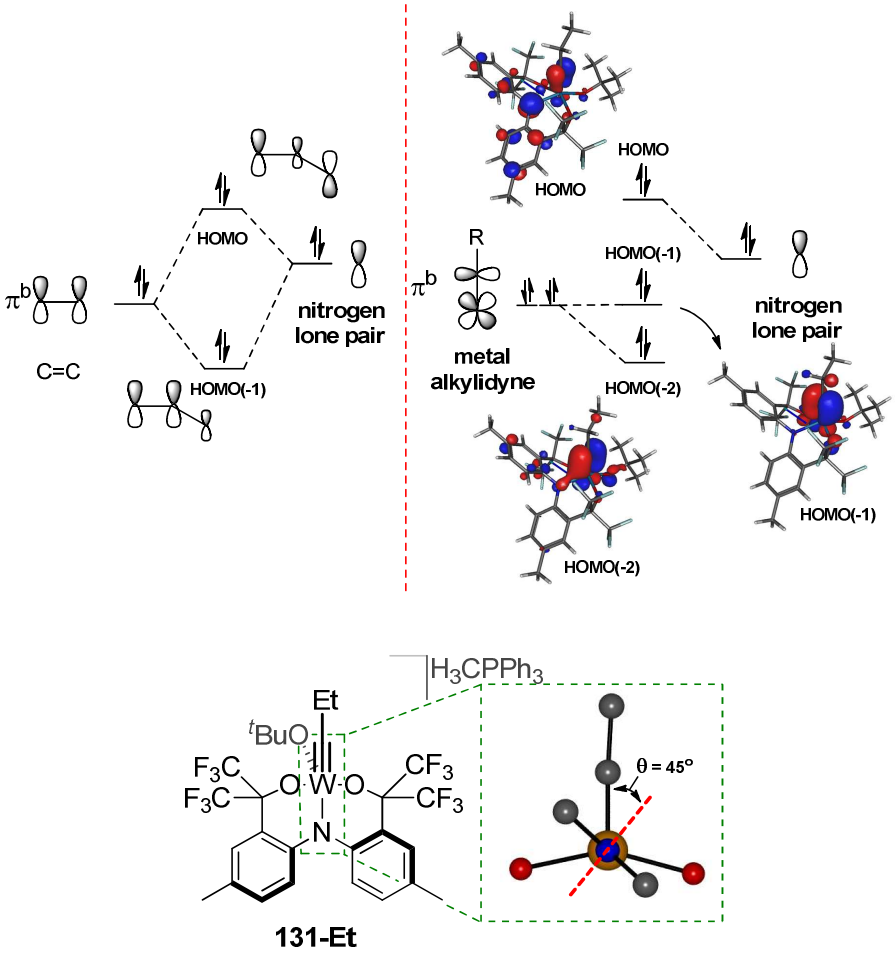


**Figure 4.** Bottom: consequence of constraining the N-atom *p*-orbital to be collinear with the M≡C multiple bond. Top: truncated molecular orbital diagram depicted the isolobal relationship between an enamine (left) and an inorganic enamine (right).

Reactivity studies of **131-Et** provide insight into the nucleophilicity of the α-C of the alkylidyne. First, adding methyl triflate to **131-Et** directly alkylates the alkylidyne carbon to yield complex **132**. Second, the larger trimethylsilyl triflate attacks the –O$^t$Bu to form Me$_3$SiO$^t$Bu, but the result is isobutylene expulsion (Scheme 60).[67] The product is the alkylidene-siloxide complex **133** that is the result of the alkylidyne carbon deprotonating the C-H bond of the *tert*-butyl group. This is unusual as *tert*-butoxide is a hallmark ancillary ligand and typically inert. The evidence points to an enhanced nucleophilic carbon to mediate C-H bond activation. The inorganic enamine interaction within complex **131-Et** provides a unique synergistic effect to allow for this C-H bond activation to occur. The aligned

amido lone pair pushes electron density two bonds away, accumulating electron density on the alkylidyne α-carbon according to Figure 4.

**Scheme 60.** Nucleophilic reactivity of **131-Et** with $CH_3OTf$ and $(CH_3)_3SiOTf$ to form complex **132** and **133**.

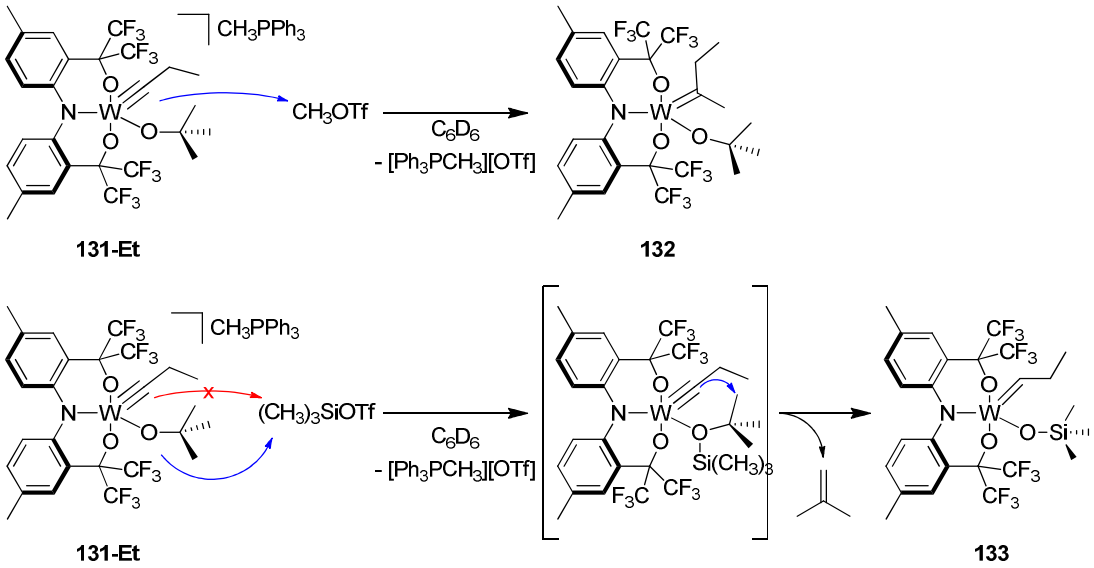


The inorganic enamine is also viable in alkylidene complexes by utilizing the M=C double bond. Adding a catalytic amount of Lewis acid, such as $CH_3OTf$, $(CH_3)_3SiOTf$, or $B(C_6F_5)_3$, to **130-Et**, similarly results in isobutylene expulsion and the formation of the tungsten-oxo complex **134** according to Scheme 61.[67]

**Scheme 61.** Proposed mechanism for isobutylene expulsion from **131-Et** with Lewis acid (LA) catalysts $CH_3OTf$, $(CH_3)_3SiOTf$, and $B(C_6F_5)_3$.

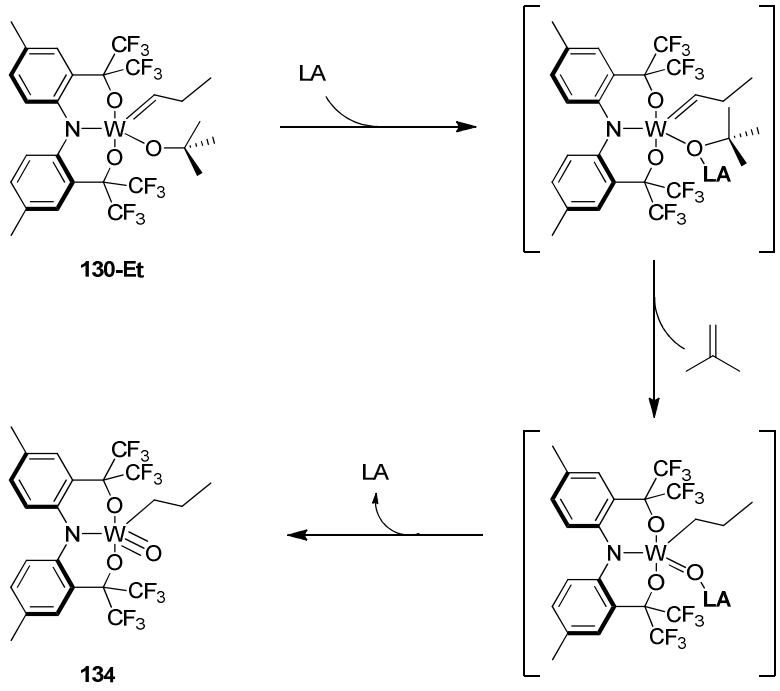


Despite similar bonding connectivity between complexes **131-$^t$Bu** and **131-Et**, their reactivity with alkylating agents is quite different. For complex **131-$^t$Bu**, the additional steric bulk ($^t$Bu) prevents alkylation upon addition of $CH_3OTf$, which is redirected towards the –O$^t$Bu ligand. Treating **131-$^t$Bu** with $CH_3OTf$ in benzene removes the –O$^t$Bu ligand, and subsequently coordinates the $^-$OTf counter anion to the tungsten alkylidyne to provide the anionic complex $\{CH_3PPh_3\}\{[CF_3\text{-}ONO]W{\equiv}C^tBu(OTf)\}$ (**135**). The triflate ion is mostly removed by dissolving complex **135** in $Et_2O$ to form the neutral complex $[CF_3\text{-}ONO]W{\equiv}C^tBu(OEt_2)$ **136**, which was confirmed via single crystal X-ray diffraction characterization (Scheme 62).[151] Consistent with previous DFT calculations, the vector representing the nitrogen lone pair is 42.3° from being collinear with the W≡C bond, and single point calculations again reveal an inorganic enamine interaction between the nitrogen lone pair and the alkylidyne π-bond.

**Scheme 62.** Synthesis of [$CF_3$-ONO]W≡C$^t$Bu($OEt_2$) (**136**).

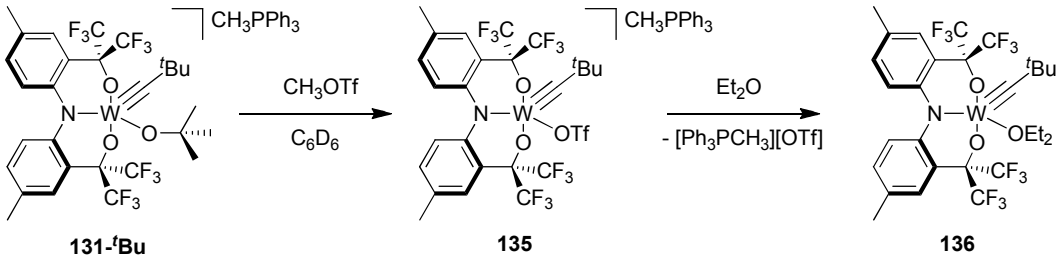


Access to complex **136** provided an opportunity to explore its potential as an alkyne metathesis catalyst. With no threat of alkyne insertion into the pincer backbone, **136** was treated with PhC≡$CCH_3$. Cycloaddition occurs rapidly at room temperature to yield the tungstenacyclobutadiene complex **137** (Scheme 63).[151] The single crystal X-ray structure of **137** contains similar bonding parameters within the $WC_3$ ring of known alkyne metathesis catalysts.[141, 154-156] Despite structural similarities, complex **137**, when treated with excess alkyne does not catalyze alkyne metathesis even at 200 °C. The tungstenacyclobutadiene is unusually stable and is thermodynamically prevented from undergoing retro-cycloaddition to release free alkyne.

**Scheme 63.** Reaction of complex **136** with alkynes to form tungstenacyclobutadiene complexes **137**, **138**, and **139**.

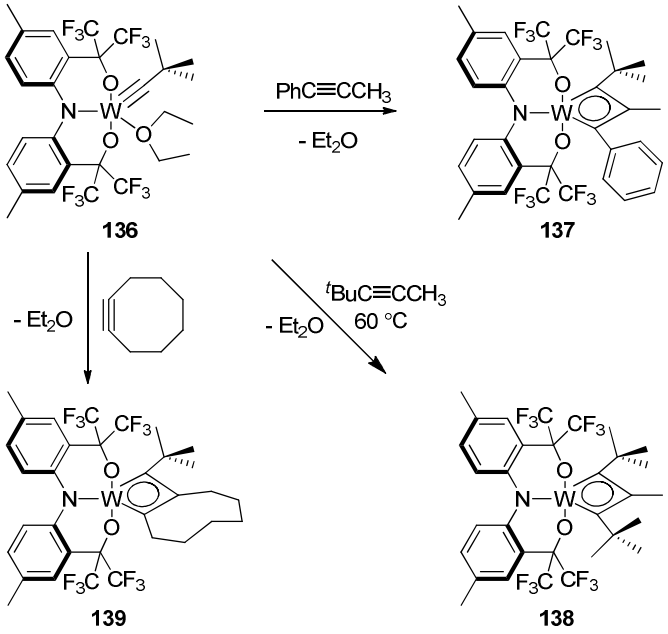

The crystallographic data of complex **137** reveals one potential flaw in the $[CF_3\text{-}ONO]^{3-}$ ligand design. The pendant $–CF_3$ groups, held back by the pincer framework, exert minimal steric pressure on the $WC_3R_3$ ring. Schrock demonstrated the importance of destabilizing the cyclobutadiene intermediate in previous work.[154-155, 157] In an effort to destabilize the ring, complex **136** was treated with the sterically bulky alkyne, 4,4-dimethyl-2-pentyne. The resulting tungstencyclobutadiene complex **138** was isolated. Despite the presence of an additional $^t$Bu substituent on the $WC_3$ ring, complex **138** does not undergo retro-cycloaddition, even at 200 °C. Moreover, treating complex **136** with cyclooctyne, in an effort to use ring strain, forms the bicyclic metallacyclobutadiene complex **139**. The solid state structure of complex **139** contains a tungstenacyclobutadiene fused to a cyclooctene ring. Despite the added ring strain, complex **139** does not undergo retro-cycloaddition at 200 °C, further indicating the impressive stability offered by $[CF_3\text{-}ONO]^{3-}$ pincer ligand to the $WC_3R_3$ ring (Scheme 64).[151] Strong donor ligands are known to promote the retro-cycloaddition. However, adding $P(CH_3)_3$ to complexes **138** and **139** does not induce metathesis at 100 °C.

The unusually stable tungstenacyclobutadiene complexes **137**, **138**, and **139** relative to the alkylidyne starting material **136** suggested a more profound influence from the $[CF_3\text{-}ONO]^{3-}$ pincer-type ligand may be involved. The inorganic enamine orbital combination, in fact, serves to destabilize the alkylidyne relative to the tungstenacyclobutadiene. An indirect test to validate the inorganic enamine effect is to treat the tungsten alkylidyne complex **136** with acetonitrile. The azametallacyclobutadiene intermediate followed by retro-cycloaddition generates a W≡N bond instead of a W≡C, which would not experience an inorganic enamine effect. Treating **136** with acetonitrile liberates free $^t$BuC≡C($CH_3$), a product from retro-cycloaddition, and the corresponding $[CF_3\text{-}ONO]W{\equiv}N$ (Scheme 64),[151] though the tungsten-nitride product could not be conclusively identified. Complex **138** is also a product in the reaction that forms via liberated $^t$BuC≡$CCH_3$ cycloaddition with the starting material (complex **136**). This study indicates that retro-cycloaddition is swift if complex **136** is still present to recombine with liberated $^t$BuC≡$CCH_3$.

**Scheme 64.** Reaction of complex **136** with acetonitrile to form free $^{t}$BuC≡CCH$_3$ and **138**.

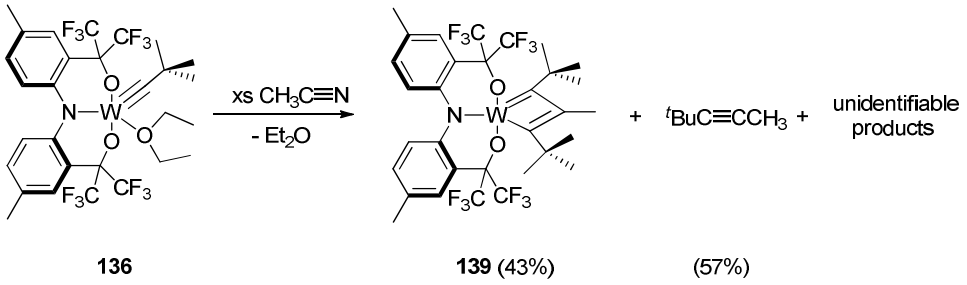


In an effort to circumvent the inorganic enamine effect in tungsten alkylidyne complexes, the pyrrolide centered trianionic pincer ligand [pyr-ONO]H$_3$ (**140**) was synthesized with the notion that the N-atom lone pair would be sequestered in the aromatic ring of the pyrrolide. Access to the alkylidene [pyr-ONO]W=CH$^{t}$Bu(O$^{t}$Bu) (**141**) and deprotonation to afford the trianionic pyrrolide pincer-type alkylidyne complex {CH$_3$PPh$_3$}{[pyr-ONO]W≡C$^{t}$Bu(O$^{t}$Bu)} (**142**) was straightforward (Scheme 65).[158] The molecular structure of complex **142** was confirmed by single crystal X-ray diffraction studies and DFT calculations confirm that minimal interaction between electron density of the N-atom π-electrons overlap with the alkylidyne W≡C bond. However, access to the neutral complex, necessary for exploring metathesis, was thwarted as attempts to liberate the *tert*-butoxide with Lewis acids lead to decomposition.

**Scheme 65.** Synthesis of the pyrrolide-centered trianionic pincer-type alkylidyne complex {CH$_3$PPh$_3$} {[pyr-ONO]W≡C$^{t}$Bu(O$^{t}$Bu)} (**142**).

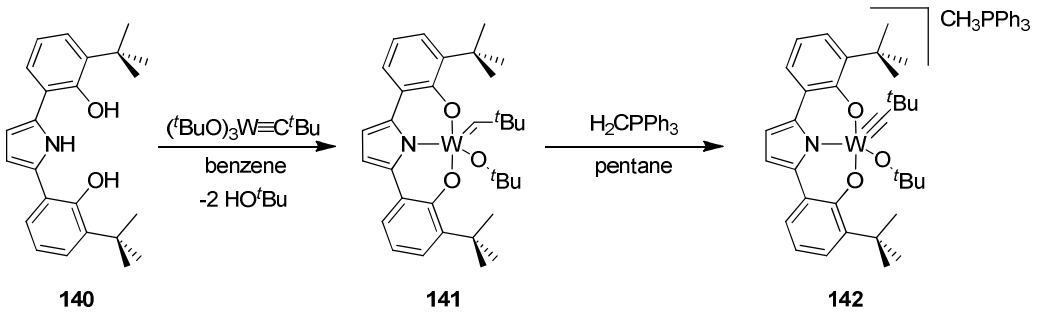

**Redox-active $ONO^{3-}$ ligands**

*6.4. $ONO^{3-}$ zirconium complexes*

Similar to redox-active $NNN^{3-}$ pincer-type ligands, an $ONO^{3-}$ donor arrangement can be used. Presented in scheme 66 is the ONO trianionic pincer-type ligand **143**. Enjoying significant attention over the past several decades, ligand **143** has been paired with several transition metals, but is most often found in its oxidized form.[47-50] Some evidence exists for the trianionic form being accessed electrochemically[159] and therefore, only clearly defined examples will be discussed in this review. Evidence for the trianionic form of the ligand comes from the work of Heyduk and coworkers,[51-53, 160] including discussions in recent reviews.[54-55] In this review, ligand **143** is presented from the chemical perspective of its trianionic form. Treating the in situ generated trilithio salt of **143** with $ZrCl_4$ in THF yields the trianionic pincer-type zirconium complex **144** (Scheme 66).[161] The Zr(IV) ion sits within an octahedral coordination field formed by the ONO ligand, two THF molecules, and a chloride. Treating the ONO ligand precursor with two equivalents of *n*-butyllithium prior to addition to $ZrCl_4$ forms the dianionic pincer-type zirconium complex **145,** with the N-H bond still intact. The N-H stretch appears at 3106 $cm^{-1}$ in the IR spectrum, and despite the ONHO ligand being distorted by the N-atom pyramidalization, the complex retains mirror-plane symmetry ($C_s$) in solution. Upon exposing complex **145** to $O_2$, the dianionic ONHO ligand is deprotonated and oxidized to the quinonate form (Scheme 66).[161] The N-H proton is transferred to form a $\mu$-OH ligand, with an O-H bond stretch at 3305 $cm^{-1}$ in the IR spectrum. X-ray analysis of the product identified it as the 7-coordinate Zr(IV) complex **146**.

**Scheme 66.** Synthesis of ONO pincer-type zirconium(IV) complexes **143**-**146**.

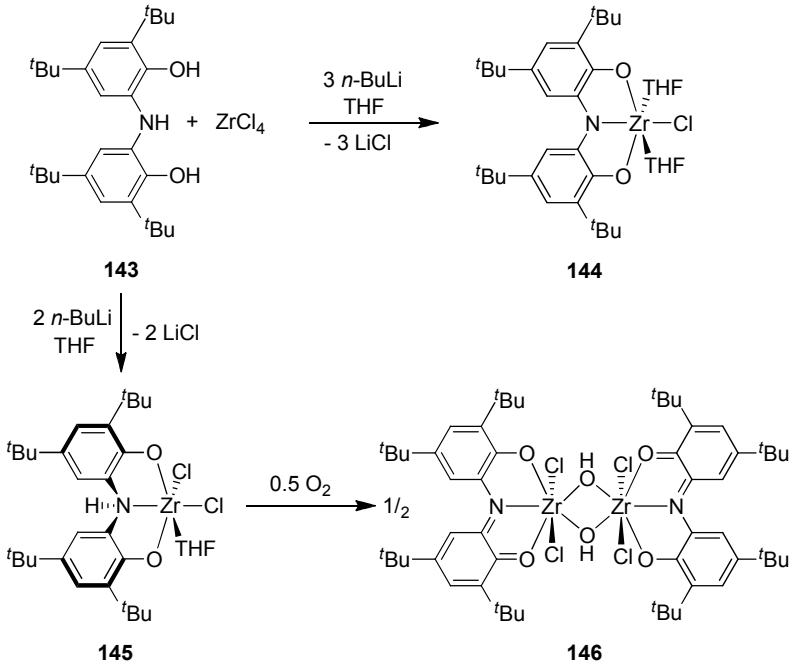


*6.5. $ONO^{3-}$ tantalum complexes*

The proligand **143** reacts with $TaCl_2(CH_3)_3$[89-91] eliminating methane to yield the $ONO^{3-}$ trianionic pincer tantalum complex **147**. Subsequent exposure to pyridine or diethyl ether forms the six-coordinate complexes **147-L** (S = py, $Et_2O$). Adding 0.5 equivalents of $PhICl_2$ to **147** generates the semiquinonate complex **148** via one-electron oxidation of the ONO pincer-type ligand. Complex **148** is paramagnetic and the EPR spectrum exhibits a prototypical eight-line pattern consistent with radical electron delocalization over the metal-ligand framework. Upon addition of a full equivalent of $PhICl_2$, a two electron oxidation of the ONO pincer-type ligand occurs to yield complex **149** (Scheme 67).[51] The X-ray structure of **149** reveals a 7-coordinate Ta(V) ion. Complex **149** is quite unique compared to other NNN and ONO complexes because it is $C_1$-symmetric in solution at room temperature. Localized bonding of the quinonate moiety with slow inter-conversion on the NMR timescale is the reason for the observed low symmetry.

**Scheme 67.** Metalation and reactivity of a redox-active ONO pincer-type tantalum complex **147**.

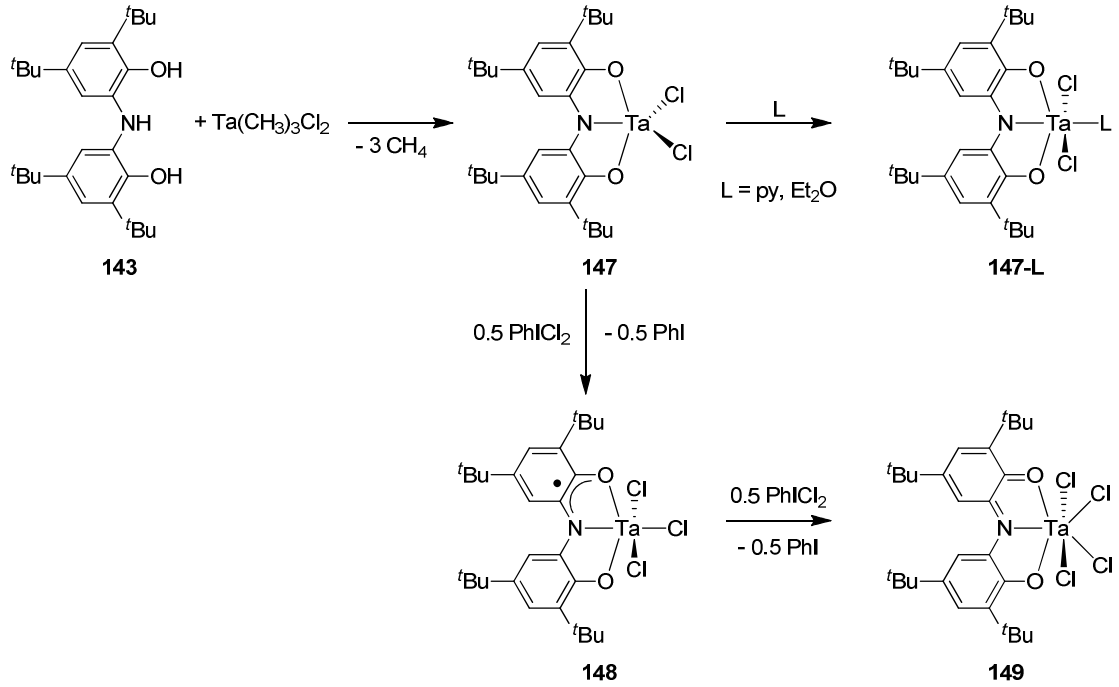


*6.5.1 Catalytic conversion of diazoalkane to ketazine*

Treating complex **147-OEt$_2$** with two equivalents of $Ph_2CN_2$ results in immediate expulsion of $N_2$ to form the ketazine complex **108** (Scheme 68).[53] The single crystal X-ray diffraction structure of **150** reveals a pentagonal bipyramidal geometry with the two chlorides occupying axial positions. The bond lengths within the ONO pincer-type ligand are consistent with its trianionic form. Similarly, $^{13}C$, IR and X-ray structures support the representation of the coordinated ketazine. The ketazine can be displaced using pyridine; however, the resulting complex **147-py** does not react with additional $Ph_2CN_2$.

**Scheme 68.** Catalyzed transformation of diazoalkane to ketazine by complex **150**.

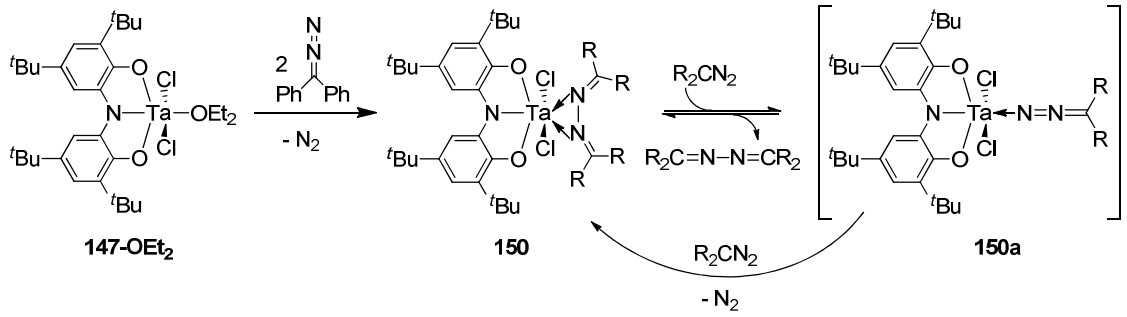


Complex **150** further catalyzes the conversion of diazoalkane to ketazine. However, after 30 turnovers, the reaction is strongly inhibited by the ketazine product. Using $PhCN_2$, diazofluorenone, $((CH_3)_3Si)HCN_2$, and ethyl diazoacetate, **147-OEt$_2$** converts these substrates to the corresponding ketazine products with similar turnover numbers. The catalysis proceeds through the proposed mechanism in Scheme 68, where $R_2CN_2$ replaces the coordinated ketazine and then $N_2$ expulsion generates a Ta carbene susceptible to nucleophilic attack by a second $R_2CN_2$ gives the ketazine. A reaction designed to probe the possible formation of a putative Ta carbene as the transfer agent involves treating complex **150** with two equivalents of $R_2CN_2$ in neat styrene (Scheme 69).[53] The reaction yielded 22% ketazine and 78% triphenylcyclopropane. The cyclopropane product would be the result of a carbene transfer to styrene, but the authors noted that Rothwell's $TaCl_2(OR)_3$[162] also provides cyclopropanes, and concluded the $ONO^{3-}$ ligand is not a redox participant in the reaction.

**Scheme 69.** Carbene transfer to styrene from diazoalkane by **150**.

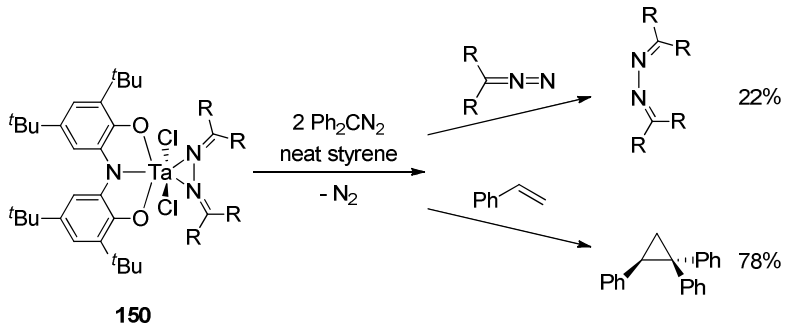


The ONO pincer-type ligand presumably remains in the trianionic form during the catalytic transformation. Though the catalyst could undergo redox changes during a catalytic cycle, it is unnecessary since $TaCl_2(OR)_3$[162] can achieve similar catalytic results. Moreover, it is interesting to compare this reactivity with the previously mentioned dichloride complex [NNN]$TaCl_2$ (**100**) and diazoalkane. The $NNN^{3-}$ pincer-type ligand reduces diazoalkane to form [NNN]Ta=N-N=$CPh_2$ (**103**), but does not eject $N_2$ to form the carbene [NNN]Ta=$CPh_2$. In contrast, [ONO]$TaCl_2(OEt_2)$ (**147-OEt$_2$**) achieves the desired transformation without oxidizing the ligand.

Treating proligand **143** with two equivalents of *n*-butyllithium prior to addition of $TaCl_2(CH_3)_3$[89-91] results in a double salt metathesis and methane elimination to yield the $ONO^{3-}$ supported dimethyltantalum complex **151-CH$_3$** (Scheme 70).[160] Complex **151-CH$_3$** is $C_{2v}$-symmetric in solution with the Ta-C$H_3$ protons resonating at 0.77 ppm in the $^1$H NMR spectrum. An alternative synthesis of complex **151-CH$_3$** involves treating [ONO]$TaCl_2(OEt_2)$ **147-OEt$_2$** with two equivalents of $CH_3Li$. In addition, a similar route provides the diphenyltantalum complex **151-Ph**. The single crystal X-ray diffraction structure of **109-CH$_3$** is consistent with the ligand in the trianionic $ONO^{3-}$ pincer form (Ta—N = 2.074(3) Å, and Ta—O = 1.890(2) Å).

**Scheme 70.** Synthesis of ONO supported dialkyltantalum complexes **151-R** (R = $CH_3$, Ph).

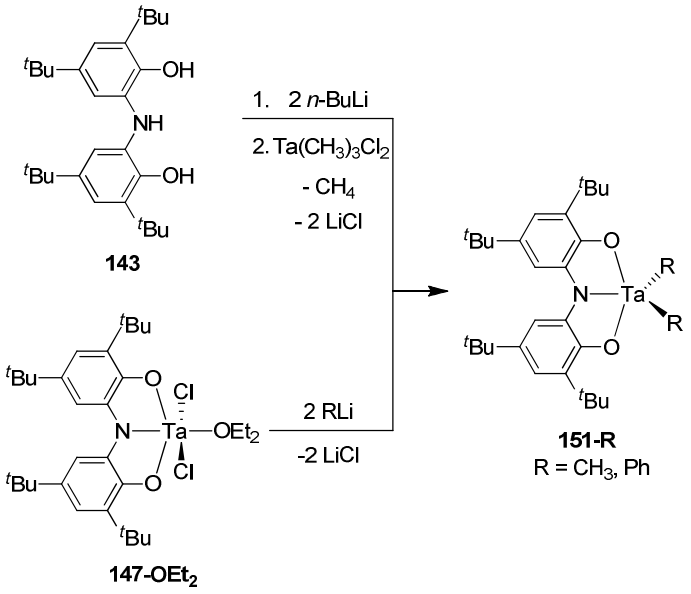


Treating complex **151-R** (R = $CH_3$, Ph) with *p*-tolylazides inserts the azide's terminal nitrogen atom into one of the Ta-R bonds forming the triazenido ligated tantalum complexes **152-R** (R = $CH_3$, Ph) (Scheme 71).[160] Subsequently, a second insertion reaction occurs with another equivalent *p*-tolylazide at 50 °C to yield complexes **153-R** (R = $CH_3$, Ph). The solid state structure of **153-$CH_3$** contains a distorted pentagonal bipyramidal Ta coordination environment with the ONO ligand and the two N-$CH_3$ fragments occupying the pentagonal plane. Again, the Ta—$N_{pincer}$ and Ta—O bond lengths are consistent with a trianionic ligand, and the O-Ta-O bite angle is 148.73(9)°.

**Scheme 71.** Azide insertion into the Ta—R of **151-R** to form **152-R** (R = $CH_3$, Ph) and **153-R** (R = $CH_3$, Ph).

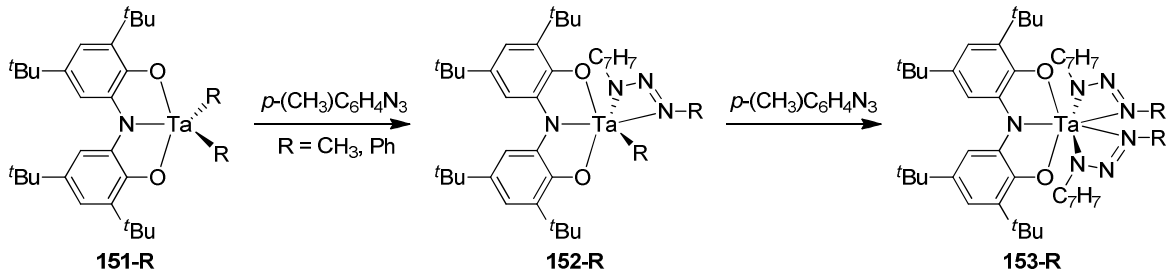

Treating complex **151-CH$_3$** with diphenylhydrazine eliminates one equivalent of methane to produce complex **154-CH$_3$** (Scheme 2.[160] However, complex **154-CH$_3$** is unstable even in the solid state by succumbing to a second methane elimination step. Addition of donor ligands (e.g. py, THF, phosphines) accelerates the second methane elimination. Adding pyridine to **154-Ph** results in benzene elimination, an equivalent of azobenzene (PhN=NPh), and the bridging *bis*-($\mu$-amido)tantalum complex **155-Ph**. An alternative route involves treating the diphenyl tantalum complex **151-Ph** with aniline and pyridine directly to release two equivalents of benzene to provide **155-Ar** (Ar = Ph, *p*-tolyl). Dinuclear **155-Ar** can be split by addition of $PhICl_2$ and pyridine to give the mononuclear dichloride complex **147-py**, an equivalent of PhI, and azobenzene.[160]

**Scheme 72.** Reactivity of complexes **151-R** (R = $CH_3$, Ph).

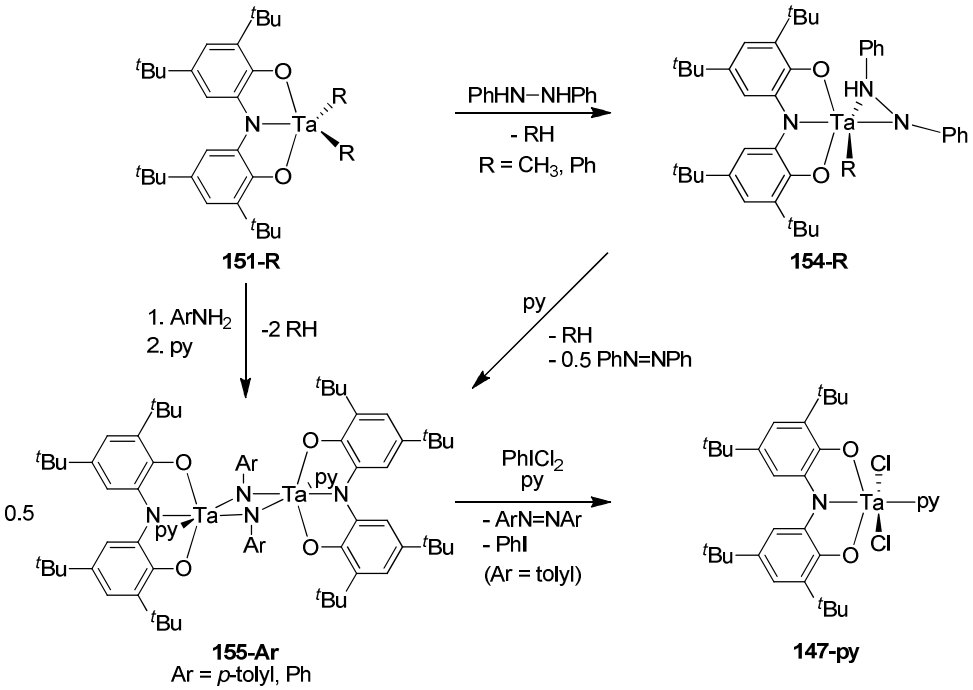

**Scheme 73.** Disproportion mechanism of hydrazine by **154-R** (R = $CH_3$, Ph).

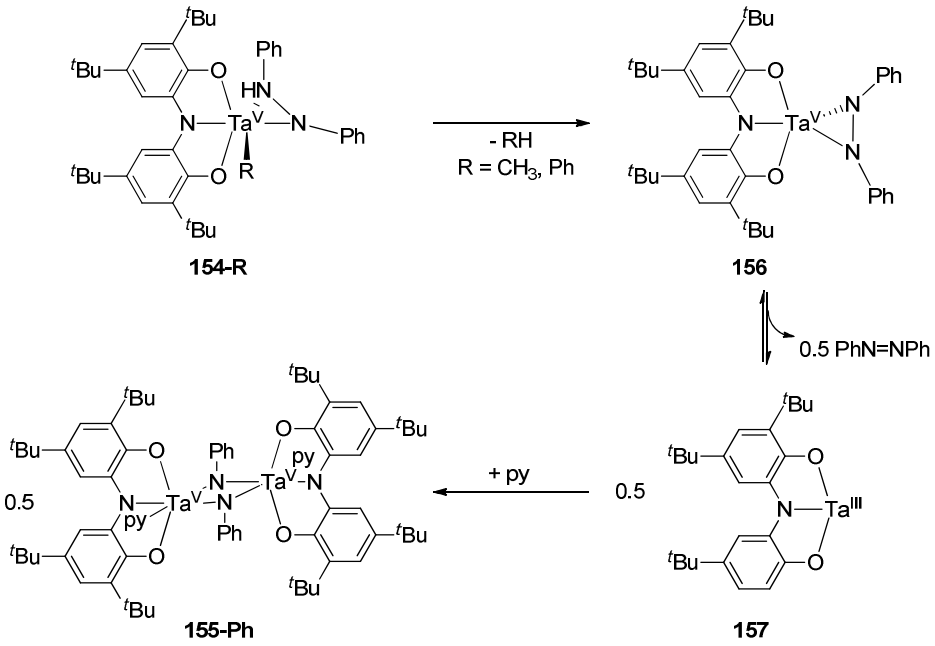


Scheme 73 highlights the proposed mechanism for the conversion of diphenylhydrazine into the *bis*-($\mu$-amido)tantalum complex **155-Ar** (Ar = Ph). Initially, the second loss of RH from **154-R** (R = $CH_3$, Ph) provides a dianionic hydrazido ligand in **156**, which reductively eliminates diazobenzene yielding a transient $Ta^{III}$ species **157**. The reduced metal ion immediately combines in a comproportionation step with **156** to yield the final product **155-Ph**. To support the validity of a [ONO]$Ta^{III}$ intermediate, [ONO]$TaCl_2(OEt_2)$ (**147-$Et_2O$)** was reduced using two equivalents of $KC_8$ in THF (Scheme 74).[160] However, upon reduction, a THF molecule ring opens to afford complex **158**. Conducting the reduction of **147-$Et_2O$** in toluene generates the [ONO]$Ta^{III}$ species and subsequent trapping with azobenzene and pyridine yields dimer **155-Ph**.

**Scheme 74.** Reactions of **147-OEt$_2$** with $KC_8$.

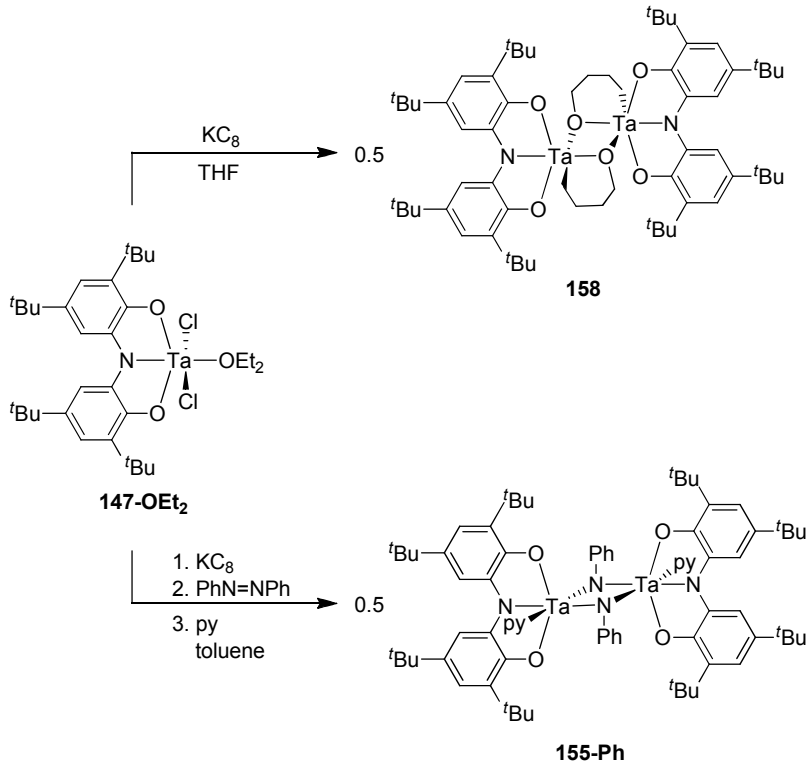


Treating **155-Ar** (Ar = Ph, p-tolyl) with two equivalents of $PhICl_2$, results in reductive elimination of diaryldiazene and the production of the dichlorotantalum complex **147-py** (Scheme 75 above). The mechanism of this transformation was explored via several experiments. One experiment involved treating a solution containing an equimolar amount of **155-tolyl** and **155-Ph** with two equivalents of oxidant. The reaction yielded the dichlorotantalum complex **147-py** and a statistical distribution of PhN=NPh, (p-tolyl)N=N(p-tolyl), and PhN=N(p-tolyl). Scheme 75 depicts the proposed mechanism. $PhICl_2$ induces a ligand-based oxidation of the pincer ligand to the quinonate form **159**.[53] The intermediate species **159** breaks into mononuclear fragments in a fast reversible process to form the terminal imido intermediate **160** that can recombine to a statistical mixture of dinuclear $\mu$-imido species. Coordination of pyridine then yields complex **147-py**. This process is irreversible, since adding azobenzene to **147-py** or **147-THF** does not result in the reverse reaction. In contrast, adding azobenzene to **147-Et$_2$O** results in an immediate color change and a paramagnetic $^1$H NMR spectrum ($\mu_{eff}$ = 1.37$\mu_B$ at

298 K and $\mu_{eff}$ = 2.18$\mu_B$ at 188 K). Adding pyridine or THF to the reaction mixture converts the products back to free azobenzene and **147-py** or **147-THF**, respectively. Using UV-vis spectroscopy, the reaction proceeds until 0.5 equivalents of azobenzene are added, suggesting the product is {[ONO]$TaCl_2$}$_2$($\mu^2$-$N_2Ph_2$) (**161**) (Scheme 76).[52] Presented are two likely resonance structures of **161**. Supporting this tentative assignment, the UV-vis spectrum of **161** contains absorptions at 590 and 950 nm that are consistent with other structures containing a semiquinonate/dianionic ONO pincer. However, complex **161** is not the same as the proposed intermediate **159** from Scheme 75, even though they appear identical. Adding equimolar amounts of PhN=NPh and (*p*-tolyl)N=N(*p*-tolyl) to **147-Et$_2$O** followed by pyridine does not result in scrambling of the ArN=NAr reagents.

**Scheme 75.** Proposed mechanism for the oxidation of **155-Ar** with $PhICl_2$ to yield **147-py**.

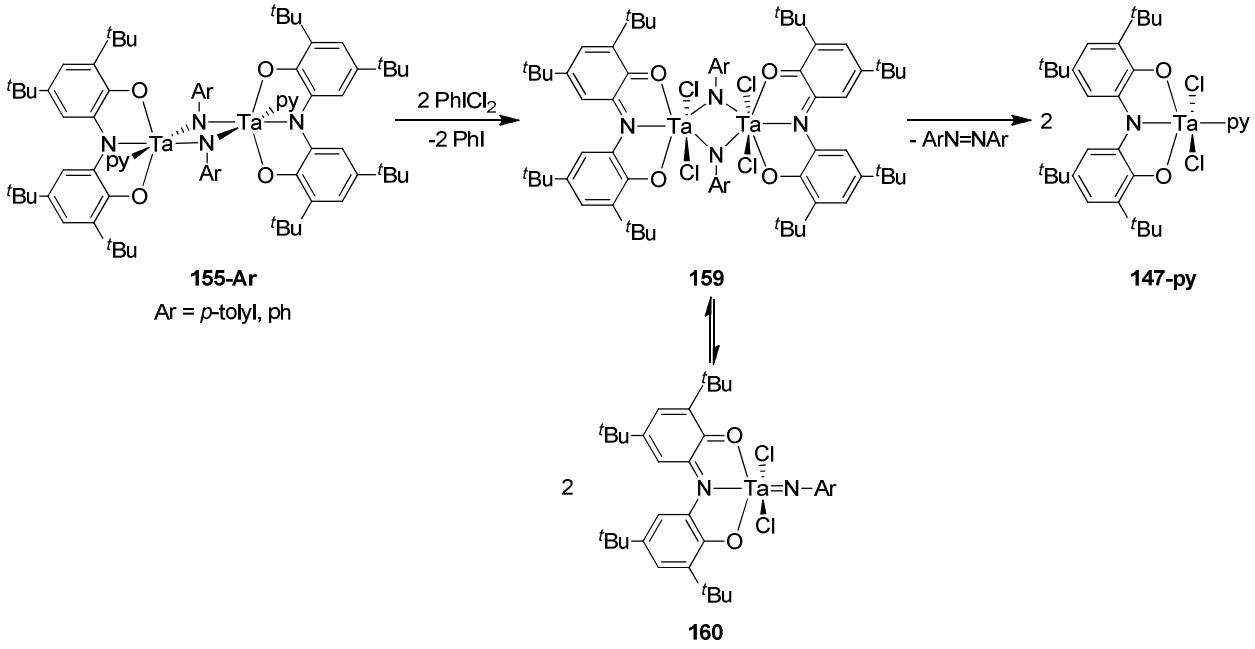

**Scheme 76.** Reaction of **147-OEt$_2$** with azobenzene to yield **161**.

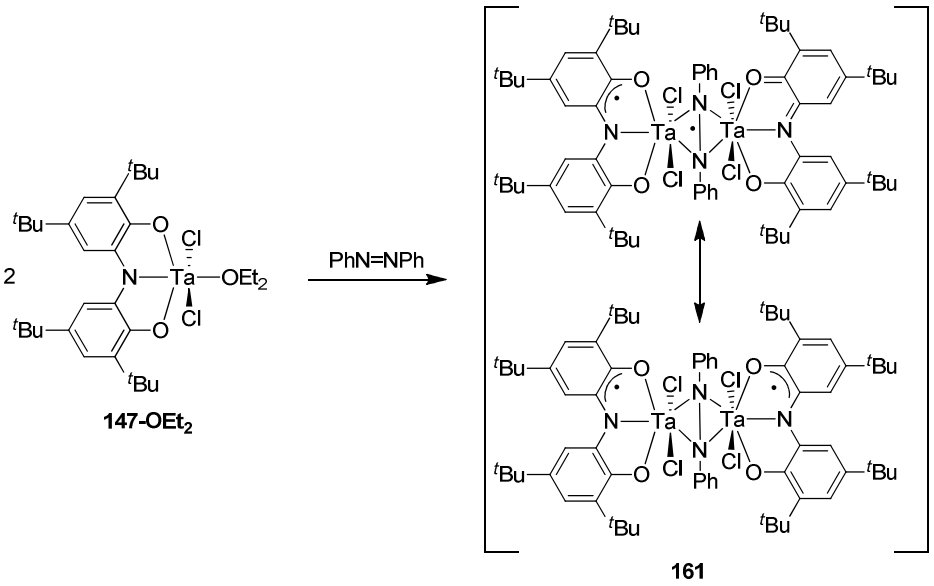


Complex **147-OEt$_2$** reacts with aryl azides ($ArN_3$) at 55 °C to release dinitrogen and azobenzene (Scheme 77).[52] However, the reaction does not occur when the more strongly coordinating ligands THF or py replace $Et_2O$. Complex **147-OEt$_2$** catalyzes the complete conversion of 10 equivalents of $PhN_3$ into azobenzene and dinitrogen. In an attempt to isolate the tantalum species after the reaction, pyridine was added, but only trace amounts of **147-py** could be isolated. The bulk of the tantalum species isolated from the reaction mixture are paramagnetic. One of these paramagnetic species is the semiquinonate product $[ONO^{2-}]TaCl_3$, which suggest a possible decomposition pathway involving chlorine atoms ($Cl^{\bullet}$). To circumvent this decomposition pathway, the chloride ligands were replaced by -O$^t$Bu.

**Scheme 77.** Catalyzed conversion of arylazide to diaryldiazene by **147-OEt$_2$**.

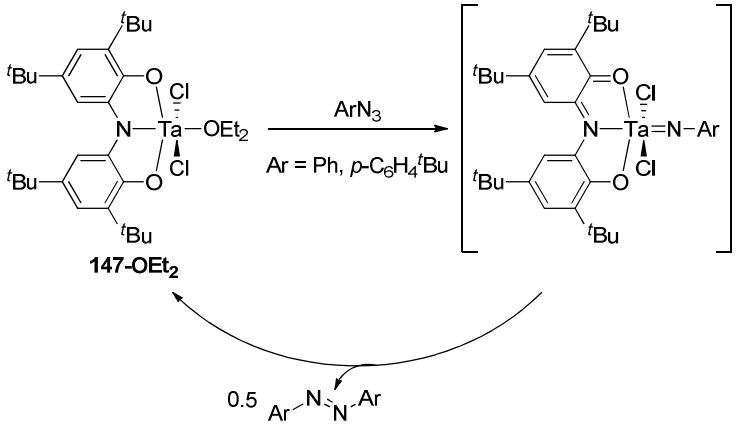

Treating the dimethyl tantalum complex **151-CH$_3$** with two equivalents of *tert*-butanol yields the *bis*-alkoxide complex **162** via methane elimination (Scheme 78).[52] The isolated yield was 41%, whereas attempting to synthesize **162** via salt metathesis of [ONO]TaCl$_2$(OEt$_2$) **147-Et$_2$O** and LiO$^t$Bu led to an intractable product mixture.

**Scheme 78.** Synthesis of **162**.

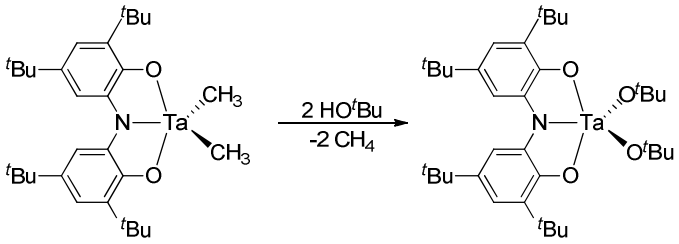


**151-Me** **162**

*6.5.2. Catalytic conversion of arylazide to diaryldiazene*

Treating complex **162** with arylazides at 55 °C oxidizes the trianionic ONO pincer-type ligand to quinonate form with concomitant loss of $N_2$ and forms the proposed arylamido intermediate **162a**. Complex **162a** readily reductively eliminates diazobenzene to regenerate complex **162** (Scheme 79) [52] However, complex **162** is considerably slower to convert arylazide to azobenzene than **147-OEt$_2$**. This is attributable to the bulkier –O$^t$Bu groups impeding both arylazide access to the metal and $N_2$ expulsion. The catalytic conversion of 10 equiv of $PhN_3$ to azobenzene by **162** at 55 °C takes nearly 7 d to complete, but starting catalyst **162** can be recovered quantitatively with no evidence for the formation of any paramagnetic material.

**Scheme 79.** Catalyzed conversion of arylazide to diaryldiazene by **162**.

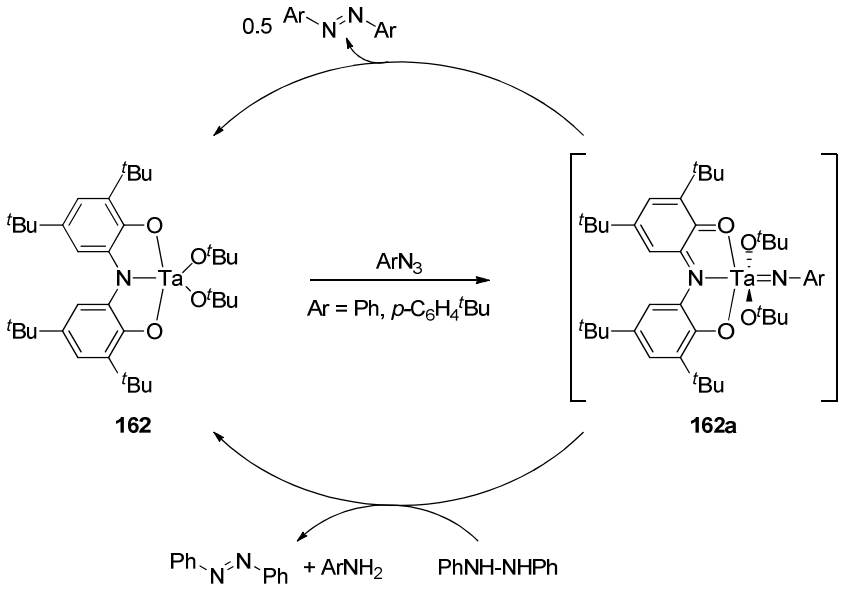


Treating complex **162** with one equivalent of *p*-tolylazide in the presence of 1,2-diphenylhydrazine results in the quantitative conversion to 4-methylaniline and azobenzene, mimicking similar reactivity observed for [NNN]Ta(=NPh)$Cl_2$ (see section 5.3). The similar reactivity supports the proposed mononuclear imido complex **162a** in the reaction mechanism.

### *6.6. $ONO^{3-}$/$SNS^{3-}$ tungsten complexes*

In contrast to ONO and NNN pincer-type ligands presented earlier, SNS versions permit redox reactivity but incorporate softer donor atoms. Heating proligand [SNS]$H_3$ (**163**) with $WCl_6$ expels HCl(g) and attaches two trianionic SNS pincer ligands to the W(VI) metal center to form **164**. For comparison, the analogous $[ONO]_2W$ complex **166** is prepared by a similar procedure (Scheme 80).[163] The solid state structures of **164** and **166** contain a distorted octahedral metal ion arising from the constrained bite angles of the pincer pendant arms. The pendant arms of the [ONO] version are significantly bent inwards to accommodate the shorter W—O bond distances of ~1.9 Å, whereas the longer W—S bond of ~2.3 Å allows more expansion. Cyclic voltammetry of **164** and **166** were performed. The first and second oxidation peaks of **164** and **166** are quasi-reversible at similar potentials (0.70 V/1.05 V and 0.63 V/1.16

V). In contrast, the reversible first and second reduction of **164** and **166** are well separated. For complex **164**, the first potential is at -1.38 V, followed by a second at -2.77 V. Quite surprisingly, complex **164** is more easily reduced (-0.61 and -1.55 V), despite coordination from the less electron donating S-atoms.

**Scheme 80.** Synthesis of $[SNS]_2W$ (**164**) and $[ONO]_2W$ (**166**).

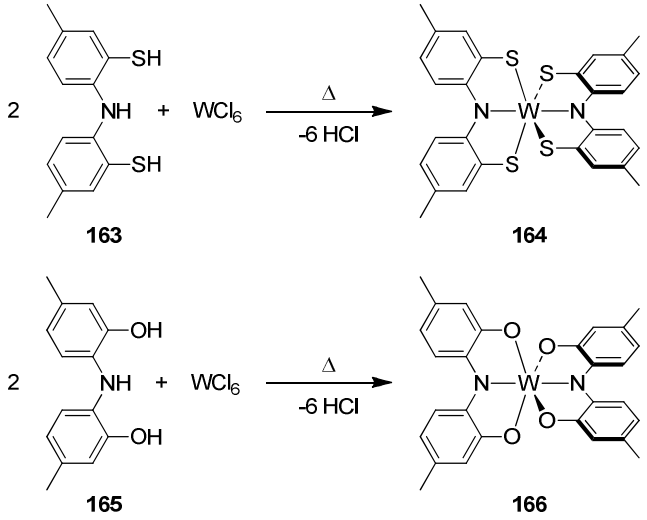


*6.7. $ONO^{3-}$ rhenium complex*

Further expansion across the periodic table employing an $ONO^{3-}$ ligand comes from the laboratories of Brown.[164] Employing an intriguing metalation technique, the authors treat $ReO_2(PPh_3)_2I$[165-166] with the transmetalating agent **167**,[167] which is an homoleptic *bis*-ONO lead(II) complex with the ONO ligand in the oxidized quinonate state. The reaction produces the Re(V) complex $[ONO]Re(O)PPh_3$ (**168**) featuring the ONO ligand in its reduced trianionic oxidation state (Scheme 81).[164] $PPh_3$ supplies the redox equivalents and is oxidized to $OPPh_3$. The reaction constitutes a non-classical oxygen atom transfer because the rhenium ion delivers the O-atom, and would normally be reduced as a consequence; however, in this case the rhenium ion remains in the 5+ oxidation state and the redox event is ligand centered. The authors note it is plausible that the ONO ligand can bind in the quinonate form, but then is reduced to the trianionic form with concomitant oxidation of the rhenium ion by two electrons to +7. Subsequent

classical oxygen atom transfer from a [ONO]Re(VII)$(O)_2$ to $PPh_3$ could occur. Deciphering between the two pathways is the subject of ongoing studies by the authors.

**Scheme 81.** Synthesis of the $ONO^{3-}$ trianionic pincer-type rhenium-oxo complex **168** via reduction by $PPh_3$ and transmetalation from lead(II); a non-classical oxygen atom transfer.

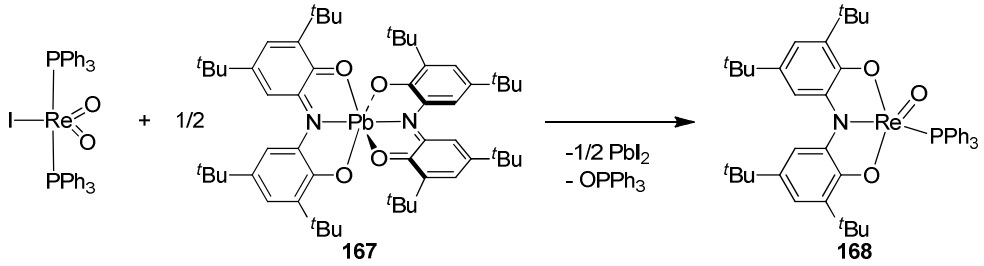


*6.8. $ONO^{3-}$ iron complexes*

In the previous sections, the redox-active $ONO^{3-}$ ligand serves as an electron reservoir to mediate 2-electron redox processes needed for bond activation/formation reactions at a formally $d^0$ metal center. Heyduk and coworkers have illustrated that the redox-active ligand coupled to the $d^0$ metal center, in fact, imitates the two-electron processes common for noble late transition metals. Two electron redox-active ligands can be applied to first row transition metals, such as Fe, which are inexpensive, but commonly undergo 1-electron redox cycles ($Fe^{2+}/Fe^{3+}$). As such, the $Fe^{2+}/Fe^{3+}$ couple catalyzes autoxidation pathways, but using a 2-electron redox-active ligand at an Fe metal center may circumvent the 1-electron redox process with a 2-electron redox cycle.[68]

Treating the semiquinonate ONO pincer-type ligand **169** with $FeCl_2$ provides an Fe(II) complex with two semiquinonate ONO pincer-type ligands attached (Scheme 82).[47, 68] The coordinatively-saturated complex **170** is rather problematic, as demonstrated earlier with [NNN]Ta complexes, in that there are no open coordination sites to investigate further oxidative/reduction reactions.

In contrast, ligating $FeCl_3$ with **169** yields the corresponding complex **171** with only one ONO ligand (Scheme 82). The solid state structure of **171** contains an iron coordination geometry that lies between square pyramidal and trigonal bipyramidal. The metric parameters of the ONO pincer-type

ligand are consistent with the quinonate form. Additional support for a high spin Fe(III) (S=5/2) oxidation state comes from Mössbauer and EPR spectroscopy. Employing a similar metalation approach, treating **169** with $Fe[N(Si(CH_3)_3)_2]_3$ yields the analogous 5-coordinate Fe(III) complex **172** (Scheme 82). The solid state structure of **172** contains a similar intermediate Fe coordination geometry.

**Scheme 82** Synthesis of the Fe(II) complex **170** featuring two semiquinonate ONO pincer-type ligands and Fe(III) complexes **171-174**.[47, 68]

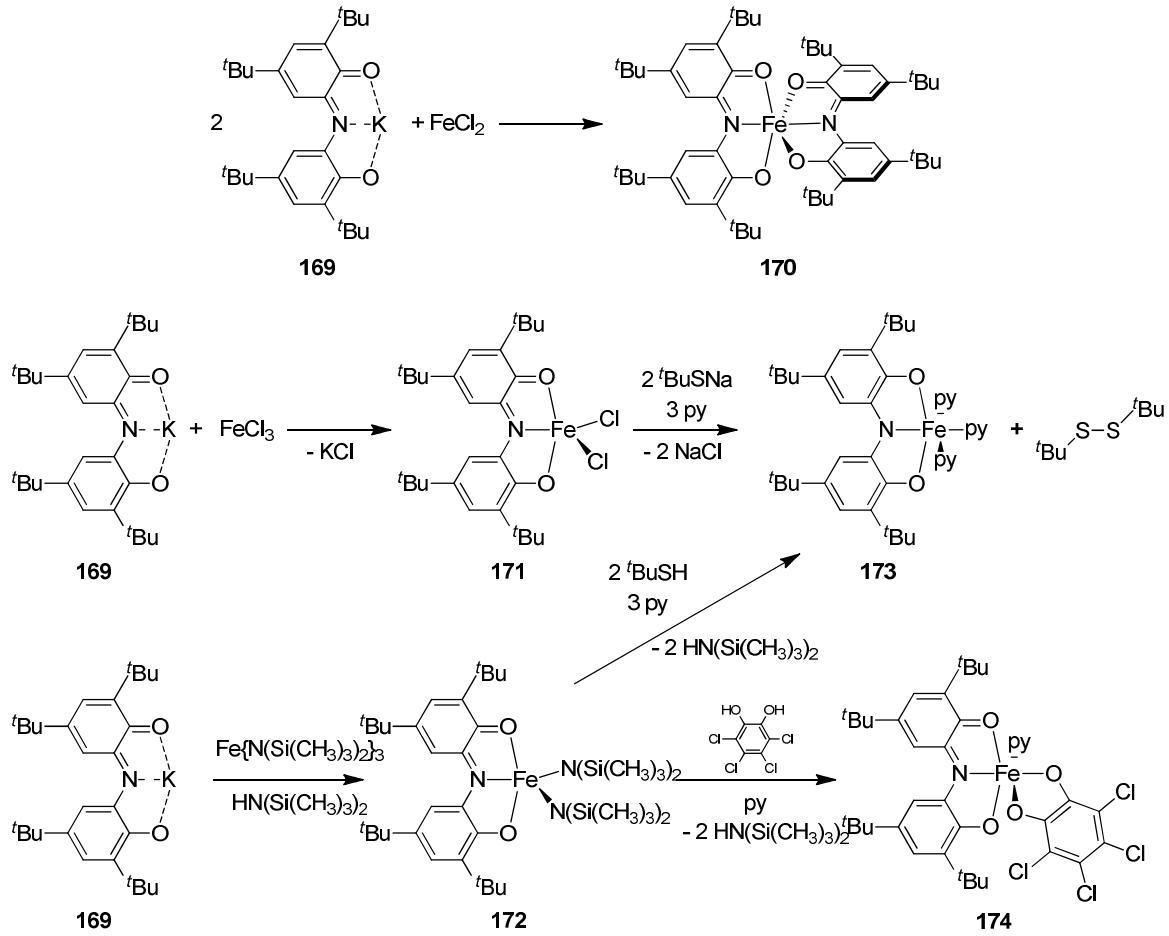


Treating complex **172** with $^t$BuSH in the presence of pyridine (py) releases two equivalents of free amine $HN(Si(CH_3)_3)_2$ via protonolysis and expulses $^t Bu_2S_2$. Accompanying the reduction to disulfide, the ONO pincer-type ligand of complex **173** is oxidized by two electrons to the trianionic form. The solid state structure of **173** supports the trianionic form of the ONO pincer-type ligand, and Mössbauer and EPR spectroscopy are consistent with a high spin $Fe^{3+}$ metal center. It is unclear whether the mechanism

occurs via reductive elimination at the metal center, or by two proton-coupled electron transfer (PCET) steps that generate $^{t}$BuS$^{\cdot}$ fragments. Another possibility involves a dimeric intermediate. It is worth noting that complex **173** and $^{t}Bu_2S_2$ also form by treating **171** with NaS$^{t}$Bu. Evidence concludes that the two electron reduction needed for the extrusion of disulfide occurs exclusively at the ligand, leaving the Fe oxidation state unchanged. Ligand reduction provides the thermodynamic driving force since neither $FeCl[N(Si(CH_3)_3)_2]_2$ or $FeCl_3$ generate disulfide in the presence of HS$^{t}$Bu or NaS$^{t}$Bu.

Treating complex **172** with a mild two electron reductant, tetrachlorocatechol, replaces the amide ligand via protonolysis to yield complex **174** (Scheme 82). The solid state structure of **174** indicates no formal oxidation state occurs at the metal; the EPR spectrum of **174** is consistent with a low spin iron(III) complex. Bond lengths within the ONO ligand indicate the semiquinonate form persists.

### *6.9. $ONO^{3-}$ rhodium complexes*

Whereas early transition metal trianionic pincer/pincer-type complexes featuring group 4-6 metals have received considerable attention, late transition metals have only recently been explored. The challenge lies in metalating hard anionic donors (suited for early transition metals in high oxidation states) with softer metals with low oxidation states and high d-electron counts. One approach to access a trianionic ONO pincer-type ligand with late transition metals utilizes low oxidation state Rh(I) and the monoanionic ONO pincer proligand **169**.[140] In the presence of strong donor ligands, the proligand **169** upon addition of 0.5 $[(cod)Rh(\mu\text{-}Cl)_2]_2$ oxidizes the metal center to Rh(III), and concomitantly the coordinated tridentate ONO ligand is reduced to its trianionic form (Scheme 83).[140] Using pyridine as a donor ligand, the octahedral Rh(III) complex **175** is obtained featuring the trianionic $ONO^{3-}$ pincer ligand and three coordinated pyridines. Similarly, replacing pyridine with either two equivalents of $P(CH_3)_3$, $PCH_3Ph_2$, or $PPh_3$ yields the 5-coordinate Rh(III) complexes **176**, **177**, or **178,** respectively.

**Scheme 83.** Synthesis of trianionic ONO pincer-type rhodium complexes **176-178**.

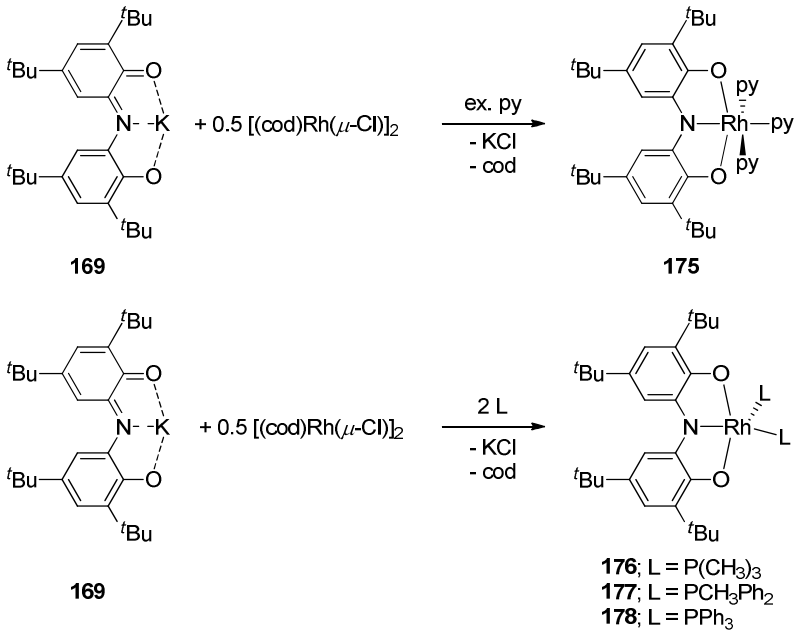


Adding excess phosphine to **176** or **177** results in the reversible coordination of a third phosphine to form **179** and **180**, respectively (Scheme 84).[140] In the case of **179**, the rapid exchange between free $P(CH_3)_3$ and coordinated $P(CH_3)_3$ yields a single resonance in the $^1H$ NMR spectrum. Lowering the temperature to 228 K slows the exchange producing unique signals for the coordinated $P(CH_3)_3$ ligands. A similar effect was observed in the $^{31}P\{^1H\}$ NMR at 213 K.

**Scheme 84.** Reversible coordination of $P(CH_3)_3$ and $PCH_3Ph_2$ to **176** and **177**.

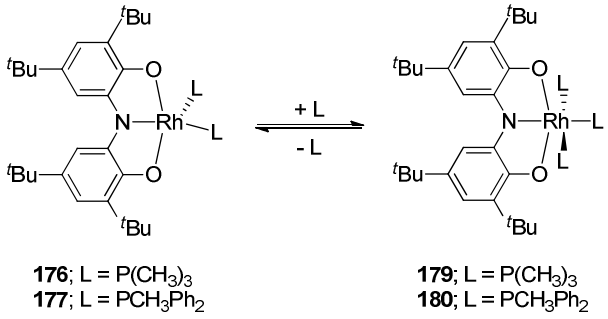


The UV-vis spectrum exhibits an interesting feature upon changing from a 5-coordinate to a 6-coordinate Rh complexes. Octahedral Rh complexes **175**, **179**, and **180** exhibit a strong absorption at 400

nm, consistent with MLCT; whereas the 5-coordinte Rh complexes **176**, **177**, and **178** contain an absorption at 300 nm and a broad absorption between 500 and 800 nm. The abrupt changes in the UV-vis spectrum suggest a significant electronic change between 5- and 6-coordinate Rh complexes. DFT calculations of the Rh complexes **175**, **176**, **178**, and **179** were employed to investigate the electronic changes for both 5- and 6-coordinate complexes. In both cases, DFT calculations unambiguously confirm the Rh(III) oxidation state and a trianionic pincer ligand. However, the single point calculations reveal a different bonding paradigm between them. Figure 5 depicts the HOMO from the 5- and 6-coordinate complexes. In the case of the 6-coordinate complexes, the nitrogen lone pair is prevented from π-donating into a filled $d_{yz}$ orbital and essentially remains non-bonding. In contrast, distortion in the square pyramidal geometry allows the N-atom lone pair to strongly π-donate into the $d_Z^2$ (σ*) orbital. The good overlap between the nitrogen p-orbital and $d_Z^2$ explains the broad π→π* absorption in the UV-vis spectra above 500 nm.

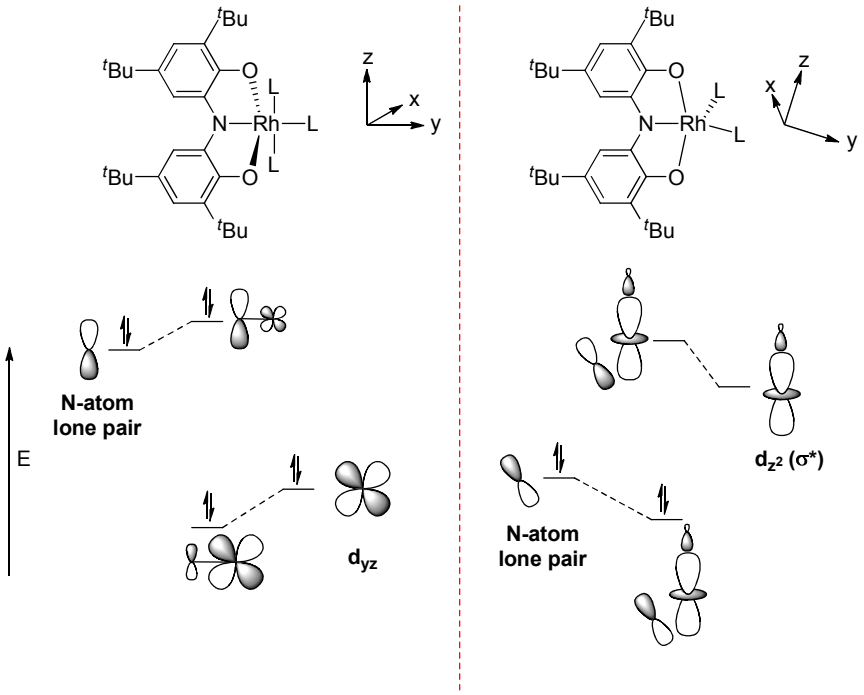


**Figure 5.** Truncated molecular orbital diagram of 6- and 5-coordinate $Rh^{3+}$ complexes.[140]

*6.10. $ONO^{3-}$ antimony complexes*

ONO and NNN redox-active pincer-type ligands mediate redox reactions at formally $d^0$ metal centers. Extension of this idea implies main group metal ions, may also facilitate two-electron processes. Heyduk et al. attempted to synthesize trianionic $ONO^{3-}$ pincer-type complexes of Al(III), but only achieved mono and dianionic versions of the ligand.[168] Poddel'sky et al. investigated the coordination chemistry of other main group elements and were successful in synthesizing and characterizing a trianionic form of the $ONO^{3-}$ ligand coordinated to antimony(V).[169-170] Treating the protio ligand $[ONO]H_3$ (**143**) with $Et_3SbBr_2$ and two equivalents of $Et_3N$ produces the triethyl complex $[ONHO]SbEt_3$ (**181-Et**) with the ONO ligand in its protonated dianionic form (Scheme 85). Complex **181** is analogous to the antimony triphenyl derivative $[ONHO]SbPh_3$ (**181-Ph**) by Poddel'sky,[171] and to an aluminum complex from Heyduk's work.[168] Interestingly, the bromide ligands are lost as opposed to protonation of the ethyl ligands to give ethane during the synthesis of **181-Et**. Whereas, **181-Ph** is stable at ambient temperature, complex **181-Et** eliminates ethane to form the trianionic pincer complex $[ONO]SbEt_2$ (**182**). The formation of **182** accelerates upon exposure of **181-Et** to oxygen, though other oxidation products are observed such as diethyl ether and ethanol. Complex **182** is stable and its characterization included a single X-ray diffraction experiment to unambiguously assign its structure. Addition of the hydroxy-quinone form of the ligand (**169-H**) to $Et_3Sb$ provides an alternative route to **181-Et**. Remarkably, reversing the order of addition ($Et_3Sb$ addition to **169-H**), provides an alternative synthesis for **182** (not shown).

Electrochemical oxidation of complex **182** provides the cationic paramagnetic semiquinonate complex $\mathbf{182}^+$ (Scheme 85). Loss of colorless **182** is evident as the solution turns intensely violet as the redox event occurs. Chemical oxidation of **182** to give $\mathbf{183}^+$ also occurs with the addition of the one-electron oxidants AgOTF and $[Fc]BF_4$. Conclusive evidence for their identity as semiquinonate complexes comes from ESR spectroscopy. Further oxidation of $\mathbf{183}^+$ produces the quinonate dication $\mathbf{183}^{++}$; however, adsorption of the product to the platinum electrode thwarted characterization.

**Scheme 85.** Synthesis of the $ONO^{3-}$ trianionic pincer-type antimony(V) complex **182** (top) and subsequent ligand centered redox processes (bottom).

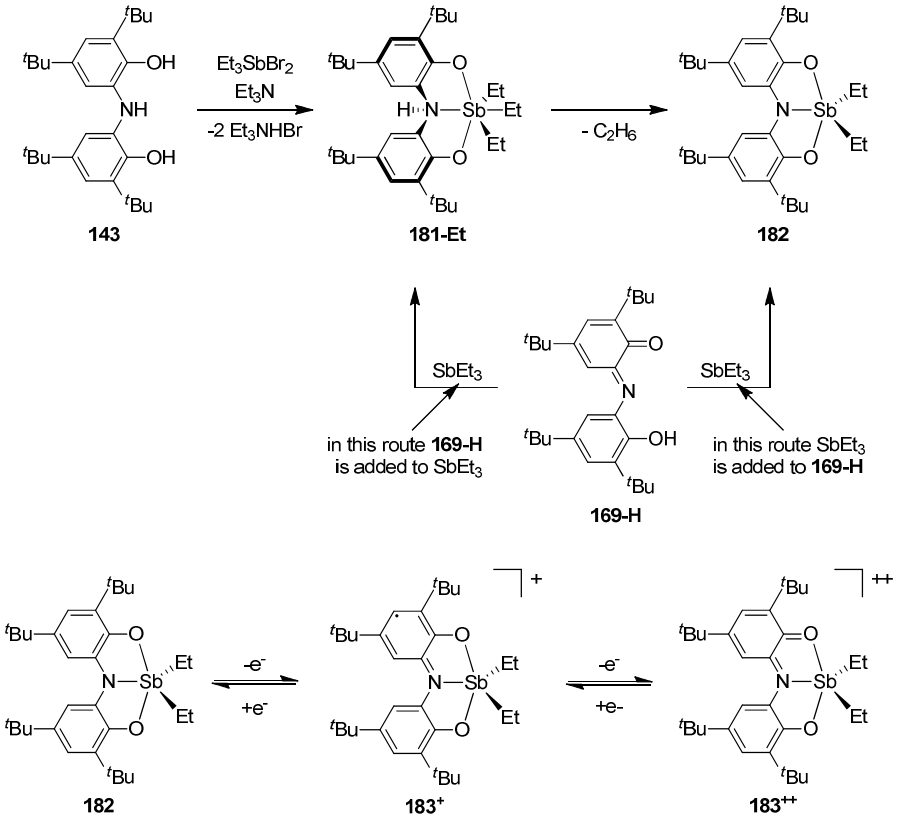


## 7. Conclusions

In this review, we provide an overview of different metalation procedures to access trianionic pincer and pincer-type complexes. Trianionic pincer ligated complexes are more difficult to synthesize than their pincer-type counterparts, due to the intensive kinetic barrier to activating the strong C-H bond. Bercaw and coworkers have quantified the kinetic barrier for C-$H_{pincer}$ activation to form OCO tantalum and titanium complexes to be ~28 kcal/mol (Section 3.3). In addition, significant steps must be taken to avoid over-metalation, over-ligation, and dimerization. Pincer-type ligand complexes, by contrast, are more easily attained. An exemplary example is the synthesis of tungsten-ONO and -SNS pincer-type complexes that only require combining the proligand with $WCl_6$ and removal of HCl by vacuum or reflux (Section 6.6).[163]

Trianionic pincer and pincer-type ligands show remarkable ability to promote a wide range of reactivity and catalysis from high valent metal complexes. The diverse selection of donor atoms available, which now includes: NCN, OCO, CCC, NNN, ONO, and SNS combinations, provide an abundance of opportunity to fine tune transition metal catalysts across the periodic table. Three predominant themes emerge from trianionic pincer and pincer-type ligands: (1) the highly charged nature of trianionic pincers coupled with strong donor atoms supports high oxidation metal ions, while the rigid tridentate architecture ensures a labile *trans*-coordination site. Evidence for the former is the unexpected stability of the [NCN]$Cr^{IV}CH_3$(THF) complex (**22**) (Section 2.2).[59] Perhaps this is most clear in the OCO supported chromium aerobic oxidation catalyst, which uses the rigid tridentate framework to avoid prototypical catalyst deactivation pathways (Section 3.4.2).[66]

(2) Trianionic pincer and pincer-type ligands are transformative by virtue of their ease of modification and their ability to access multiple oxidations states. The most notable examples are the redox-active ONO, NNN, and SNS pincer-type ligands that shuttle between trianionic, dianionic, and monoanionic forms. Accessing multiple ligand oxidation states can drive redox chemistry at a redox-inert metal center. Another aspect of transformative behavior is that trianionic pincer ligands can transform themselves into new ligand structures to generate highly active catalysts. For example, Cr—$CH_3$ bond homolysis within [NCN]$Cr^{IV}CH_3$(THF) (**22**) affords the dianionic pincer complex [NCN*H*]$Cr^{II}$ (**23**) that is a highly selective catalyst for alkene isomerization.[59] More recently, we demonstrated W-alkylidyne insertion into the W-$C_{pincer}$ bond to form a tetraanionic $OCO^{4-}$ pincer complex that is highly active for alkyne polymerization (Section 3.6).[61] By similar merit, a ligated metal complex can be transformed into trianionic pincer and pincer-type complexes. Schrock[43-44] demonstrated the conversion of an NNN tripodal ligand into an $NNN^{3-}$ trianionic pincer-ligand, and A. V. Churakov[139] transformed a dianionic ONO pincer-type ligand into a trianionic version upon metalation with $TiBn_4$. Generating the trianionic pincer when already bound to a metal ion provides a new approach to access highly active catalysts, since it is likely the trianionic pincer complex desired may not always be isolable.

(3) Trianionic pincer and pincer-type ligands, by nature of their rigid framework, can constrain the orientation of donor atom lone pairs with respect to the metal. The constrained orientation is most evident in trianionic NNN and ONO pincer-type ligands, where the lone pair on the amido donor atom is not free to rotate. Schrock and coworkers report a drastic angle change between coordinated methyl ligands upon changing the basicity of the central amido donor (Section 5.1),[124] and Heyduk observed significant changes in the UV-vis spectrum between 5- and 6-coordinate [ONO]Rh(III) complexes due to changes in the N-atom lone pair π-donation.[140] Using the pincer framework to constrain an N-atom lone pair to be collinear with W-C π-bonds enhances the nucleophilicity of tungsten alkylidene and alkylidyne complexes via an inorganic enamine effect (Section 6.3).[67]

There is now ample evidence that trianionic pincer ligands will continue to deliver fascinating transition metal complexes, and importantly, complexes that act as catalysts. Considering the diverse range of complexes presented within this review and their reactivity, it is not unreasonable to suggest that many more catalytic applications of trianionic pincer ligand complexes will be forthcoming. Given the number and type of ligands now available, and an already deep understanding of their metalation chemistry, it is only a matter of pairing the correct trianionic pincer with the appropriate metal ion to achieve the desired reactivity.

## 8. Acknowledgements

ASV acknowledges the NSF (CHE-1265993) for support of ongoing work in the area of trianionic pincer ligands.

## 9. References

1 R. L. O'Connell, *The ghosts of Cannae : Hannibal and the darkest hour of the Roman republic*, Random House, New York, 2010.
2 E. J. Stackpole, *Chancellorsville; Lee's greatest battle*, Stackpole Co, Harrisburg, Pa, 1958.
3 A. Beevor, *Stalingrad*, Viking, New York, 1998.
4 G. Roberts, *Victory at Stalingrad: The Battle that Changed History*, Longman, London ; New York, 2002.
5 http://commons.wikimedia.org/wiki/File:Battle_of_Stalingrad.png.

6 L. A. Watson, J. N. Coalter, O. Ozerov, M. Pink, J. C. Huffman and K. G. Caulton, *New J. Chem.*, 2003, **27**, 263-273.
7 G. van Koten and D. Milstein, *Top. Organomet. Chem.*, 2013, **40**, 1-356.
8 Z.-X. Wang and N. Liu, *Eur. J. Inorg. Chem.*, 2012, 901-911.
9 G. van Koten, *J. Organomet. Chem.*, 2012, **730**, 156-164.
10 S. Schneider, J. Meiners and B. Askevold, *Eur. J. Inorg. Chem.*, 2012, 412-429.
11 H. Zhang and A. Lei, *Dalton Trans.*, 2011, **40**, 8745-8754.
12 N. Selander and K. J. Szabo, *Chem. Rev.*, 2011, **111**, 2048-2076.
13 L. T. Pilarski and K. J. Szabo, *Curr. Org. Chem.*, 2011, **15**, 3389-3414.
14 J.-L. Niu, X.-Q. Hao, J.-F. Gong and M.-P. Song, *Dalton Trans.*, 2011, **40**, 5135-5150.
15 J. Kisala and T. Ruman, *Curr. Org. Chem.*, 2011, **15**, 3486-3502.
16 C. Gunanathan and D. Milstein, *Top. Organomet. Chem.*, 2011, **37**, 55-84.
17 P. Bhattacharya and H. Guan, *Comments Inorg. Chem.*, 2011, **32**, 88-112.
18 M. Albrecht and M. M. Lindner, *Dalton Trans.*, 2011, **40**, 8733-8744.
19 D. Milstein, *Top. Catal.*, 2010, **53**, 915-923.
20 J. I. van der Vlugt and J. N. H. Reek, *Angew. Chem. Int. Ed.*, 2009, **48**, 8832-8846.
21 J. M. Serrano-Becerra and D. Morales-Morales, *Curr. Org. Synth.*, 2009, **6**, 169-192.
22 I. Moreno, R. SanMartin, B. Ines, M. T. Herrero and E. Dominguez, *Curr. Org. Chem.*, 2009, **13**, 878-895.
23 D. Morales-Morales, *Mini-Rev. Org. Chem.*, 2008, **5**, 141-152.
24 W. Leis, H. A. Mayer and W. C. Kaska, *Coord. Chem. Rev.*, 2008, **252**, 1787-1797.
25 D. Benito-Garagorri and K. Kirchner, *Acc. Chem. Res.*, 2008, **41**, 201-213.
26 M. Q. Slagt, G. Rodriguez, M. M. P. Grutters, R. J. M. K. Gebbink, W. Klopper, L. W. Jenneskens, M. Lutz, A. L. Spek and G. van Koten, *Chem. Eur. J.*, 2004, **10**, 1331-1344.
27 D. Morales-Morales, *Rev. Soc. Quim. Mex.*, 2004, **48**, 338-346.
28 J. T. Singleton, *Tetrahedron*, 2003, **59**, 1837-1857.
29 M. Albrecht and G. van Koten, *Angew. Chem. Int. Ed.*, 2001, **40**, 3750-3781.
30 W. Leis, H. A. Mayer and W. C. Kaska, *Coord. Chem. Rev.*, 2008, **252**, 1787-1797.
31 D. Morales-Morales and C. M. Jensen, eds., *The Chemistry of Pincer Compounds*, Elsevier, Amsterdam, 2007.
32 C. J. Moulton and B. L. Shaw, *J. Chem. Soc., Dalton Trans.*, 1976, 1020-1024.
33 C. Crocker, R. J. Errington, W. S. Mcdonald, K. J. Odell, B. L. Shaw and R. J. Goodfellow, *J. Chem. Soc., Chem. Comm.*, 1979, 498-499.
34 C. Crocker, R. J. Errington, R. Markham, C. J. Moulton, K. J. Odell and B. L. Shaw, *J. Am. Chem. Soc.*, 1980, **102**, 4373-4379.
35 C. Crocker, H. D. Empsall, R. J. Errington, E. M. Hyde, W. S. Mcdonald, R. Markham, M. C. Norton, B. L. Shaw and B. Weeks, *J. Chem. Soc., Dalton Trans.*, 1982, 1217-1224.
36 C. Crocker, R. J. Errington, R. Markham, C. J. Moulton and B. L. Shaw, *J. Chem. Soc., Dalton Trans.*, 1982, 387-395.
37 R. J. Errington, W. S. Mcdonald and B. L. Shaw, *J. Chem. Soc., Dalton Trans.*, 1982, 1829-1835.
38 M. D. Fryzuk and P. A. Macneil, *J. Am. Chem. Soc.*, 1981, **103**, 3592-3593.
39 M. D. Fryzuk, C. D. Montgomery and S. J. Rettig, *Organometallics*, 1991, **10**, 467-473.
40 L. Fan, B. M. Foxman and O. V. Ozerov, *Organometallics*, 2004, **23**, 326-328.
41 L. C. Liang, *Coord. Chem. Rev.*, 2006, **250**, 1152-1177.
42 J. Koller, S. Sarkar, K. A. Abboud and A. S. Veige, *Organometallics*, 2007, **26**, 5438-5441.
43 J. S. Freundlich, R. R. Schrock and W. M. Davis, *J. Am. Chem. Soc.*, 1996, **118**, 3643-3655.
44 J. S. Freundlich, R. R. Schrock and W. M. Davis, *Organometallics*, 1996, **15**, 2777-2783.
45 T. Watanabe, T. Matsuo and H. Kawaguchi, *Inorg. Chem.*, 2006, **45**, 6580-6582.
46 H. Sugiyama, I. Korobkov, S. Gambarotta, A. Moller and P. H. M. Budzelaar, *Inorg. Chem.*, 2004, **43**, 5771-5779.
47 A. Y. Girgis and A. L. Balch, *Inorg. Chem.*, 1975, **14**, 2724-2727.

48 S. K. Larsen and C. G. Pierpont, *J. Am. Chem. Soc.*, 1988, **110**, 1827-1832.
49 C. L. Simpson, S. R. Boone and C. G. Pierpont, *Inorg. Chem.*, 1989, **28**, 4379-4385.
50 P. Chaudhuri, M. Hess, T. Weyhermuller and K. Wieghardt, *Angew. Chem. Int. Ed.*, 1999, **38**, 1095-1098.
51 R. A. Zarkesh, J. W. Ziller and A. F. Heyduk, *Angew. Chem. Int. Ed.*, 2008, **47**, 4715-4718.
52 A. F. Heyduk, R. A. Zarkesh and A. I. Nguyen, *Inorg. Chem.*, 2011, **50**, 9849-9863.
53 R. A. Zarkesh and A. F. Heyduk, *Organometallics*, 2009, **28**, 6629-6631.
54 R. F. Munha, R. A. Zarkesh and A. F. Heyduk, *Dalton Trans.*, 2013, **42**, 3751-3766.
55 O. R. Luca and R. H. Crabtree, *Chem. Soc. Rev.*, 2013, **42**, 1440-1459.
56 V. K. K. Praneeth, M. R. Ringenberg and T. R. Ward, *Angew. Chem. Int. Ed.*, 2012, **51**, 10228-10234.
57 V. Lyaskovskyy and B. de Bruin, *ACS Catal.*, 2012, **2**, 270-279.
58 M. O'Reilly, J. M. Falkowski, V. Ramachandran, M. Pati, K. A. Abboud, N. S. Dalal, T. G. Gray and A. S. Veige, *Inorg. Chem.*, 2009, **48**, 10901-10903.
59 K. P. McGowan, K. A. Abboud and A. S. Veige, *Organometallics*, 2011, **30**, 4949-4957.
60 K. P. McGowan and A. S. Veige, *J. Organomet. Chem.*, 2012, **711**, 10-14.
61 K. P. McGowan, M. E. O'Reilly, I. Ghiviriga, K. A. Abboud and A. S. Veige, *Chemical Science*, 2013, **4**, 1145-1155.
62 S. Sarkar, K. P. McGowan, S. Kuppuswamy, I. Ghiviriga, K. A. Abboud and A. S. Veige, *J. Am. Chem. Soc.*, 2012, **134**, 4509-4512.
63 A. I. Nguyen, R. A. Zarkesh, D. C. Lacy, M. K. Thorson and A. F. Heyduk, *Chem. Sci.*, 2011, **2**, 166-169.
64 M. E. O'Reilly, T. J. Del Castillo, K. A. Abboud and A. S. Veige, *Dalton Trans.*, 2012, **41**, 2237-2246.
65 S. Sarkar, K. A. Abboud and A. S. Veige, *J. Am. Chem. Soc.*, 2008, **130**, 16128-16129.
66 M. E. O'Reilly, T. J. Del Castillo, J. M. Falkowski, V. Ramachandran, M. Pati, M. C. Correia, K. A. Abboud, N. S. Dalal, D. E. Richardson and A. S. Veige, *J. Am. Chem. Soc.*, 2011, **133**, 13661-13673.
67 M. E. O'Reilly, I. Ghiviriga, K. A. Abboud and A. S. Veige, *J. Am. Chem. Soc.*, 2012, **134**, 11185-11195.
68 J. L. Wong, R. H. Sanchez, J. G. Logan, R. A. Zarkesh, J. W. Ziller and A. F. Heyduk, *Chem. Sci.*, 2013, **4**, 1906-1910.
69 H. Lang, R. Packheiser and B. Walfort, *Organometallics*, 2006, **25**, 1836-1850.
70 S. Sarkar, K. P. McGowan, J. A. Culver, A. R. Carlson, J. Koller, A. J. Peloquin, M. K. Veige, K. A. Abboud and A. S. Veige, *Inorg. Chem.*, 2010, **49**, 5143-5156.
71 S. Brenner, R. Kempe and P. Arndt, *Zeitschrift Fur Anorganische Und Allgemeine Chemie*, 1995, **621**, 2021-2024.
72 D. J. Liston and B. O. West, *Inorg. Chem.*, 1985, **24**, 1568-1576.
73 A. C. Filippou and S. Schneider, *Organometallics*, 2003, **22**, 3010-3012.
74 E. S. Gould, *Coord. Chem. Rev.*, 1994, **135**, 651-684.
75 M. P. McDaniel, *Advances in Catalysis*, 2010, **53**, 123-606.
76 J. P. Hogan, *J. Polym. Sci., Part A: Polym. Chem.*, 1970, **8**, 2637-2652.
77 C. Schulzke, D. Enright, H. Sugiyama, G. LeBlanc, S. Gambarotta, G. P. A. Yap, L. K. Thompson, D. R. Wilson and R. Duchateau, *Organometallics*, 2002, **21**, 3810-3816.
78 K. H. D. Ballem, V. Shetty, N. Etkin, B. O. Patrick and K. M. Smith, *Dalton Trans.*, 2004, 3431-3433.
79 R. Schmid and T. Ziegler, *Can. J. Chem.*, 2000, **78**, 265-269.
80 J. A. N. Ajjou and S. L. Scott, *J. Am. Chem. Soc.*, 2000, **122**, 8968-8976.
81 J. A. N. Ajjou, G. L. Rice and S. L. Scott, *J. Am. Chem. Soc.*, 1998, **120**, 13436-13443.
82 J. A. N. Ajjou, S. L. Scott and V. Paquet, *J. Am. Chem. Soc.*, 1998, **120**, 415-416.
83 S. Nuckel and P. Burger, *Organometallics*, 2000, **19**, 3305-3311.

84 I. Korobkov, S. Gorelsky and S. Gambarotta, *J Am Chem Soc*, 2009, **131**, 10406-10420.
85 S. R. Golisz and J. E. Bercaw, *Macromolecules*, 2009, **42**, 8751-8762.
86 S. R. Golisz, J. A. Labinger and J. E. Bercaw, *Organometallics*, 2010, **29**, 5026-5032.
87 S. Kuppuswamy, I. Ghiviriga, K. A. Abboud and A. S. Veige, *Organometallics*, 2010, **29**, 6711-6722.
88 T. Agapie and J. E. Bercaw, *Organometallics*, 2007, **26**, 2957-2959.
89 G. L. Juvinall, *J. Am. Chem. Soc.*, 1964, **86**, 4202-4203.
90 G. W. A. Fowles, D. A. Rice and J. D. Wilkins, *J. Chem. Soc., Dalton Trans.*, 1973, 961-965.
91 R. R. Schrock and P. R. Sharp, *J. Am. Chem. Soc.*, 1978, **100**, 2389-2399.
92 T. Agapie, M. W. Day and J. E. Bercaw, *Organometallics*, 2008, **27**, 6123-6142.
93 T. Funabiki, in *Catalysis by Metal Complexes*, Kluwer, Dordrecht, 1997.
94 L. Que and W. B. Tolman, *Nature*, 2008, **455**, 333-340.
95 M. Costas, M. P. Mehn, M. P. Jensen and L. Que, *Chem. Rev.*, 2004, **104**, 939-986.
96 M. M. Q. Simoes, C. M. B. Neves, S. M. G. Pires, M. G. P. M. S. Neves and J. A. S. Cavaleiro, *Pure Appl. Chem.*, 2013, **85**, 1671-1681.
97 S. I. Murahashi and D. Zhang, *Chem. Soc. Rev.*, 2008, **37**, 1490-1501.
98 E. M. McGarrigle and D. G. Gilheany, *Chem. Rev.*, 2005, **105**, 1563-1602.
99 T. Katsuki, *Coord. Chem. Rev.*, 1995, **140**, 189-214.
100 S. Caron, R. W. Dugger, S. G. Ruggeri, J. A. Ragan and D. H. B. Ripin, *Chem. Rev.*, 2006, **106**, 2943-2989.
101 K. P. Bryliakov and E. P. Talsi, *Inorg. Chem.*, 2003, **42**, 7258-7265.
102 E. N. Jacobsen, L. Deng, Y. Furukawa and L. E. Martinez, *Tetrahedron*, 1994, **50**, 4323-4334.
103 S. Kuppuswamy, A. J. Peloquin, I. Ghiviriea, K. A. Abboud and A. S. Veige, *Organometallics*, 2010, **29**, 4227-4233.
104 R. R. Schrock, J. S. Murdzek, G. C. Bazan, J. Robbins, M. Dimare and M. Oregan, *J. Am. Chem. Soc.*, 1990, **112**, 3875-3886.
105 M. T. Jan, S. Sarkar, S. Kuppuswamy, I. Ghiviriga, K. A. Abboud and A. S. Veige, *J. Organomet. Chem.*, 2011, **696**, 4079-4089.
106 Z. J. Tonzetich, R. R. Schrock and P. Muller, *Organometallics*, 2006, **25**, 4301-4306.
107 J. M. Blackwell, J. S. Figueroa, F. H. Stephens and C. C. Cummins, *Organometallics*, 2003, **22**, 3351-3353.
108 Y. C. Tsai, P. L. Diaconescu and C. C. Cummins, *Organometallics*, 2000, **19**, 5260-5262.
109 R. R. Schrock, D. N. Clark, J. Sancho, J. H. Wengrovius, S. M. Rocklage and S. F. Pedersen, *Organometallics*, 1982, **1**, 1645-1651.
110 D. N. Clark and R. R. Schrock, *J. Am. Chem. Soc.*, 1978, **100**, 6774-6776.
111 Z. J. Tonzetich, Y. C. Lam, P. Müller and R. R. Schrock, *Organometallics*, 2007, **26**, 475-477.
112 M. L. Listemann and R. R. Schrock, *Organometallics*, 1985, **4**, 74-83.
113 K. Jyothish and W. Zhang, *Angew. Chem. Int. Ed.*, 2011, **50**, 3435-3438.
114 H. M. Cho, H. Weissman, S. R. Wilson and J. S. Moore, *J. Am. Chem. Soc.*, 2006, **128**, 14742-14743.
115 W. Zhang, S. Kraft and J. S. Moore, *J. Am. Chem. Soc.*, 2004, **126**, 329-335.
116 E. A. Ison, K. A. Abboud and J. M. Boncella, *Organometallics*, 2006, **25**, 1557-1564.
117 J. H. Hardesty, J. B. Koerner, T. A. Albright and G. Y. Lee, *J. Am. Chem. Soc.*, 1999, **121**, 6055-6067.
118 K. Kirchner, M. J. Calhorda, R. Schmid and L. F. Veiros, *J. Am. Chem. Soc.*, 2003, **125**, 11721-11729.
119 R. Matusiak and A. Keller, *J. Mol. Catal. A: Chem.*, 2003, **195**, 29-35.
120 V. V. Saraev, P. B. Kraikivskii, A. Vilms, S. N. Zelinskii, A. Y. Yunda, E. N. Danilovtseva and A. S. Kuzakov, *Kinet. Catal.*, 2007, **48**, 778-784.
121 A. Sattler and G. Parkin, *J. Am. Chem. Soc.*, 2012, **134**, 2355-2366.
122 A. Sattler, S. Ruccolo and G. Parkin, *Dalton Trans.*, 2011, **40**, 7777-7782.

123 R. R. Schrock and P. Meakin, *J. Am. Chem. Soc.*, 1974, **96**, 5288-5290.
124 R. R. Schrock, J. Lee, L.-C. Liang and W. M. Davis, *Inorg. Chim. Acta*, 1998, **270**, 353-362.
125 A. I. Nguyen, K. J. Blackmore, S. M. Carter, R. A. Zarkesh and A. F. Heyduk, *J. Am. Chem. Soc.*, 2009, **131**, 3307-3316.
126 A. F. Heyduk, R. A. Zarkesh and A. I. Nguyen, *Inorg. Chem.*, 2011, **50**, 9849-9863.
127 R. F. Munha, R. A. Zarkesh and A. F. Heyduk, *Inorg. Chem.*, 2013, **52**, 11244-11255.
128 Q. Knijnenburg, S. Gambarotta and P. H. M. Budzelaar, *Dalton Trans.*, 2006, 5442-5448.
129 S. C. Bart, E. Lobkovsky and P. J. Chirik, *J. Am. Chem. Soc.*, 2004, **126**, 13794-13807.
130 A. M. Tondreau, C. C. H. Atienza, K. J. Weller, S. A. Nye, K. M. Lewis, J. G. P. Delis and P. J. Chirik, *Science*, 2012, **335**, 567-570.
131 S. K. Russell, E. Lobkovsky and P. J. Chirik, *J. Am. Chem. Soc.*, 2011, **133**, 8858-8861.
132 K. T. Sylvester and P. J. Chirik, *J. Am. Chem. Soc.*, 2009, **131**, 8772-8774.
133 D. Enright, S. Gambarotta, G. P. A. Yap and P. H. M. Budzelaar, *Angew. Chem. Int. Ed.*, 2002, **41**, 3873-3876.
134 D. P. Cladis, J. J. Kiernicki, P. E. Fanwick and S. C. Bart, *Chem. Commun.*, 2013, **49**, 4169-4171.
135 A. M. Tondreau, S. C. E. Stieber, C. Milsmann, E. Lobkovsky, T. Weyhermuller, S. P. Semproni and P. J. Chirik, *Inorg. Chem.*, 2013, **52**, 635-646.
136 J. M. Darmon, Z. R. Turner, E. Lobkovsky and P. J. Chirik, *Organometallics*, 2012, **31**, 2275-2285.
137 L. R. Avens, C. J. Burns, R. J. Butcher, D. L. Clark, J. C. Gordon, A. R. Schake, B. L. Scott, J. G. Watkin and B. D. Zwick, *Organometallics*, 2000, **19**, 451-457.
138 J. J. Kiernicki, B. S. Newell, E. M. Matson, N. H. Anderson, P. E. Fanwick, M. P. Shores and S. C. Bart, *Inorg. Chem.*, 2014, **53**, 3730-3741.
139 I. E. Nifant'ev, P. V. Ivchenko, V. V. Bagrov, S. M. Nagy, S. Mihan, L. N. Winslow and A. V. Churakov, *Organometallics*, 2013, **32**, 2685-2692.
140 G. Szigethy, D. W. Shaffer and A. F. Heyduk, *Inorg. Chem.*, 2012, **51**, 12606-12618.
141 S. Beer, C. G. Hrib, P. G. Jones, K. Brandhorst, J. Grunenberg and M. Tamm, *Angew. Chem. Int. Ed.*, 2007, **46**, 8890-8894.
142 M. Tamm and X. Wu, *Chim Oggi*, 2010, **28**, 60-63.
143 X. A. Wu and M. Tamm, *Beilstein J. Org. Chem.*, 2011, **7**, 82-93.
144 X. Wu, C. G. Daniliuc, C. G. Hrib and M. Tamm, *J. Organomet. Chem.*, 2011, **696**, 4147-4151.
145 S. VenkatRamani, M. E. Pascualini, I. Ghiviriga, K. A. Abboud and A. S. Veige, *Polyhedron*, 2013, **64**, 377-387.
146 R. Fandos, I. López-Solera, A. Otero, A. Rodríguez, M. J. Ruiz and P. Terreros, *Organometallics*, 2004, **23**, 5030-5036.
147 A. Conde, R. Fandos, C. Hernandez, A. Otero and A. Rodriguez, *Chem. Eur. J.*, 2010, **16**, 12074-12078.
148 A. Conde, R. Fandos, C. Hernandez, A. Otero, A. Rodriguez and M. J. Ruiz, *Chem. Eur. J.*, 2012, **18**, 2319-2326.
149 A. Conde, R. Fandos, A. Otero and A. Rodriguez, *Organometallics*, 2009, **28**, 5505-5513.
150 D. H. Nguyen, I. Greger, J. J. Pérez-Torrente, M. V. Jiménez, F. J. Modrego, F. J. Lahoz and L. A. Oro, *Organometallics*, 2013, **32**, 6903-6917.
151 M. E. O'Reilly, I. Ghiviriga, K. A. Abboud and A. S. Veige, *Dalton Trans.*, 2013, **42**, 3326-3336.
152 B. Kempf, N. Hampel, A. R. Ofial and H. Mayr, *Chem. Eur. J.*, 2003, **9**, 2209-2218.
153 A. G. Cook, ed., *Enamines: synthesis, structure, and reactivity*, Marcel Dekker, Inc., New York, 1988.
154 M. R. Churchill, J. W. Ziller, J. H. Freudenberger and R. R. Schrock, *Organometallics*, 1984, **3**, 1554-1562.
155 J. H. Freudenberger, R. R. Schrock, M. R. Churchill, A. L. Rheingold and J. W. Ziller, *Organometallics*, 1984, **3**, 1563-1573.

156 S. F. Pedersen, R. R. Schrock, M. R. Churchill and H. J. Wasserman, *J. Am. Chem. Soc.*, 1982, **104**, 6808-6809.
157 M. R. Churchill, Y. J. Li, L. Blum and R. R. Schrock, *Organometallics*, 1984, **3**, 109-113.
158 M. E. O'Reilly, S. S. Nadif, I. Ghiviriga, K. A. Abboud and A. S. Veige, *Organometallics*, 2014, **in press**, DOI: 10.1021/om4009422.
159 S. Bruni, A. Caneschi, F. Cariati, C. Delfs, A. Dei and D. Gatteschi, *J. Am. Chem. Soc.*, 1994, **116**, 1388-1394.
160 R. A. Zarkesh and A. F. Heyduk, *Organometallics*, 2011, **30**, 4890-4898.
161 F. Lu, R. A. Zarkesh and A. F. Heyduk, *Eur. J. Inorg. Chem.*, 2012, 467-470.
162 R. W. Chesnut, L. D. Durfee, P. E. Fanwick, I. P. Rothwell, K. Folting and J. C. Huffman, *Polyhedron*, 1987, **6**, 2019-2026.
163 D. W. Shaffer, G. Szigethy, J. W. Ziller and A. F. Heyduk, *Inorg. Chem.*, 2013, **52**, 2110-2118.
164 D. D. Wright and S. N. Brown, *Inorg. Chem.*, 2013, **52**, 7831-7833.
165 G. F. Ciani, G. Dalfonso, P. F. Romiti, A. Sironi and M. Freni, *Inorg Chim a-Article*, 1983, **72**, 29-37.
166 J. J. Kennedy-Smith, K. A. Nolin, H. P. Gunterman and F. D. Toste, *J. Am. Chem. Soc.*, 2003, **125**, 4056-4057.
167 B. R. Mcgarvey, A. Ozarowski, Z. G. Tian and D. G. Tuck, *Can. J. Chem.*, 1995, **73**, 1213-1222.
168 G. Szigethy and A. F. Heyduk, *Dalton Trans.*, 2012, **41**, 8144-8152.
169 A. I. Poddel'sky, N. N. Vavilina, N. V. Somov, V. K. Cherkasov and G. A. Abakumov, *J. Organomet. Chem.*, 2009, **694**, 3462-3469.
170 I. V. Smolyaninov, A. I. Poddel'skii and N. T. Berberova, *Russ. J. Electrochem.*, 2011, **47**, 1211-1219.
171 A. I. Poddel'sky, N. V. Somov, Y. A. Kurskii, V. K. Cherkasov and G. A. Abakumov, *J. Organomet. Chem.*, 2008, **693**, 3451-3455.


This review provides a comprehensive examination of the synthesis, characterization, properties, and catalytic applications of trianionic pincer metal complexes.